UNIVERSITY OF COPENHAGEN
FACULTY OF SCIENCE

Master's thesis

Sofie Gyritia Weitzmann van't Veen

Hydrogeology and groundwater chemistry in riparian lowland

– An investigation of nitrate transport and groundwater flow for an agricultural, riparian area with sandy aquifer located at a subglacial stream trench near Holtum Stream, Denmark

Supervisor: Peter Knudegaard Engesgaard
Department of Geosciences and Natural Resource Management
University of Copenhagen

Co-supervisors: Søren Jessen
Department of Geosciences and Natural Resource Management
University of Copenhagen

Anker Lajer Højberg
Geological Survey of Denmark and Greenland, GEUS

ECTS: 45 ECTS points

Title of thesis:	Hydrogeology and groundwater chemistry in riparian lowland – An investigation of nitrate transport and groundwater flow for an agricultural, riparian area with sandy aquifer located at a subglacial stream trench near Holtum Stream, Denmark
Student:	Sofie Gyritia Weitzmann van't Veen Department of Geosciences and Natural Resource Management University of Copenhagen
Degree:	Master of Science in Geology-Geosciences with qualification profile in Water Resources
Submission date:	November 8th 2016
ETCS credits:	45 ECTS points
Supervisor:	Peter Knudegaard Engesgaard Department of Geosciences and Natural Resource Management University of Copenhagen
Co-supervisors:	Søren Jessen Department of Geosciences and Natural Resource Management University of Copenhagen Anker Lajer Højberg Geological Survey of Denmark and Greenland, GEUS
Number of characters:	170,992 / 71.2 pages

Acknowledgements

I would like to thank my supervisors Peter Engesgaard, Søren Jessen and Anker Højberg for help and support during the process. A special thanks to Mads Steiness for lot of guidance, help and many nice field trips.

Also thanks to Anne Thoisen for support and help in the laboratory, none of the chemical data could have been conducted without her help. Thanks to Catharina Madsen, Per Jensen and Tue Kofod for help during field trips and to Sasha Müller for help understanding the isotope data. I would also thank Per Rasmussen, Maria Skjerbæk, Laura Krohn, Lukas Stray and Kim Schwartz Madsen for general support during this thesis.

I would also like to thank GEUS for support and for making a thesis office available for me and to the project TReNDS for finance during field trips and for letting me be a part of the project.

Hydrogeology and groundwater chemistry in riparian lowland– An investigation of nitrate transport and groundwater flow for an agricultural, riparian area with sandy aquifer located at a subglacial stream trench near Holtum Stream, Denmark

Author: Sofie Gyritia Weitzmann van't Veen

Abstract: This study investigates the hydrogeology and groundwater chemistry for an agricultural riparian area, EVI2, located at a subglacial stream trench with a sandy aquifer near Holtum stream, Denmark. The groundwater flow, nitrate transport and removal were explored in the riparian area in order to understand small-scale nitrate removal processes and parameters.
Different data were collected during field trips. Data investigations consisted of analysis of chemistry measurements, geology data as well as 1D PHREEQC modeling, 2D PHAST modeling and 3D MODFLOW modeling.

The results show that a 3D model at catchment scale can be used to examine the groundwater flow and origins of the water in the riparian area EVI2 at local scale. It was observed that nitrate is removed at the agricultural field and that nitrate-polluted water is presence in springs at the wetland area of the study site. Nitrate reduction appeared possible in presence of pyrite and organic material at the agricultural field. The analyses show that the processes controlling the water chemistry at the agricultural field with high probability are denitrification with pyrite and organic material as the electron donors, reductive dissolution of iron oxides and sulfate reduction with organic material.

Keywords: Denitrification, groundwater chemistry, riparian area, nitrate removal, small-scale investigations

Table of content

1. Introduction and objectives

Over the last few years, there has been more and more focus on groundwater quality and pollution. In the European countries and North America, there is a problem with nitrate in the groundwater which mainly originates from the use of fertilizer at the agriculture sites since the early sixties (Appelo and Postma, 2005).
Nitrate is a major problem because it threatens the groundwater resources (Appelo and Postma, 2005, Jessen et al, 2016). A high level can cause unwanted algae growth in lakes, streams and coastal environments. It also causes human health problems because it can reduce the oxygen supply to the body, which can contribute to the development of stomach cancer (Postma et al, 1991). The algae growth in lakes, streams and coastal environments can give problems since it can result in oxygen depletion (Jessen et al, 2016). The threshold value for nitrate in groundwater is 50 mg/L, which corresponds to 0.8 mmol/L, but the recommended concentration is less than 25 mg/L (Appelo and Postma, 2005).

Nitrate pollution from agriculture is a problem in Denmark and therefore, the understanding of nitrate pollution is of great concern. Since the mid-1980'ies, the Danish national water action plans have been implemented. These are made in order to improve the Danish water environment with the aim of ensuring more clean water in Denmark's coastal waters, lakes, streams and groundwater in accordance with the EU Water Framework Directive. A new updated and extension of the water action plan has been implemented in June 2016 and applies from 2015 to 2021 (SVANA, 2016).
The regulation of nitrogen in Denmark has always been consistent with the same restriction everywhere, which is not cost-effective. The Danish Commission on Nature and Agriculture are currently developing new regulation strategies in Denmark, based on a more spatially nitrate regulation. This is done in order to find methods, which can distinguish between areas where denitrification is present with a high rate and more vulnerable areas where the denitrification is much slower or absent.

By developing a new spatially differentiated regulation where nitrate restrictions are focused in areas with low capacity for reduction of nitrate, a further reduction in N-load can be obtained. Such a distinction between natural variations in nitrate reduction is new and requires knowledge on small-scale nitrate removal which is not jet excising (TRENDS, 2016).

Riparian areas are important and of great concern because they lie as a sandwich between aquifers and streams and thus control not only the exchange of water, but also nitrate removal. The hydrogeology of stream aquifer valleys and riparian areas is therefore important because it controls the connection between the riparian area and the aquifer. This connection needs to be good in order to optimize the rate of denitrification in specific riparian lowland (Vidon and Hill, 2004).
Riparian areas' importance of removing nitrate are investigated and discussed in different studies and articles, which include the following: Vidon and Hill (2004), Dahl (et al. 2007) and Karan (et al. 2013).

Vidon and Hill (2004) found that the riparian area needs to be in good connection with the aquifer in order to have the optimal denitrification rate in an area, and that this connection is highly affected by the landscape topography and geology in the area. Dahl (et al. 2007) made a classification of flow path types through riparian areas in Denmark in order to evaluate the denitrification capacities of different riparian areas. Karan (et al. 2013) investigated the groundwater flow and mixing in a wetland-stream system and found that nitrate reduction was occurring in the anoxic deeper parts of the wetland but not in the upper part, which was the area receiving the most nitrate-polluted water. This means that the wetland area did not act like a buffer for removing nitrate from the water before entering the stream. Hence the site-specific geological and hydrogeological conditions of a given riparian area are important to investigate, in order to understand the capacity of nitrate transport and removal.

This study investigates the hydrogeology and geochemistry in a specific riparian area. The study area is an agricultural riparian area located in Holtum catchment close to Holtum Stream.
The area is investigated in order to understand the nitrate transport and removal which can give some knowledge on small-scale nitrate removal. This will be done by collection of data in the field. The collection of data will include MEP lines to investigate the geology composition in the area, establishing of a number of new wells where slugtests are carried out together with water level measurements and water samples collection. In addition, an investigation of the pyrite content and water samples from the stream, drain and from some naturally occurring springs will be conducted.

Preexisting data from previous studies will also be included in the study. All the data will be used to develop groundwater chemistry models at local scale in both 1D and 2D. In addition, the new data will also be implemented in an already existing 3D groundwater model at catchment scale.

This thesis is carried out in cooperation with the research project TReNDS that investigates the importance of Transport and Reduction of Nitrate in Danish landscapes at various Scales www.trends.nitrat.dk. The project is a four-year project started in January 2015, funded by the Innovation Fund Denmark and hosted by GEUS.

The specific objectives and aims of this thesis are the following:

- To investigate the hydrogeology and groundwater chemistry for an agricultural riparian area located at a subglacial stream trench with sandy aquifer near Holtum Stream, Denmark
- To examine the groundwater flow in the riparian area by use of field work and hydrogeological modeling
- To investigate if a pre-developed 3D model at catchment scale can be used to examine the groundwater flow and origins of the water in the riparian area at local scale
- To examine the nitrate transport and removal in the riparian area in order to understand small-scale nitrate removal processes and parameters

2. Study area

This study was conducted in Holtum catchment, located in the western part of Denmark in the middle of Jutland (figure 2.1). The land use in the catchment contains 54% agriculture, 32% forest and 14% urban area (Karan et al, 2013). The catchment is located west of the main stationary line from the last glacial period Weichsel, from approximately 12.000 years ago. From a geomorphologic point of view, it consist of glacial deposits at the eastern part of the main stationary line and at the western part of outwash plains with hill islands and a subglacial stream trench (figure 2.2).

The annual precipitation for the catchment is 888 mm/year, while the actual evapotranspiration is 460-480 mm/year (Jessen et al., 2016 and Poulsen et al., 2015). The large amount of precipitation is mainly due to the location west of the Main Stationary Line, where the precipitation is generally higher than in the rest of Denmark, due to western wind and the topography. The average net precipitation in Denmark is approximately 350 mm (Scharling and Kern-Hansen, 2002).

The composition of the geology and precipitation has a great impact on the land use, how the groundwater is formed and how the streams and groundwater interact.

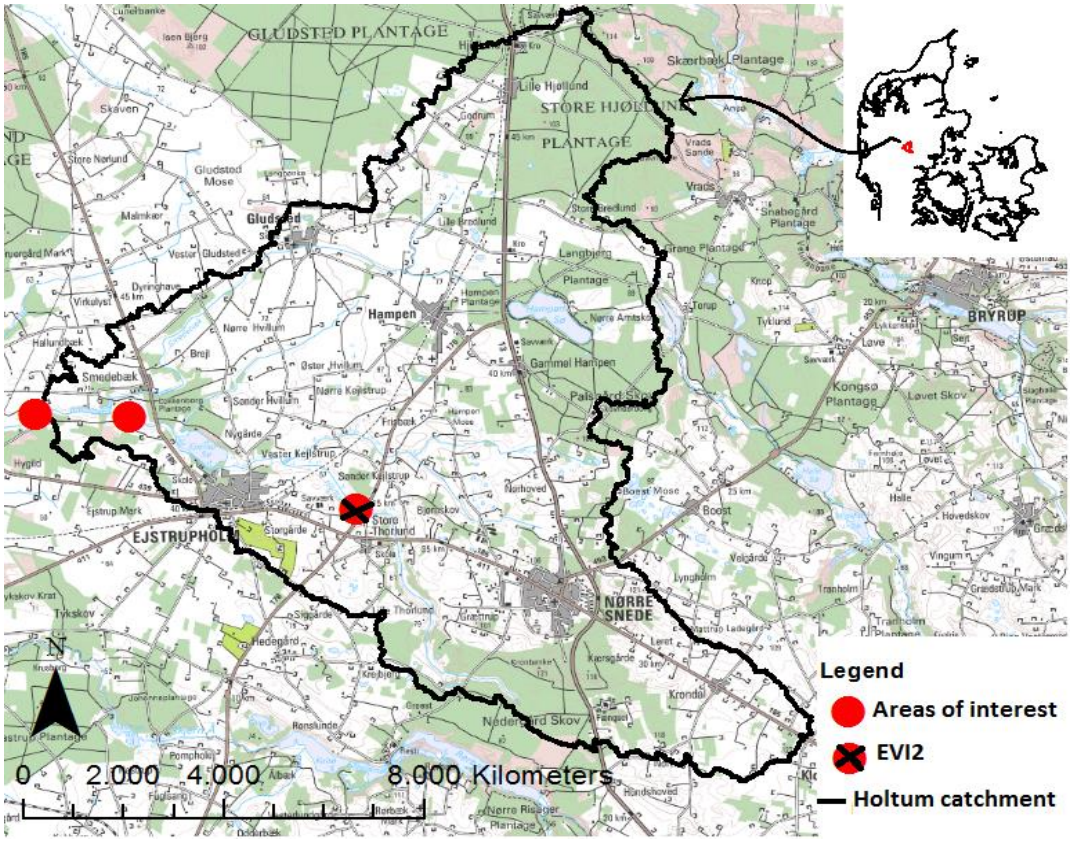

Figure 2.1: Holtum catchment with illustration of areas of interest in the TRENDS project and the study area, EVI2

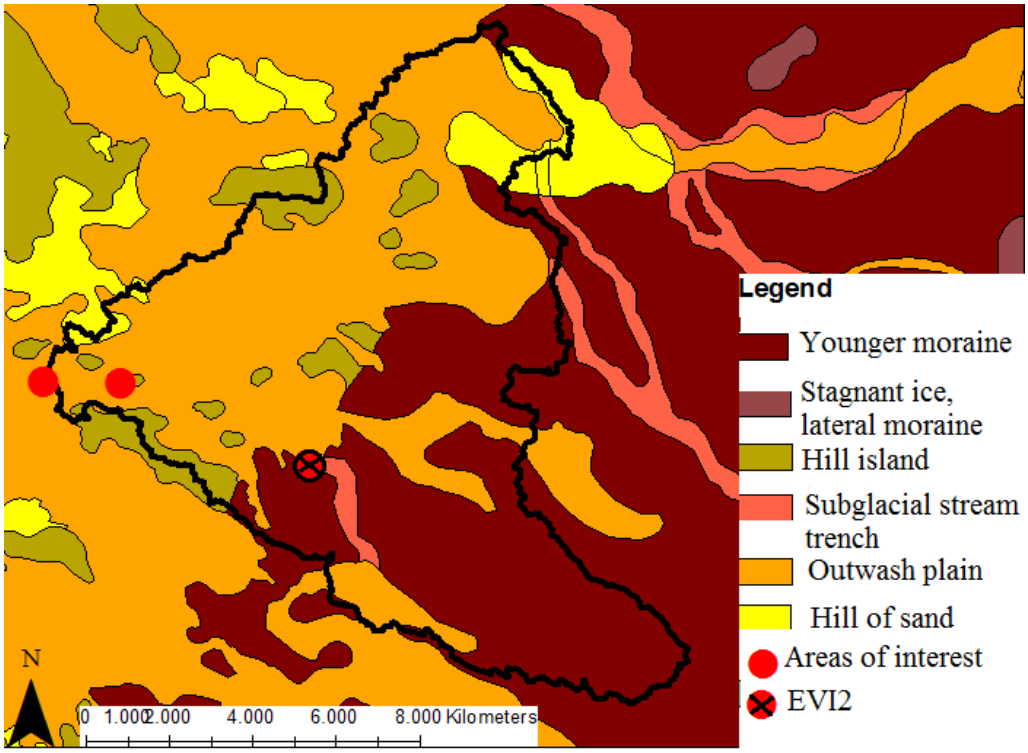

Figure 2.2: Geomorfology of Holtum Catchment with illustration of areas of interest in the TReNDS project and the study area, EVI2.

The TReNDS project focus on Holtum catchment in three different areas of interest (figure 2.1). This thesis is limited to one of those areas, which will hereafter be called EVI2. EVI2 is located in the middle part of the catchment in the Ejstrupholm area (figure 2.1). This area is located upstream in the Holtum catchment and includes Holtum stream. Holtum stream has a width of approximately 2 m and a depth of 1-1.5 m depending on the season, and the mean annual discharge is 0.17m^3/s (Poulsen et al., 2015). The area around EVI2 is dominated by different agricultural fields, and in the northern part, a forest plantation is to be found. By looking at the study area, it is seen that three different kind of land use are found (figure 2.3). Close to the stream and in the northern part of EVI2, an agricultural field is placed. Towards the east and close to the stream a wetland area with grassing, livestock is to be found. A buffer zone consisting of grass with a width of approximately 40 meter is located between the stream and the agricultural field (figure 2.3). As for all other areas, there are some site-specific geological and hydrogeological conditions for EVI2.

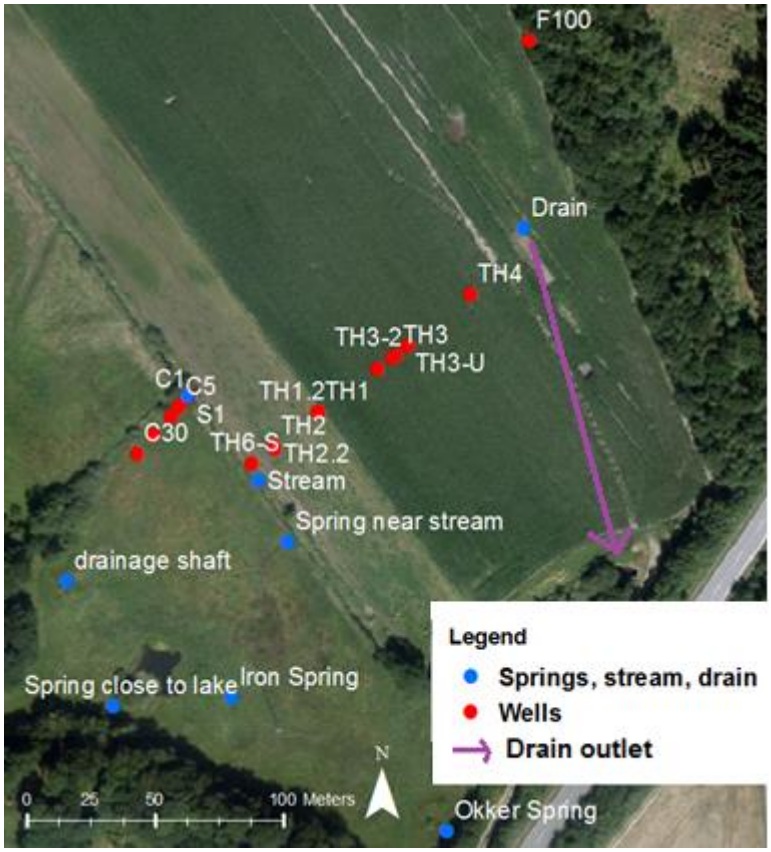

Figure 2.3: The study area, EVI2

The topography of the area shows that Holtum stream is located in the bottom of a valley and that the southern shoulder of the valley is steeper than the northern (figure 2.4).

The fact that EVI2 is located in the termination of a subglacial stream trench (figure 2.2) means that the area has been an environment with frequent floods and a meandering stream over time. The area is nowadays affected by humans and the stream is not meandering anymore.

It can be assumed that before the stream was affected by humans, it was meandering freely in the subglacial stream trench and thereby deposited both sandy and gravel sediments in the stream channels and organic material at the bank deposits by flooding occasions (Nichols, 2009).

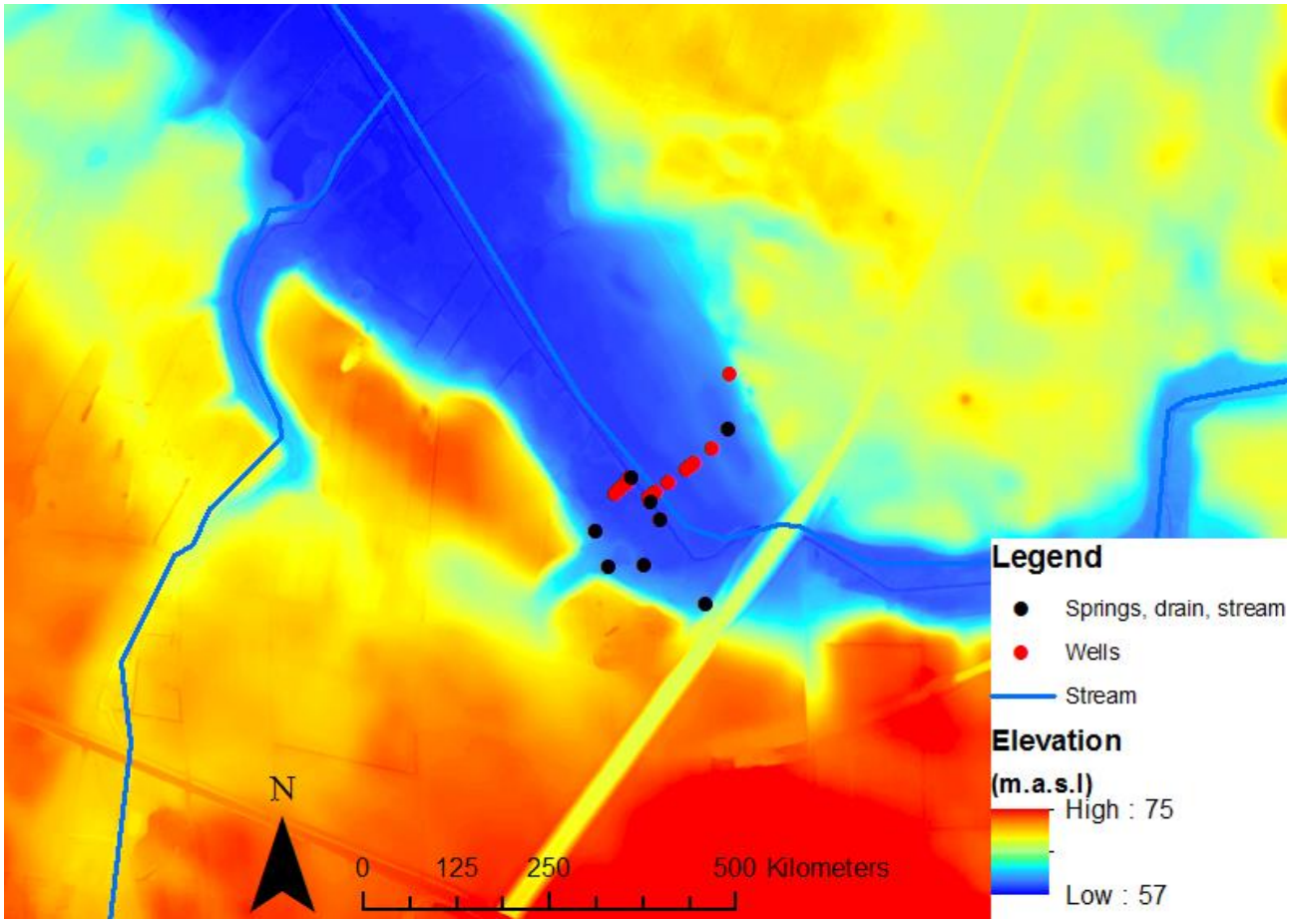

Figure 2.4: The topography of EVI2. The units is in meter about sea level (m.a.s.l)

The period of this thesis is limited and the TReNDS project will continue to investigate the study area and use the collected data. The data is collected in November 2015, February 2016, March 2016 and September 2016. Some of the wells are already installed in a former study and the head measurements from this study are included in this thesis (Poulsen et al., 2015).

3. Theoretical background

In the following, the most relevant theoretical background regarding this thesis will be described. First, the nitrogen cycle will be described and second the denitrification of nitrate with the possible electron donors followed by a description of the different redox steps regarding the chemical processes in the soil, which is important for the analysis later in this thesis.
In addition, the 3D groundwater flow equation will be described, as well as the equation for the conductance and how the transport of chemical components in a groundwater system occurs.

3.1 The nitrogen cycle

Nitrate is a part of the complicated nitrogen cycle (figure 3.1). In the nitrogen cycle, the nitrogen is found in different forms. Organic nitrogen is found in living or dead animals and plants, while inorganic nitrogen is found in nutrients in soil and water and as different nitrogen gasses. When animals and plants decay, the organic nitrogen is reduced to inorganic nitrogen. This process is called *mineralization*. A lot of different organisms like bacteria are a part of the process (Ernstsen, 2014). In microbiology the two reactions *nitrification* and *denitrification* are the overall most important processes in the nitrogen cycle (Appelo and Postma, 2005).

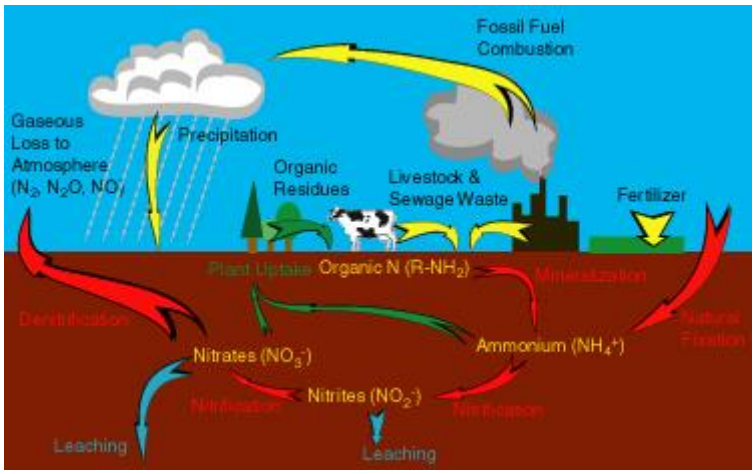

Figure 3.1: The nitrogen cycle. Red arrows illustrate the processes where microorganisms transform the nitrogen. Yellow arrows illustrate human sources of nitrogen. Blue arrows illustrate physical forces acting on nitrogen and the green arrows illustrate the natural processes that do not include microorganisms. (Harrison, 2016).

The nitrogen can be reduced to ammonium (NH_4^+) which by nitrification can be transformed into nitrite (NO_2^-) and nitrate (NO_3^-). Nitrification affects the nitrogen mobility in soils, since ammonium ions are positive charged and therefore, retained in the soil by cation exchange whereas the nitrate

ion is negatively charged and therefore may be leached (Borggaard and Elberling, 2013). Plants can only absorb inorganic nitrogen, which is highly affected by the mineralization that transforms the organic nitrogen to available inorganic nitrogen for the plants. Nitrate is an anion which means that it normally does not go together with the soils organic particles or mineral particles. Therefore, the nitrate can be found in the soil water and is moving with the water to the groundwater aquifers, lakes or streams (Borggaard and Elberling, 2013). In order to ensure an optimum profit of the crops, many farmers supply their fields with inorganic nitrogen in the fertilizer and if the plants do not manage to take up the nitrate, the nitrate will be transported with the water into streams and groundwater aquifers (Erstsen, 2014).

Denitrification describes the microbial reduction of nitrate to N_2 or N_2O. This process can only occur under anaerobic conditions (Borggaard and Elberling, 2013).

3.2 Nitrate reduction

Nitrate in the groundwater can only be effectively removed by the process denitrification (Postma et al, 1991). Denitrification involves different processes where microorganisms, by reduction of organic material, pyrite or other electron donors, reduce nitrate (NO_3^-) to nitrogen (N_2). Denitrification can be explained by the following equation:

$$NO_3^- \rightarrow NO_2^- \rightarrow NO \rightarrow N_2O \rightarrow N_2 \qquad \text{(Eq. 1)}$$

Denitrification requires the presence of microorganisms, nitrate, a type of electron donors and anoxic conditions. In addition, the denitrification is affected directly by the temperature of the soil and pH and indirectly by the soil, crops and cultivation factors at the different fields (Breuning-Madsen and Krogh, 2005). Denitrification is most effective at a pH ranging from 5 to 8 and a temperature around 8 $°C$ (Breuning-Madsen and Krogh, 2005).

In the following denitrification with organic material, pyrite and iron will be described.

The most common denitrification is with organic material as electron donor, which can be described by eq. 2(Appelo and Postma, 2005). The nitrate is reduced to nitrogen and the organic material is reduced to bicarbonate (assuming a pH around 6), carbon acid and water, which in total will give an increase in alkalinity.

$$5(CH_2O) + 4\,NO_3^- \rightarrow 4\,HCO_3^- + 2\,N_2 + H_2CO_3 + 2\,H2O \quad \text{(Eq. 2)}$$

Denitrification with pyrite (FeS_2) as an electron donor can be described with eq. 3, where nitrate is reduced to nitrogen while sulfate and Fe2+ is formed (Appelo and Postma, 2005):

$$5\,FeS_2 + 14\,NO_3^- + 4\,H^+ \rightarrow 7\,N_2 + 10\,SO_4^{2-} + 5\,Fe^{2+} + 2\,H_2O \quad \text{(Eq. 3)}$$

Denitrification can also take place with iron 2 as the electron donor which can be described with eq. 4 (Appelo and Postma, 2005):

$$10\,Fe^{2+} + 2NO_3^- + 14\,H_2O \rightarrow 10\,FeOOH + N_2 + 18\,H^+ \quad \text{(Eq. 4)}$$

3.3 Berner's (1981) classification of redox environments

The ongoing redox processes are often used to characterize the Redox environments and the water chemistry in the soil. When taking organic matter as the driving reductant, the water chemistry may change in depth as seen in figure 3.2. Berner(1981) classified the redox environment between oxic and anoxic environments by the present of oxygen concentration (figure 3.2) (Appelo and Postma, 2005). Figure 3.2 shows which type of electron acceptor that is preferred in the different depths. In the oxygen rich environment, the oxygen is reduced. In the anoxic environment, the nitrate is first reduced due to denitrification and then Fe-oxides are reduced which leads to an increase in the Fe2+ concentration, which can be described by eq. 5 (Appelo and Postma, 2005).

$$CH_2O + FeOOH + 7H \rightarrow 4Fe^{2+} + HCO_3^- + 6H_2O \quad \text{(Eq. 5)}$$

Then the sulfate is reduced. Sulfate reduction causes the sulfide concentration to increase and the Fe2+ concentration to decrease due to precipitation of iron sulfides. This is followed by an increase in the methane concentration (figure 3.2) (Appelo and Postma, 2005).

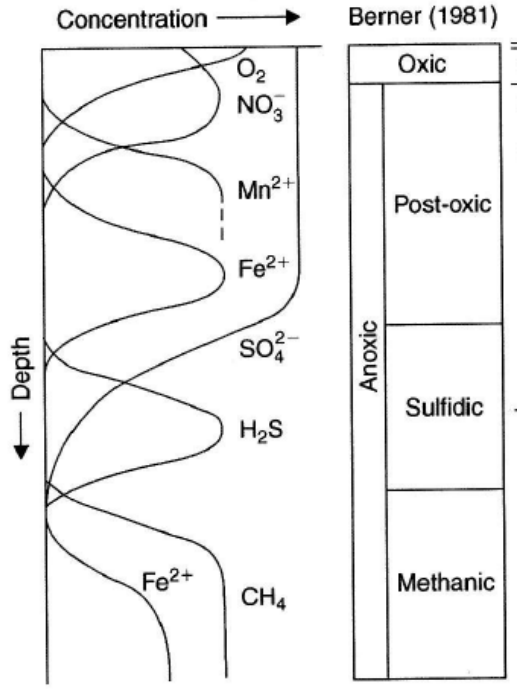

Figure 3.2: The sequential of reduction processes in groundwater chemistry (left) and Berner's (1981) classification schema of redox environments (right) (Appelo and Postma, 2005 p. 440).

Oxidation of pyrite can also occur with oxygen as electron donor. This can be explained by eq. 6 (Appelo and Postma, 2005):

$$4FeS_2 + 15O2 + 14H_2O \Rightarrow 4(OH)_3 + 16H^+ + 8SO_4^{2-} \quad \text{(Eq. 6)}$$

Reduction of sulfate can happen by organic matter, here represented as CH_2O, both with or without the presence of Fe-oxide (Eq. 7 and 8). Without the presence of Fe-oxide, the sulfate reduction leads to hydrogen sulfide formation (Appelo and Postma, 2005):

$$4CH_2O + 2FeOOH + 2H^+ + 2SO_4^{2-} \Rightarrow Fe^{2+} + FeS_2 + 4HCO_3^- + 4H_2O \quad \text{(Eq. 7)}$$

$$2CH_2O + SO_4^{2-} \Rightarrow 2HCO_3^- + H_2S \quad \text{(Eq. 8)}$$

3.4 3D groundwater flow

The following 3D equation explains how the groundwater flow can be calculated. The equation in 3D is deduced from the general equation for groundwater flow in 1D, which is found using Darcy's law and the principle of continuity. The 3D flow equation in this study assumes steady state groundwater flow conditions, which means that there is no change in hydraulic head over time (Fitts, 2013):

$$\frac{\partial}{\partial x}\left(K_x \frac{\partial h}{\partial x}\right) + \frac{\partial}{\partial y}\left(K_y \frac{\partial h}{\partial y}\right) + \frac{\partial}{\partial z}\left(K_z \frac{\partial h}{\partial z}\right) - Q + R = 0 \qquad \text{(Eq. 9)}$$

Where:

x, y and z: point in the x, y or z direction [m]

Kx/y/z: the hydraulic conductivity in the x, y and z direction [m/day]

∂h: change in the hydraulic head [m]

t: Time [days]

R: Recharge [m/day]

Q: Discharge to stream [m^3/day]

The change in the hydraulic head is zero because the model is in a steady state and not time dependent.

3.5 Conductance

Darcy's law can be used to describe the leakage between two water reservoirs. The layer that separates the stream from the groundwater has a conductance that is controlling for the leakage. To determine the size of the conductance the leakage parameter is determined by the following method. The equation for the specific Darcy flux is the first step (Fitts, 2013).

$$q = -K_m \frac{H-h}{D} = p'(H-h) \qquad \text{(Eq.10)}$$

Where

q: The specific discharge [m/s]

K_m: The vertical hydraulic conductivity in the layer which divide the stream and groundwater [m/day]

H: The hydraulic head in the upper stream [m]

h: The hydraulic head in the groundwater [m]

D: The thickness of the layer [m]

p': The leakage factor ($\frac{-K_m}{D}$) [*day/1*]

Which result in:

$p' * A * (H-h) = Q$

It is known that:

$p' * A = cond$

Which result in:

$Cond\ (H-h) = Q = -K_m * A * \frac{H-h}{D}$

The conductance can then be expressed as:

$$Cond = \frac{-K_m * A}{D} \quad \text{(Eq.11)}$$

Where

Cond: The conductance [m^2/day]

Q: The flow between the streams and the groundwater aquifer [m^3/day]

A: The streambed area [m^2]

$\frac{-K_m}{D}$: *The leakage factor (p') [day/1]*

3.6 Solute transport

Transport of different chemical components in a groundwater system occurs in two ways but is also affected by the chemical processes in the environment. The two transport ways are advection and diffusion. Advection can be a rather fast form of transport and diffusion is often a much slower form of transport and therefore often not as evident as the advection, but this depends on the geology (Pepper et al., 2006). Dispersion is also an important factor caused by advection, which affects the groundwater flow (Fetter, 1999).

Advection can be described with eq.12, which is used to describe the transport of a particle by the water flow. This means that the transport velocity is dependent on the groundwater velocity (Fitts, 2013).

$$F_{ax} = q_x * c = (-K_x * \frac{\Delta h}{\Delta x}) * c = \overline{V_x} * n_e * c \quad \text{(eq. 12)}$$

Where:

F_{ax}: advection flux of a solute in the x-direction [minimoles/day/m2]

c: the solute concentration [mM]

q_x: The specific discharge [m/dag]

$-K_x$: The hydraulic conductivity [m/day]

$\frac{\Delta h}{\Delta x}$: The hydraulic gradient [-]

$\overline{V_x}$: Average linear velocity [m/dag]

n_e: The effective porosity [-]

Diffusion, also called molecular diffusion, can be described with the following equation 13. Diffusion is a spread of contamination due to molecular motions and is not dependent on the water-movement, but on the concentration rate and the geology (Pepper et al., 2006).

$$F_{dx}=-n*T_x*D*\frac{\Delta c}{\Delta x} \quad \text{(eq. 13)}$$

Where:

F_{dx}: Diffusion mass flux for a solute in a saturated porous medium [minimoles/day/m^2]

n: porosity [-]

T_x: Tortuosity [-]

D: molecular diffusion coefficient [$m^{2/}$day]

$\frac{\Delta c}{\Delta x}$: Concentration gradient [minimoles/l/m]

The transport equations are solved for the different chemical components in the 2D PHAST models.

4. Methods

This section describes the different methods used for collecting data in the field, lab work and groundwater modeling in GMS, PHREEQC and PHAST.
The data collected for this project and for further use in the TReNDS project is collected in November 2015, February 2016, March 2016 and September 2016. In the following, the different methods will be explained.

4.1 Wells

In EVI2, 7 wells was already installed from previous work and eleven new wells have been installed during this project (figure 2.3). In November 2015, TH1 and TH2 were installed in 16 meters below surface (m.b.s.) and 12 m.b.s. at the bufferzone close to the stream (figure 2.3). In the middle of the agricultural field, TH3 (2 m.b.s) and TH4 (3 m.b.s.) were installed. TH4 was installed in a deeper depth because the well did not give any water in 2 m.b.s. The wells were installed as a transect, located across the EVI2 field site. This was done in order to investigate the groundwater flow system and the nitrate transport and removal in the area.

In March 2016, four new wells were installed. TH6s (2 m.b.s.) is located only 2 meters from the stream. TH1.2 (5 m.b.s.) and TH2.1 (5 m.b.s.) are located close to TH1 and TH2 in order to get more samples due to the results from February. TH3 and TH4 were hammered deeper down to 6 and 8 m.b.s. TH5(10 m.b.s.) was installed in the edge of the agricultural field, at the beginning of the northern shoulder. This was done in order to investigate this part of the study area and maybe get a boundary condition for the hydrogeological model. This well did not give any water.

In September 2016, three new wells were installed at the agricultural field close to the former location of the well TH3 was removed in March 2016 due to sowing of the agricultural field. This was done in order to investigate a snapshot of the groundwater chemistry in the summer season at the agricultural field and especially the nitrate content. TH3.2, TH3-U (upstream) and TH3-D (downstream) was installed. TH3.2 was installed in 3 m.b.s. and water samples were taken every half meter from the top 1-2 meter and then in 3 m.b.s. This depth was chosen in order to make a Push-pull test of the denitrification rate (appendix 18). It was only possible to install TH3-U in 2 m.b.s. due to

a broken thread. TH3-D was installed in 4 m.b.s. and water samples were taken every half meter from 1-2 meter and then every meter.

4.2 Hydraulic conductivity - Slugtest

The hydraulic conductivity was investigated in the area and found by slugtests. Slugtests were conducted in TH6-S (2m.b.s.), TH2.2 (5m.b.s.), TH2 (2, 6 and 10 m.b.s.), TH1.2 (5 m.b.s.), TH1 (2, 5 and 8 m.b.s.), TH3 (2 and 6 m.b.s.) and TH4 (3 and 8 m.b.s.). Each slugtest are repeated three times, in order to reduce the uncertainty and find the most reliably hydraulic conductivity.

The slugtests are performed by installing a pressure transducer in the well above the filter and below the static water level. Afterwards, the well is filled with water and the pressure transducer records the height of the water column in the well until the water falls to the static water level. The data is then analyzed in the software AQTESOLV by the use of the Hvorslev (1951) solution for an unconfined aquifer (Fitts, 2002).

4.3 Geology

In order to examine the geology in the study area, the geophysical method Multi Elektrode Profilering (MEP) is used. In addition, data from a Geoscene model of Holtum catchment developed by Enemark (2015), is used to make a conceptual model of the geology at EVI2.

4.3.1 Jupiter boreholes

Jupiter is GEUS's database of geological and hydrological data. The database contains groundwater, drinking water, raw materials, environmental and geotechnical data (GEUS, 2016). For this thesis, data from two different Jupiter boreholes located close to EVI2 are used to investigate the geology in the area. In the eastern part of the agricultural field at EVI2, the closest Jupiter borehole is found called 96.1026 and 1 km in the southern direction, the Jupiter borehole 96.2187 is located (GEUS, 2016).

4.3.2 Geophysics - Multi Elektrode Profilering

Three different MEP profile lines are made at EVI2, the location is seen in figure 4.1. The three profiles represent the geology at the following locations:

Profile 1: Along the stream at the bufferzone (west -east)

Profile 2: Across the agricultural field (south – north)

Profile 3: Along the northern shoulder at the agricultural field (west-east)

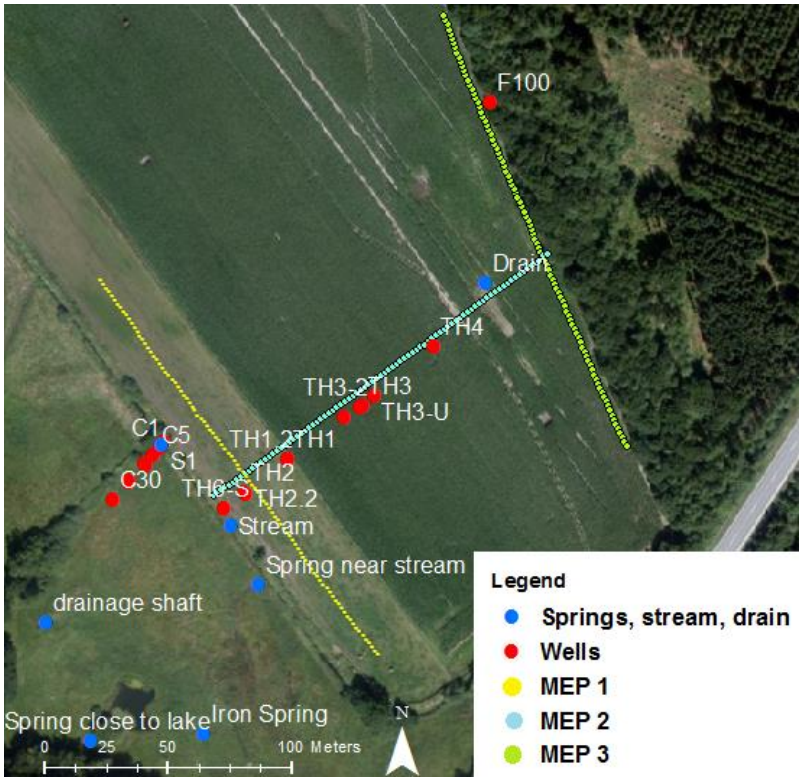

Figure 4.1: Location of the MEP profiles at EVI2.

The MEP analyze is performed by a one kilometer long cable that is connected to the ground by iron sticks. The resistivity is measured between the iron sticks, which is done by a mathematical program that simulates the observed flow and voltage between the connected sticks indicating the electrical resistance / conductivity in the materials 30 meters into the ground, which is the resistivity (Fitts, 2013).

The measured MEP lines are analyzed in the program RES2DINV by log interpolation and by importing the topography. First, incorrect measurements are deleted that differ much from the rest of the line. However, the line is not changed more than 10 percent. Then the starting value for the resistivity is selected.

The produced MEP lines are used to analyze the different layers and material in the underground. The different materials resistivity used for the analysis are illustrated in figure 4.2.

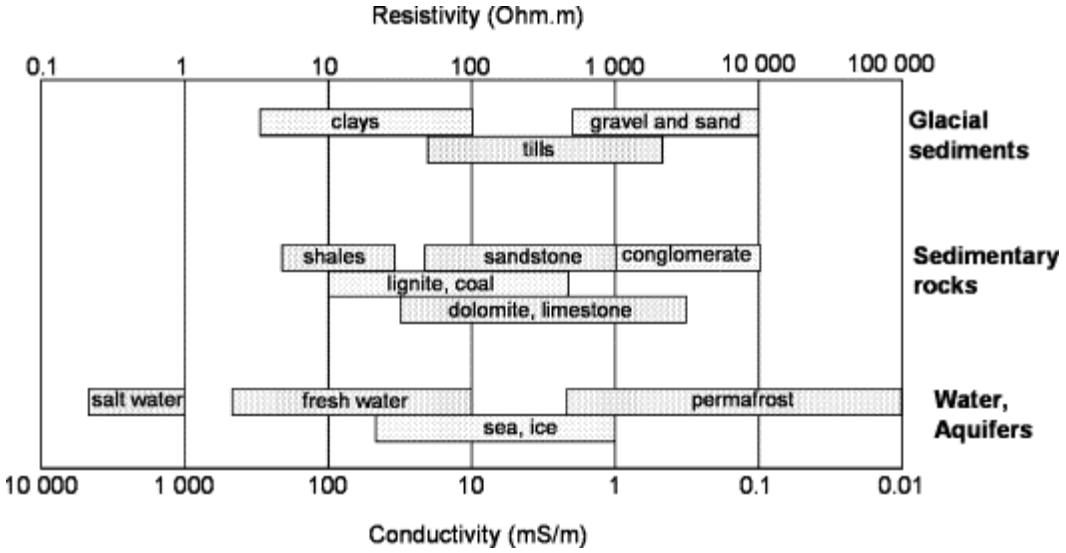

Figure 4.2: Resistivity values for different materials (Skov og Naturstyrelsen, 1987)

4.3.3 Geoscene

An already existing Geoscene model based on Jupiter boreholes data from Holtum catchment is used to create a conceptual description of the geology at EVI2. The Geoscene model is created by Enemark (2015), and is used to define the geology layers in a 3D GMS model, which will be described later. The model contains eight geological layers and the materials in the different layers are interpolated from Jupiter boreholes by kriging to a net of 50x50 m (Enemark, 2015).

4.4 Isotopes

Stable isotopes are used for characterizing and tracing of the water in the study area. The two elements that water consists of (H_2O) have different isotopes. For oxygen, two of the stable isotopes are called ^{16}O and ^{18}O. When the water evaporates the water goes from liquid to gas phase. Some of the molecules in the water have lower diffusivity than others, which means that it is more difficult for them to evaporate meaning that they have a larger tendency to stay in liquid phase. ^{16}O is a light isotope while ^{18}O is a heavy isotope (Fitts, 2013).

With the purpose of comparing the degree of fractionation for the groundwater at EVI2, the notation $\delta^{18}O$ is used. $\delta^{18}O$ is defined as the following equation 14, using a deviation from the isotopic ratio in the common isotopic standard for oxygen which is called Vienna Standard Mean Ocean Water (VSMOW) (Fitts, 2013):

$$\delta^{18}O = \frac{(^{18}O/^{16}O)_{sample} - (^{18}O/^{16}O)_{standard})}{(^{18}O/^{16}O)_{standard}} * 1000 \quad \text{(Eq. 14)}$$

Where:

$\delta^{18}O$: The deviation of the $^{18}O/^{16}O$ isotope ratio (parts per thousand)

Sample: The sample fraction

Standard: The VSMOW level

The $\delta^{18}O$ depends on the surface temperature where evaporation occur and of the distance from where the water was exposed to evaporation. This means that the $\delta^{18}O$ depends on the season. Due to seasonal change in precipitation and by that recharge, the levels of $\delta^{18}O$ vary. This means that the groundwater $\delta^{18}O$ levels are equal to the average annual precipitation $\delta^{18}O$ level. Because of that, it can be assumed that water samples with a $\delta^{18}O$ level equal to the bulk precipitation can be groundwater and if the water in the sample is different than the bulk precipitation level, it can be assumed to be water that is mixed with surface water and/or affected by evaporation. The bulk precipitation average of $\delta^{18}O$ for the catchment is measured to $\delta^{18}O$ = -7.84 δ‰ (Müller, S. unpublished).

The influence of the infiltration through the soil is illustrated in figure 4.3 from Clark and Fritz (1997). It is seen that the seasonal variation in the signal gets lost during the infiltration as a function of the physical characteristics of the unsaturated zone, the flow path length and the residence time and equals the bulk average of $\delta^{18}O$ with the depth (Clark and Fritz, 1997).

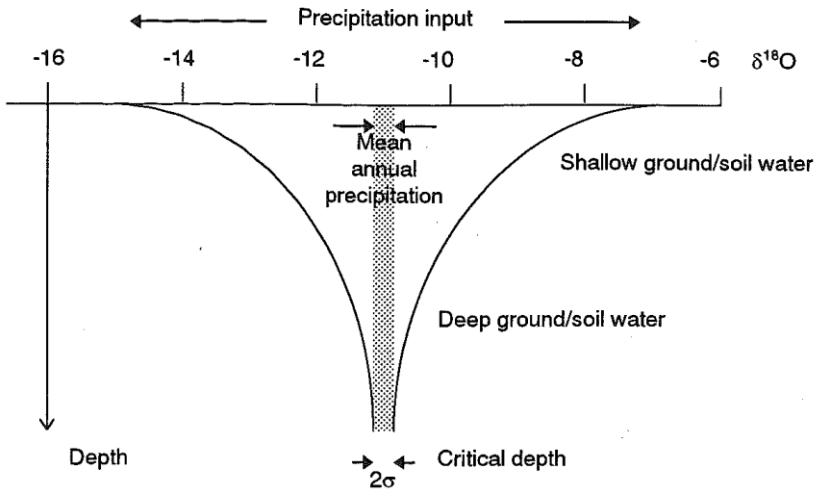

Figure 4.3: Attenuation of seasonal isotope variations in $\delta^{18}O$ in recharge water during infiltration (Clark and Fritz, 1997).

The isotope $\delta^{18}O$ and δD was measured from water samples taken at EVI2. δD corresponds to $\delta^{18}O$ just for hydrogen instead of oxygen and is calculated from the isotopes ^{1}H and ^{2}H (deuterium, D). The isotope analyzes was conducted at a laboratory at GEUS in a Picarro and the δ‰ result is given relative to the VSMOW.

4.5 Water samples

Water samples were collected at EVI2 from the springs at the wetland area, the stream, the drain and from the wells, in order to investigate the groundwater quality (figure 2.3).
When taking water samples from the wells, the wells were first clean pumped, in order to make sure that the water were fresh and that the well were not broken. The water was pumped into a flow cell were the oxygen, pH and EC were measured directly in the field. When the values for the three parameters were stable, samples were taken by use of a 60 ml and a 10 ml syringe. The syringes were filled with water from the well at least three times before the sample was taken. This was done to minimize the impact of the groundwater sample.

In order to keep the samples anoxic, a vacuum was applied by the use of a 60 ml syringe and two three-way valves. This vacuum was used to conserve the water with 0.2 µm filters before putting the water into different containers depending on the different analysis to be performed. This was done in order to make the samples less contaminated by the surroundings. Samples for anions and stable isotopes were stored frozen.

0.1 ml reagent ferrozin to 3 ml groundwater was added to the samples for Fe2+ and 0.3 ml zinkaccetat to 3 ml groundwater had been added to the H_2S samples in order to preserve the water samples.
Samples for cations were acidified at the fieldtrips in the winter season by adding 2vol% 7M HNO3‡ before storing the samples. It was found that this acid was too strong and therefore, the procedure was changed to acidify by only adding 1vol% 1M HNO3‡ to the cations samples conducted in August.

4.6 Chemical analyses of the groundwater

In the following, the different chemical analysis used to analyze the groundwater chemistry is described. All chemical analyses were conducted at the laboratory except for analysis of pH, O_2 and EC which were conducted directly in the field. The stable isotopes were analyzed at GEUS and the rest of the analysis was done in the laboratory at KU.

4.6.1 pH, O_2 and EC

pH, O_2 and EC were measured in the field. This was done by using a flow cell where the pumped-up groundwater is passed through three closed cells (figure 4.4). In the first cell, the O_2 was measured because this parameter is higher affected by the surroundings than the two others. O_2 was measured with a WTW oxi 3310 IDS Portable Dissolved Oxygen Meter. pH was measured with an IntelliCALTM PHC101 Standard Gel Filled pH Electrode probe in the next cell. In the last cell, the EC was measured with an IntelliCALTM CDC401 Standard Conductivity probe. The O_2 and pH probes were connected to an HQ40d Portable Multi-Parameter Meter. All the probes were calibrated before use.

Figure 4.4: The flow cell and the pump. In the flow cell the different probes are installed. These probes are used to measure the oxygen, pH and EC in the water that is pumped up from the well.

4.6.2 Fe^{2+} and H_2S

The Fe^{2+} and H_2S concentrations in the samples were found by using a spectrophotometer.
0.1 ml Natrium-accetat buffer was added to the Fe^{2+} samples and afterwards the Fe^{2+} concentration was measured in the spectrophotometer (Stookey, 1970). The spectrophotometer measures the absorbance by a wavelength at 560 nm. If the absorbance is above 1.5 the sample has to be diluted with milliQ water.
The H_2S concentrations were found by the same method with a spectrophotometer (Cline, 1969). This was done by adding 300-microliter reagent A for hydrogen sulfide analysis. For H_2S, the absorbance was measured at a wavelength at 666 nm and the samples have to be diluted with milliQ water if the absorbance is above 1.385.

For both analyses, the absorbance is used to calculate the different concentrations by the use of the equation of the standard curve. A blank sample was made for both analyses consisting of the spectrophotometric reagent and milliQ water. For both analyses, the sample containers were weighted before and after the samples were taken and then corrected to match exactly 3 ml sample. In addition, the values were converted to mg/L by using the conversion factor found by the standard curve. The conversion factor was 1.39 for H_2S and 2.22 for Fe^{2+}.

4.6.3 Alkalinity

The alkalinity was measured by the use of GRAN titration using a standardized HCL 0.1 M solution. Alkalinity is a measure for the acid neutralizing capacity of a groundwater sample. This is strongly related to the amount of bicarbonate because bicarbonate at pH 5-7 represents the majority of the substances that can neutralize acid (Borggaard and Elberling, 2013). In practice, this means that the amount of dissociated carbonic acid is determined in a groundwater solution.
The principle of GRAN titration is to monitor the H+ increase with volume tirant, past the equivalent point and afterwards extrapolate backwards to the equivalent point. (Appelo and Postma, 2005, and Gieskes and Rogers 1973).

The HCl was titrated into the samples to lower the pH down to 2.5 or slightly below and the change in pH was noticed down. Afterwards the GRAN function F is calculated:

$$F = (v + V_0) * 10^{-pH} \quad \text{(Eq. 15)}$$

Where:
F: The GRAN function
V_0: The original sample volume
V: The added volume of acid

A plot of F vs. ml acid added was then done in an already existing EXCEL file and a linear relationship was showed past the equivalent point. This was used to extrapolate to F=0 and gives the ml of acid corresponding to the equivalent point (Appelo and Postma, 2005 and Gieskes and Rogers 1973).
The acid that was used for the titration of the samples taken in February and March 2016 was not strong enough. Therefore are all the alkalinity measurements from the winter season multiplied with 0.1.

4.6.4 Cations and anions

The major anions (chloride, flouride, sulfate, phosphate, bromide, nitrate and nitrite) and the major cations (sodium, potassium, calcium, ammonium and magnesium) are measured. Both cations and anions were analyzed by the use of ion chromatography. Different eluents were used for the cations and anions. For cations 1,7 mM HNO_3 + 0,7 mM, dipicolonic acid was used and for measuring the anions the eluent 3,2 mM Na_2CO_3 + 1,0 mM $NaHCO_3$ was used.

The analysis of the anions and cations using chromatography, works in the way that the sample passes through a stationary phase through a column in which the sample is flushed through the system by a mobile phase which is the eluent. The column works like that the sample is retained in the column in which it is dissolved. Depending on the resistivity, it is released through some of the sample. For every time a substance leaves the column, it is analyzed by a detector, which gives a peak in a chromatogram. When the entire sample has passed the column, the total chemistry is found.
All anion and cation concentrations are recalculated from mg/L to mM. The samples from February and March are multiplied with 1.02 because it was acid conserved with 2% acid in the field. The samples from September are multiplied with 1.01 because it was acid conserved with 1% acid.

4.6.5 Sources of error

In the following, some of the sources of error regarding chemistry sampling will be explained. A lot of different sources of error can happen which gives some uncertainty that can affect the results. In the field sources of error can occur if the wells are not cleanly pumped enough before taking samples or if it is not the right conservation or if it is not the right concentration that is added to the conservation.

By taking the alkalinity samples, problems of $CaCO_3$ precipitation do to CO_2 degassing or precipitation of iron oxyhydroxides ect. can occur if the samples are not fully filled with groundwater. Because of that, the alkalinity containers should be fully filled with water and the alkalinity determinations should be conducted as quickly as possible. Additionally, it is important to freeze the samples of anions just after the samples are taken. In the lab. it is also important to be very precise with the pipettes and with for example in GRAN titration so as to not put too much acid into the sample at one time.

In order to make sure that the samples are reliable and the results can be trusted, the electrical balance for every sample is measured. The electrical balance is between +/-5. This means that the samples are acceptable (Jessen et al, 2016) (appendix 2)

4.7 Pyrite extraction

In order to investigate if pyrite is present in the soil at EVI2 some measurements were conducted. The conduction was done by installing a metal pipe at 1 m with a plastic pipe inside and a metal ring at the end, preventing the soil to get out of the plastic pipe. The core was taken up for every one meter and a new plastic pipe was installed in the core. This means that the top of every soil core can be contaminated by soil from the upper meters.

At one location, close to EVI2 soil cores were taken for the first 2 m.b.s. At the third m.b.s. the plastic pipe was stuck in the core and impossible to get out. This means that the soil sample from 2-3 meter is a mixture. The equipment failure means that it was not possible to get any more core samples, despite that it would have been preferred to have core samples down to 5 m.b.s. at two different locations at the agricultural field. The soil cores were stored at freezing temperature and analyzed in the lab. This was done taking samples of the soil core from every 10 cm and freeze-dry the samples. In total, the soil cores were only half a meter each because the soil was getting compact. Afterwards,

the samples were ready for distillations for silver sulfide. Some of the samples were crushed before the experiment.

The pyrite extraction was done by use of distillation for silver sulfide. In practice, the idea with the experiment is that the content of pyrite are found by capturing the degassed sulfur from a sample in a “trap” with water and silver nitrate as Ag2S (figure 4.5). The sulfur degasses by adding acid and chromium. 2 g sample was weighted and put into a reaction flask with 10 ml 50% ethanol. Then the trap was created consisting of 0.5 ml 1M silver nitrate ($AgNO_3$) and 10 ml water. The reaction flask was then mounted on the distillation unit with N_2 bubbling into the liquid. This was done in order to keep the experiment under anoxic conditions. The N_2 was bubbling to degas for 10 min. After the degassing, 6M HCl was slowly added and then 16 ml of reduced chromium. Then the experiment was left for boiling in approximately 60 min. Afterwards, the traps was filtered through pre weighted filters and dried for one day before weighting again. The weight of the Ag2S that was captured in the trap was then converted into mol S and % FeS2 and mM FeS2 of the 2 g sample can then be found. The Ag2S can also be other forms of sulfate, but in this experiment it is assumed that all the Ag2S is pyrite (Antivakis, 2012).

Figure 4.5: The setup of the distillation for silver sulfide in the laboratory.

The extracted amount of pyrite was afterwards used to calculate the redox front progression as a function of groundwater nitrate concentration and pyrite contents of the sediment. This was calculated by the following retardation equation (appendix 8) (Appelo and Postma, 2005).

$$V_{FeS_2} = V_{H2O}/R = V_{H2O}/(1 + \frac{\Delta q}{\Delta c}) \quad \text{(Eq. 16)}$$

Where:

V_{FeS_2}: The pyrite front progressing [m/yr]

V_{H2O}: The downward flow velocity [m/yr]

Δq: The change in the electron balance for the electron donors [mmol/L]

Δc: The change in the electron balance of the FeS2 concentrations [mmol/L]

R: The retardation factor

4.8 Groundwater modeling

In this study, groundwater modeling is used to investigate the groundwater flow, the origins of the water, the nitrate reduction and the controlling chemistry processes and distribution of the groundwater chemistry in the study site. The modeling will be structured as the following:

1. 3D MODFLOW of Holtum catchment to understand 2D/3D flow near the study site
2. 1D reactive transport modeling using PHREEQC below field to study geochemical processes in the study site
3. 2D reactive transport using PHAST, with 2D homogeneous/heterogeneous flow and geochemistry for the study site

A 3D MODLOW groundwater model is used to investigate the groundwater flow and the origins of water found in the stream and in the springs at the wetland area at EVI2. The 3D model is a pre-existing model developed by Enemark, 2015 and the conductance for the drain and wetland areas are the only parameters calibrated in this model. The conductances are calibrated against hydraulic head measurements in the catchment.

In order to make quantitative analysis of the groundwater chemistry in the study site the programs PHREEQC and PHAST are used. A 1D PHREEQC model is constructed in order to investigate the

chemical processes in a simple way and calibrated by changing the amount of the different chemical components in order to match the chemical concentrations that were measured in the well TH3.
2D PHAST models are used to investigate both the groundwater flow and the chemical processes at the same time and to better represent 2D groundwater flow and transport effects on geochemical processes. Three different models are constructed and calibrated against hydraulic head observations and the chemical measurements in the wells TH3 and TH4. This is done by changing the location of the different processes in the model, the nitrate content in the agricultural recharge water and for the heterogeneous model by adjusting the geology composition in the model. Two homogeneous models with and without drain included and one heterogeneous model with drain was constructed.

4.8.1 3D Groundwater modeling in MODFLOW

The 3D MODFLOW model used in this study is a modification of an already existing model developed by Enemark, 2015. The model is a modification of the model A in her thesis that was most reliable for the area. The model extent of the previous model is modified to only include Holtum catchment and not the area at the other side of the water divide. The modification is described in the following and it is assumed that the previous calibration done by Enemark, 2015 is acceptable for the new model.
The 3D model for Holtum catchment is based on a predefined spatial discretization of 100 x 100 meters for each cell in X and Y direction while the grid in the Z direction follows the vertical extent of the different geological layers, which is called a layered grid (Sonnenborg and Henriksen, 2005). The model contains eight geological layers and is by Enemark, 2015 developed in a Geoscene model based on Jupiter boreholes as describes earlier. In the area around EVI2, a finer grid size is implemented in the model because the purpose is to investigate the groundwater flow in this specific area. Therefore, the grid size in the model around EVI2 made smaller to 50x50m and specifically for EVI2 the grid size is made even smaller to 25x25m. The grid size of 25x25m for EVI2 was the smallest grid size for this area the model would accept (figure 4.6).

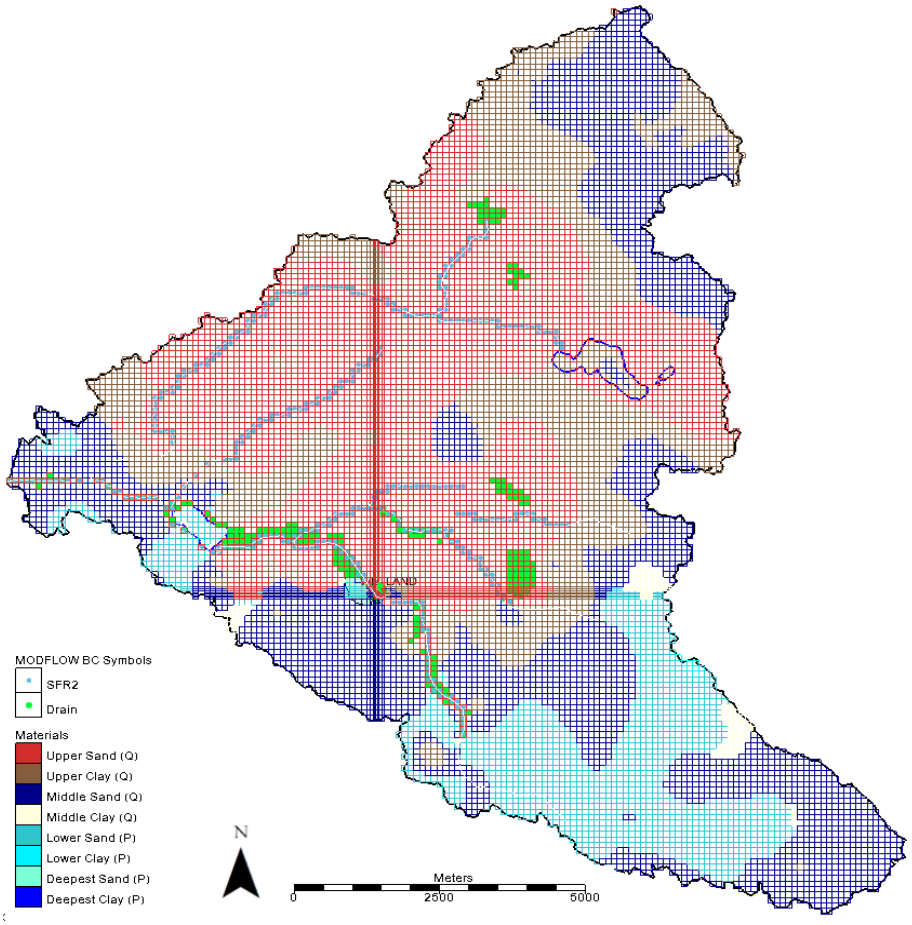

Figure 4.6: Model domain and grid of the 3D model of Holtum catchment, modified after Enemark, 2015.

The measured average of the hydraulic head in the wells at EVI2 is imported to the model and evaluated based on calibration targets as well as the observed heads that was imported to the model by Enemark, 2015. A calibration target is a visual impression on the calibration quality since they represent the relationship between observed and simulated data. A green calibration target represents that the simulated values is closer than +/1 standard deviation. A yellow represents that the simulated value is between +/1 and 2 standard deviations and a red represents that the simulated value is worse than +/2 standard deviations (Aquaveo, 2016). The same standard deviation is used as by Enemark (2015).

Additionally, the lakes are modified from the previous model. They were converted to general heads instead of Lake Package based on the hydraulic head and conductance from Enemark, 2015. Furthermore drain is included in the model. This is done in two ways. For EVI2 the drain (figure 2.3) is installed as drain package in GMS MODFLOW based on the conductance from Petersen, 2016.

To represent the springs at the wetland area the drain package in GMS MODFLOW are used. The same method is used to represent wetland areas along the stream in the catchment based on a map showing flooded areas in the catchment. Figure 4.7 shows an example of some of the areas that are assumed to be wetland in the catchment. This is not the optimal solution because the drain package simply removes the water from the model which removes the surface flow to the stream. The distribution of drain in the model is seen in figure 4.6. The calibrated conductance results for the drains, wetland springs and wetlands along the stream are found in table 4.1. For the wetland area, the conductance was set as high as possible to 0.001 [$(m^2/day)/m^2$]. The steam conductance in the model is 6 m/day (Enemark, 2015).

Table 4.1: The conductance of the drains in the 3D GMS MODFLOW model.

Drain	Conductance of the drains in the MODFLOW model [$(m^2/day)/m^2$]
Drain at the agricultural field	0.05
Springs at wetland side of the stream	0.12
Wetland areas along the stream in the catchment	0.001

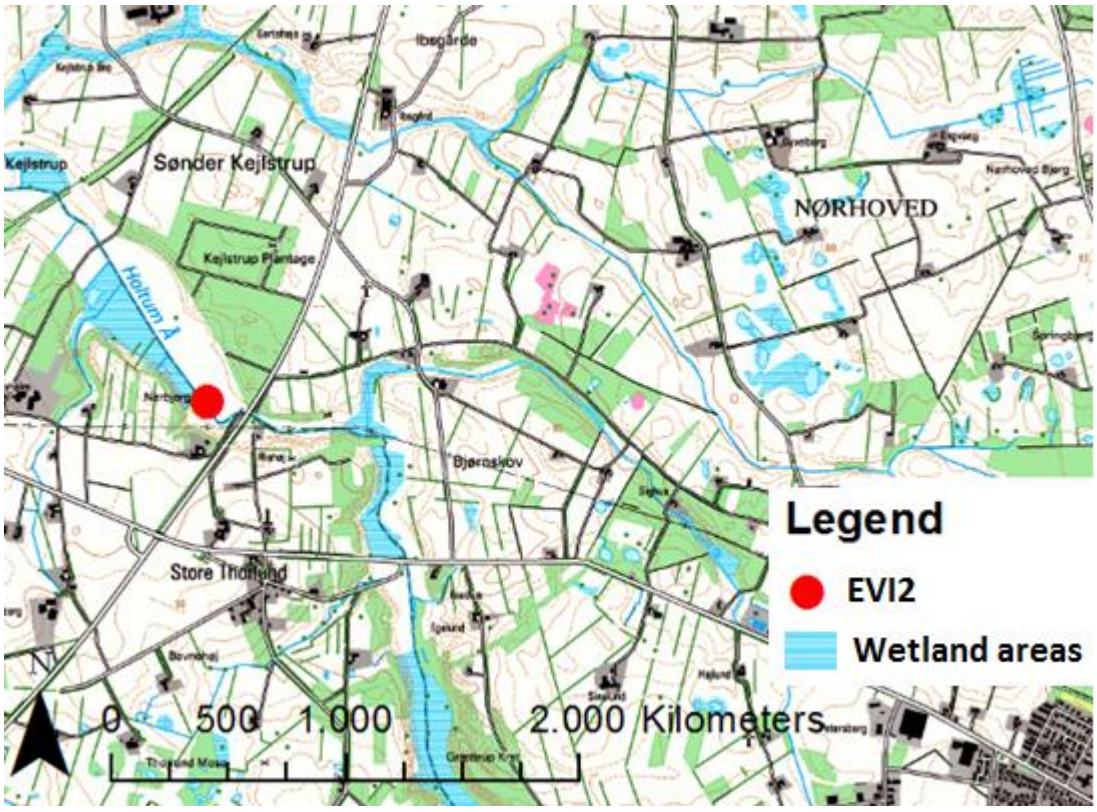

Figure 4.7: The wetlands areas in Holtum catchment

The flow budget is investigated for the entire model with and without drain. For the agricultural field at EVI2, the flow budget is also explored, in order to investigate the water flow in this area. As a statistical measure for the performance of the model, RMSE is calculated. The RMSE is the average numerical residuals between observed and simulated values. This objective function is chosen because it is the most commonly used criteria for a model because it is comparable to the uncertainty of the measurements (Sonnenborg and Henriksen, 2005). The expression is found in the following (Sonnenborg and Henriksen, 2005):

$$RMSE = \sqrt{\frac{\sum_{i=1}^{n} (X_{obs,i} - X_{model,i})^2}{n}} \quad \text{(Eq. 17)}$$

Where:

RMSE: Root Mean squared error [m]

n: Number of observations [-]

Obs: The observed data [m]

Mod: The simulated data[m]

i: time/place

In order to investigate the origins of the water particles in the stream and in the springs at the wetland area at EVI2, particle tracking is used in GMS. GMS is using MODPATH to investigate the flow path by doing backward tracking particles and to analyze the age distribution. The particle pathway simulation is generated by releasing 100 particles that are distributed within cells in the stream and in the wetland at EVI2. The velocity of the particle is defined as the following expression (Sonnenborg & Henriksen 2005):

$$V_i = \frac{q}{n} = \frac{K_i}{n} \frac{\partial h}{\partial x_i} \quad \text{(Eq. 18)}$$

Where:

v_i: velocity of the particle [m/day]
q: the Darcy flux [m/day]
K_i: the hydraulic conductivity [m/day]
dh/dx_i: the gradient [m]
n: the porosity [-]

4.8.2 1D groundwater chemistry modeling in PHREEQC

In order to examine the chemical processes at EVI2, PHREEQC is used. PHREEQC is a program for speciation, batch-reaction, one-dimensional transport, and inverse geochemical calculations (Parkhurst and Appelo, 2013).

To investigate the chemical processes, a speciation is made in PHREEQC based on the chemical observations. To explore if there is dissolution or precipitation going on in the soil, the saturation index for calcite (Si calcite) Si CO2, Si siderite and Si mackinawite are calculated in PHREEQC.

With the aim of investigate the nitrate transport and removal quantitatively a simple 1D model is developed. The model is used to examine whether it can be explained with a relatively simple model what happens chemically in the soil, despite the fact that in reality it is a complicated as well as a wide variety of chemical processes that may take place. This means that the qualitative analysis, which was first made, perhaps can be quantified and in some degree validated in a quantitative way.

In PHREEQC a Solution 0 is defined which is the infiltration solution. The composition of the Solution 0 corresponds to the chemical composition measured in TH3 in 2 m.b.s. but without the small amount of oxygen that was measured. The oxygen is removed in order to make the model as simple as possible. In that way, the model does not simulate the processes from the surface but from the first measurement in 2 m.b.s.

The same composition is chosen as initial values in all the cells. The model cover 10 m.b.s. and 10 cells are therefore defined, with a cell length at 1m. The dispersivity is set to 0.1 m and the diffusion coefficient $0.3e^{-9}$ m^2/s. 20 shifts are used which corresponds to 2 x pore volume. For the time step, it is assumed that the water flows 1 meter every year. The processes defined in the model for the different cells are found in table 4.2. The *Equilibrium_phases* in the PHREEQC model controls if a given phase will dissolve or precipitate to achieve equilibrium (Parkhurst and Appelo, 2013).

The *reaction* in the PHREEQC model means that the defined reaction transfer amounts of the element to or from the solution instantly. This means that the process is not time or solution composition dependent (Parkhurst and Appelo, 2013). The processes follows the results from the qualitative analyzes of the main processes going on in EVI 2 based on chemical measurements from TH3.

Table 4.2: The defined processes in the PHREEQC model. The cells represent meter below surface.

Cell	PHREEQC process
2	- Equilibrium_phases with Goethite
2-3	- Reaction with pyrite
3-10	- Equilibrium_phases Pyrite (in total pyrite can only precipitates) and stable goethite.
4-10	- Reaction with organic material

4.8.3 2D groundwater flow and chemistry modeling in PHAST

In order to investigate the chemical processes and groundwater flow at EVI2, and to better represent 2D groundwater flow and transport effects on geochemical processes, the program PHAST is used to make 2D groundwater flow and solute transport models for the study area.
PHAST is a program for simulating groundwater flow, solute transport, and geochemical reactions which is done by defining different equilibrium and kinetic geochemical reactions (Parkhurst et al, 2010). In PHAST, some numerically equations are solved. These are saturated groundwater flow equation, a set of solute-transport equations, and a set of chemical-reaction equations comprising mass-balance equations, mass-action equations, and kinetic-rate equations (Parkhurst et al, 2010).

Additionally, PHAST is using the same format for the chemistry as PHREEQC, which makes the chemical simulation for the 1D PHREEQC model comparable with the PHAST model in 2D. MATLAB is used to analyze the results and to plot figures from the PHAST 2D models (appendix 12, 13, 14 and 15).

In the following, the constructions of the 2D models are explained. In total three models are developed.
MODEL A: Homogeneous model without drain.
MODEL B: Homogeneous model with drain.
MODEL C: Heterogeneous model with drain.

The drain is excluded for model A in order to explore the drains influence at the chemical concentrations. The model domain, boundary conditions and location of the chemistry processes are the same in all the models.

4.8.3.1 Model domain

The model domain for the 2D PHAST models is a transect across the agricultural field at EVI2. This transect is chosen because the aim with the model is to investigate what happens with the nitrate at the agricultural field. The transect is located from the stream in south to the end of the agricultural field in north at the northern shoulder figure 4.8). This means, that the transect is following the location of MEP profile 2 and includes the different wells located at the transect (figure 4.1).

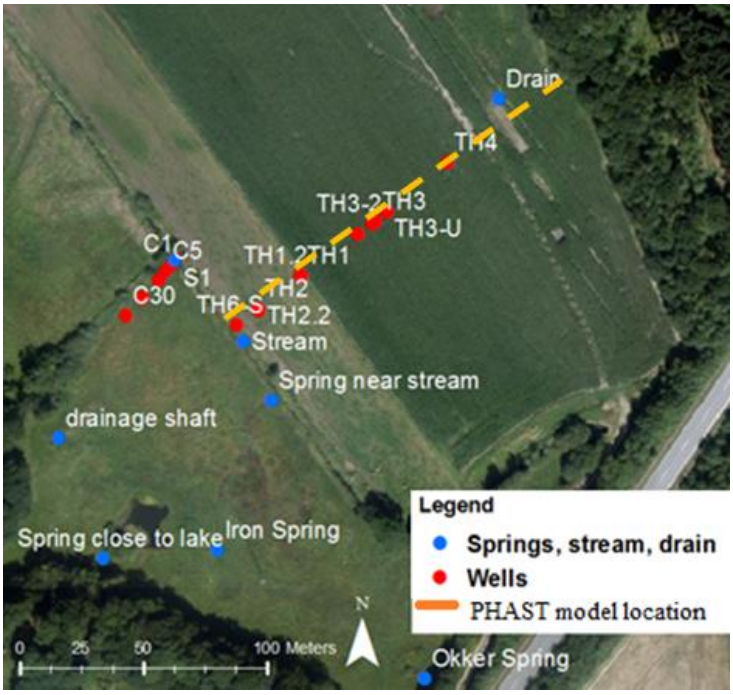

Figure 4.8: The location of the PHAST model at EVI2.

The orientation of the model is chosen based on the assumption that the groundwater is flowing perpendicular to the stream, which can be seen from the hydraulic head measurements (figure 5.1). Therefore, and in order to make the models as simple as possible, the models are developed in 2D in X-Z direction, which neglects the flow in Y direction. The 3D model also tests this assumption.

A fine temporal and spatial grid was used for the 2D PHAST models. The model domain was chosen to 170x21 m in x, z direction. The y direction only includes 1 cell (2 nodes) because it is not possible to totally neglect the y dimension due to computational calculations. The chemical calculations in the model are only made in x-z dimensions.

The model domain was discretized by a uniform regular 88x84 node grid, with a node spacing of Δx = 1.93 m and Δz = 0.25 m. This means that every cell is 1.93 x 0.25 m. The thickness of the model is 21 meter (from 37 to 58 m DVR90). This assumption is based on the assumption about a lower clay

layer in the area (section 5.1.2.3) that "works" as a bottom for the aquifer and the assumption about the groundwater is flowing perpendicular to the stream. At the same time, the aim with the model is to investigate the chemical processes in the upper 10 meter.

The time step is 1 year and the model is run for 10 years in total to make sure that the model is flushed one time. To make sure that the model avoids numerical discretization and that the 1 year time step is small enough, the model was run with a smaller time step and grid size and no differences was found.

The dispersion in the model has a great impact on the solute transport. The longitudinal dispersion was set to 1 m. Based on a study on dispersivity in sandy aquifers, the vertical dispersivity was set to 0.01m. (Frind and Hokkanen,1987). This also follows the general assumption that states the vertical dispersivity to be a factor of 100 less than the longitudinal (Engesgaard, 2003).
The porosity was unknown and a value of 0.3 was chosen, representing sand (Karan et al, 2013). A value of 3 was applied for the anisotropy based on a sensitivity analyze of the anisotropy factor and a further study of the study site Hygild, located further downstream in Holtum catchment (Karan et al, 2013) (appendix 6).

4.8.3.2 Boundary conditions

The recharge in the model is uniformly distributed in the uppermost cells with a rate of 434 mm/year (0.00115 m/day) based on the previously study from Rabis creek and Holtum catchment (Jessen et al., 2016 and Poulsen et al., 2015).

The average measured hydraulic head at the stream is 57.4 m, which is used as a boundary condition. The best estimate for the conductance for the stream bed is found to be 13.3 m^2/day. A sensitivity analysis of the conductance is found in appendix 6. The calculation of the conductance is based on an assumption about the stream bed material is consisting of sand. Assuming an anisotropy at 3 (Karan et al., 2013), gives a hydraulic conductivity at 20/3=6.7m/day. The calculation is found in appendix 5.
A conductance at 13.3 m^2/day seems to be a bit high compared with the previously model created by Petersen (2016) that found a conductance at 7.5 m^2/day for the leakage between the stream and groundwater in the area. In addition, a previous study of the study site EVI1, located further

downstream in the catchment area found a conductance at 0.9 m^2/day (Nørrevang and van't Veen, 2014). Another study that investigated the vertical and horizontal conductance in the streambed at five different test locations in the Holtum catchment area, found that the Kv ranges a lot and by that also the conductance (Sebok et al., 2014). This means that the found conductance can be representative.

There is a drain installed at the northern part of the agricultural field. This drain discharges 34.56 m^3/day (24L/min) and is 117 m long. By taking the assumption that the drain removes the same amount for its length it gives, that 1 m drain removes 0.295 m^3/day. The depth for the drain is 57.7 m and the conductance is 5 m^2/day (Petersen, 2016), which corresponds to a hydraulic conductivity of 25 m/day by isolating the hydraulic conductivity in the equation for the conductance (see appendix 5 for the calculation). In PHAST, the drain is defined by defining the location, thickness (0.1), hydraulic conductivity (25m/day), width (0.2 m) and z (57.7m).

The boundary conditions at the northern edge of the model are a specified head. The specified head is 58 m. based on a previous model for the area (Petersen, 2016) but is in fact unknown because of a not working well (TH5). It is assumed, that the water flowing into the model from this direction is "natural water" that is not affected by agriculture and by that nitrate-pollution.

Table 4.3: The boundary conditions in the 2D PHAST models

Boundary conditions	Fixed hydraulic head (m)
Northern boundary	58
Stream	57.4
Drain	57.7

4.8.3.3 Chemical processes in the model

The chemical processes included in the PHAST models are based on the 1D PHREEQC model and defined at a PHREECQ script (appendix 4). Three different solutions are defined. Each represents different chemical composition. Solution 1: Natural recharge water. Solution 2: agricultural recharge water and Solution 3: Initial natural water without oxygen (appendix 4). Solution 1 is representing the natural recharge water without nitrate-pollution. This solution is used as recharge for the buffer zone and the incoming water at the northern boundary in the model. The solution is based on the measurement in TH3 in 2m.b.s. without nitrate and Fe2. Oxygen corresponding to the atmospheric

pressure is added to the solution because it is impossible to not have oxygen in an infiltration precipitation. Solution 3 is the initial solution for the water in all cells in the model and content is almost the same chemical composition as solution 1, just without added oxygen and with a small amount of sulfate. Solution 2 represents the agricultural recharge water, which means that the water is nitrate-polluted due to fertilizer. This solution is also based on the measured concentrations in TH3 in 2m.b.s. without Fe2 and with added oxygen and nitrate. The nitrate concentration in TH3(2m.b.s.) is already affected by 2 meters transport down though the soil. Therefore, it is assumed that the nitrate concentration in solution 2 must be higher than 1.25 mM. Based on that assumption, the nitrate concentration in Solution 2 is calibrated to match the nitrate concentration in TH3 and TH4 in the model. The locations of the different solutions are seen in figure 4.9.

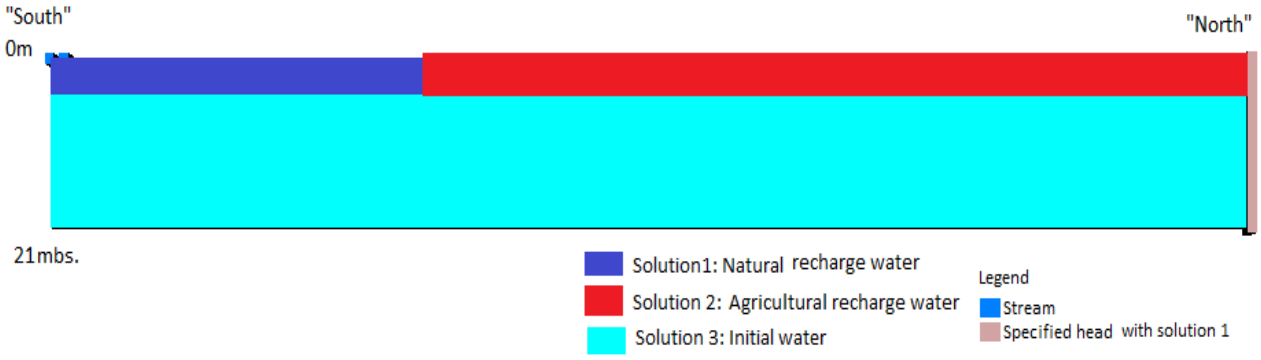

Figure 4.9: The locations of the three defined solutions in the PHAST 2D models. The chemical composition of the different solution is found in appendix 4.

The same processes as defined in the 1D PHREEQC model is also used in PHAST. However, PHAST does not provide the *Reaction* process from PHREEQC. Therefore, the function *Kinetics* is used to define the present of pyrite and organic material in the model. The kinetics of pyrite and organic material are from the database in PHREEQC and the degradation rates are fitted to match the chemical measurement in TH3. This was done in PHREEQC.

For pyrite, the kinetic rate is based on dissolution of pyrite in the presence of dissolved oxygen from Williamson and Rimstidt (1994) (Parkhurst and Appelo, 2013). The kinetic rate is modified by incorporating nitrate in the rate and then fitting parameter 1 and 3 (called parm in the script, appendix 4). This was done because these two parameters control the reaction order with respect to the nitrate and the area available per. liter pore water. The fitting resulted in a 5. order reaction for the pyrite oxidation (appendix 4).

The kinetic rate for organic material is a monod kinetic with means that it is not defined by orders but by the rate constant and concentration. This rate was also fitted to match the chemical measurements in TH3. The fitting was done by adjusting the m and m0 in the expression, which are the moles of reactant and the initial moles of reactant (appendix 4).
Table 4.4 shows the processes defined in different depth in the PHAST models.

Table 4.4: The defined processes in the PHAST model

Meter (z)	**PHAST process**
56-57	- Equilibrium_phases with Goethite
53-55	- Kinetic pyrite
	- Equilibrium_phases Pyrite (in total pyrite can only precipitates) and stable goethite and siderite (in total siderite can only precipitates).
48-54	- Kinetic organic material

4.8.3.4 Hydraulic conductivity distribution

Three different models are as described created in PHAST. Model A and B are homogeneous. A value of 10 m/day was applied for the hydraulic conductivity of the geology, based on the assumption of sandy material and an average hydraulic conductivity measured in the area (section 5.1.3.). Model C is heterogeneous and six different geology types are chosen for this model based on the MEP profile 3 and hydraulic conductivity measurement at EVI 2 in the wells assuming a correlation between the hydraulic conductivity and the resistivity in a material (Karan et al. 2013) (figure 4.10).

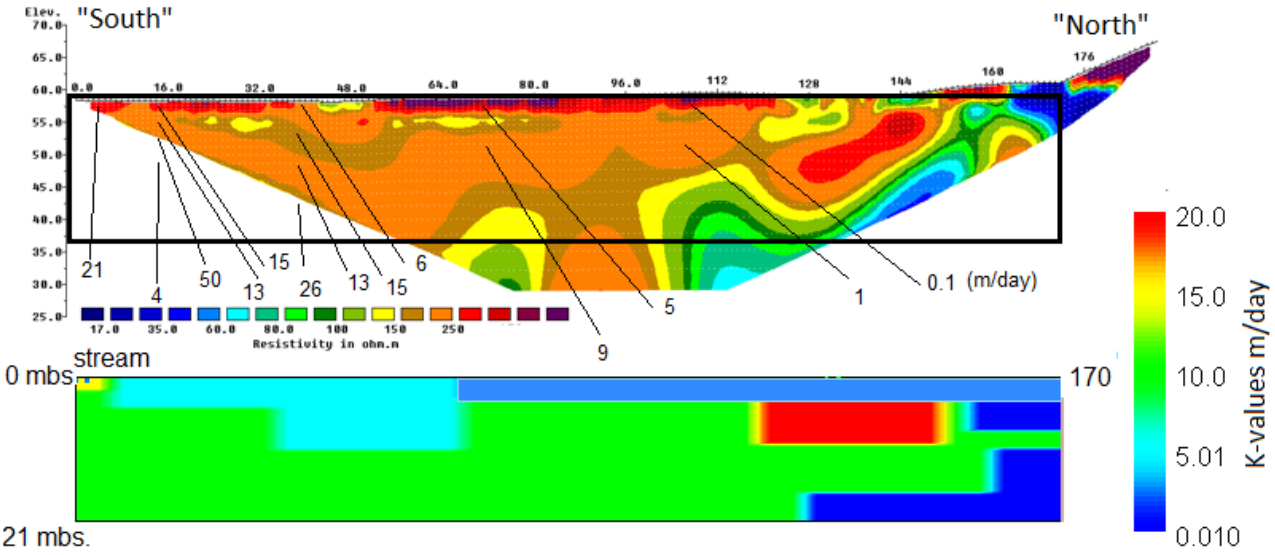

Figure 4.10: The horizontal hydraulic conductivity in the PHAST model C based on the MEP profile 2 and hydraulic conductivity (m/day) measured in the wells and seen at the MEP profile in the figure.

In order to analyze the performance of the different models compared to reality, the average hydraulic head in the cells that corresponds to the locations of the wells placed at the transect in the study area are found by use of MATLAB and plotted against the measured hydraulic head in a 1-1 line. In addition, the RMSE is calculated (appendix 11).

In PHAST, the function *print locations* is used to find the chemical concentrations in the specific cells corresponding to the samples depth for TH3, TH4, TH1 and TH2 which by use of MATLAB is compared to the observed values for every well in different depth.

5. Results and analysis

In the following, the results will be described and analyzed. First the hydrogeology and geology for the area will be analyzed. Second, the different chemical results will be analyzed and third the results from the 3D model will be presented and analyzed followed by the results from the chemical 1D model and 2D groundwater chemical and hydrogeological modeling at local scale.

5.1 Hydrogeology

In the following, the hydrogeology in the study area will be investigated based on field measurements.

5.1.1 Groundwater flow – hydraulic heads

The isopotential map based on the average hydraulic head in the wells located at EVI2, shows a cross section of how the groundwater flows in the study area (figure 5.1). The groundwater flows from both the agricultural side of the stream and the wetland side of the stream toward the stream (figure 5.1). At the same time the isopotential lines illustrates that the groundwater can flow under the agricultural field from further away against the stream (figure 5.1).

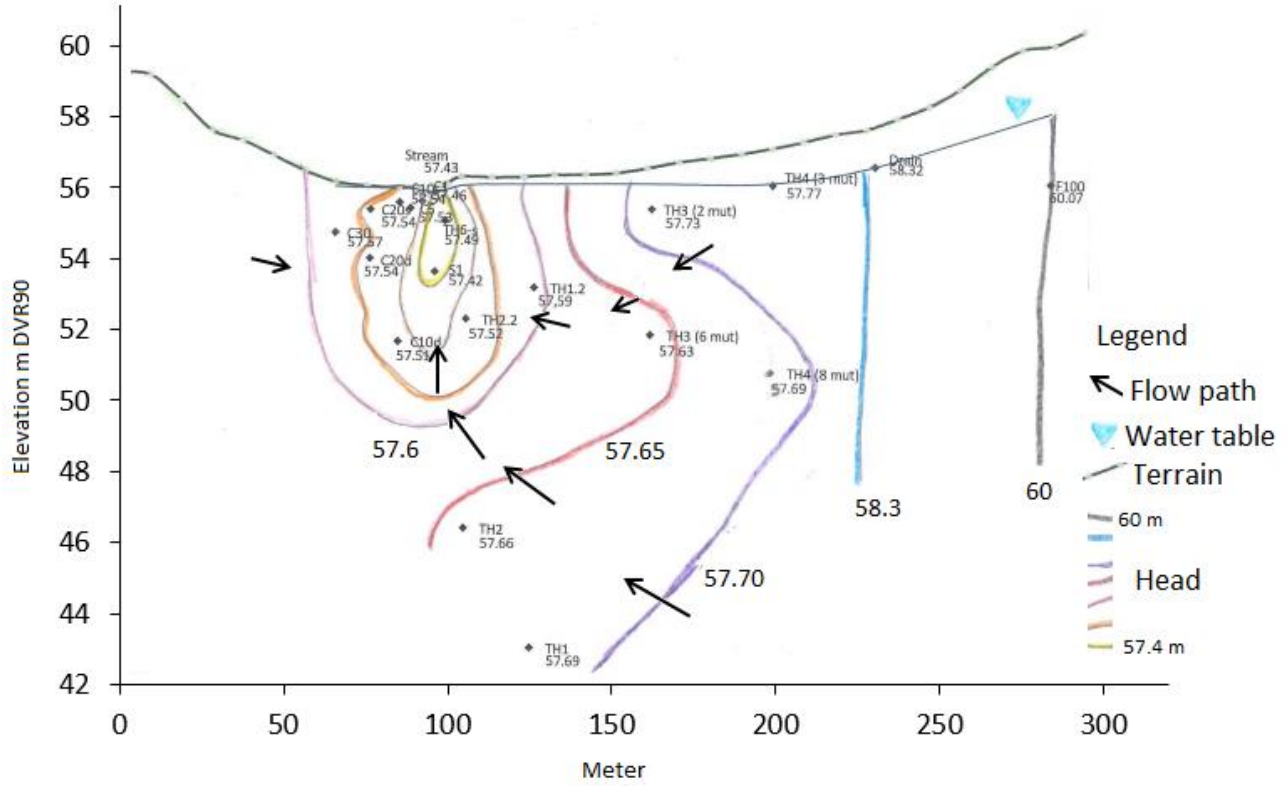

Figure 5.1: Isopotential map of the average hydraulic heads measured in all wells at EVI2

5.1.2 Geology – Jupiter boreholes, MEP and Geoscene

In the following, the geology at EVI2 will be analyzed based on two Jupiter boreholes, three MEP profiles and results from the Geoscene model developed by Enemark (2015).

5.1.2.1 Jupiter boreholes

The Jupiter boreholes located closest to EVI2 are seen in figure 5.2. 96.1026, located in the eastern part of EVI2 and 96.2187, located 1 km south from EVI2. The Jupiter borehole 96.1026 shows that from 0 - 7.6 m.b.s. the geology consist of sand and from 7.6 to 15.2 m.b.s. clay mixed with sand is present followed by clay from 15.2 to 18.3 m.b.s. (figure 5.2).

96.2187 shows that the material consist of sand from 0.5 - 2.5 m.b.s. From 2.5 to 6 m.b.s. clay is present and from 6 to 15.5 m.b.s. the material consists of sand, followed by a clay layer that goes deeper down to 44 m.b.s. (figure 5.2). The clay layer is followed by a sand layer from 44 to 55 m.b.s. and a silt layer from 55 to 70 m.b.s (GEUS, 2016).

Figure 5.2: The Jupiter borehole number. 96. 1026 and 96. 2187. Modified after GEUS, 2016

5.1.2.2 MEP

The two Jupiter boreholes are both localized at the shoulders of the sub glacial stream trench which means that they do not provide information about the geology in the sub glacial stream trench and therefore MEP profiles are conducted for EVI2.

The three different MEP profiles are presented in figure 5.3, 5.4 and 5.5. The MEP profiles give a detailed picture of the geology at EVI2. Profile 1 that is located along the stream at the bufferzone from west to east shows that the resistivity values vary from 85 to 550 Ω*m (figure 5.3). The lowest values are found in the western part of the profile in 45 m DVR90 with values from 85 to 100 Ω*m. Values from 10-500 Ω*m indicates sand and values from 5-100 Ω*m indicates clay (figure 4.2). This means that the material at Profile 1 is mainly consisting of sand and the area with lower values in the deeper western part can consist of clay. The fact that the different sediments have overlapping and varying resistivity values means that it can be difficult to assess between the different materials in a MEP profile without additional studies of the area's geology.

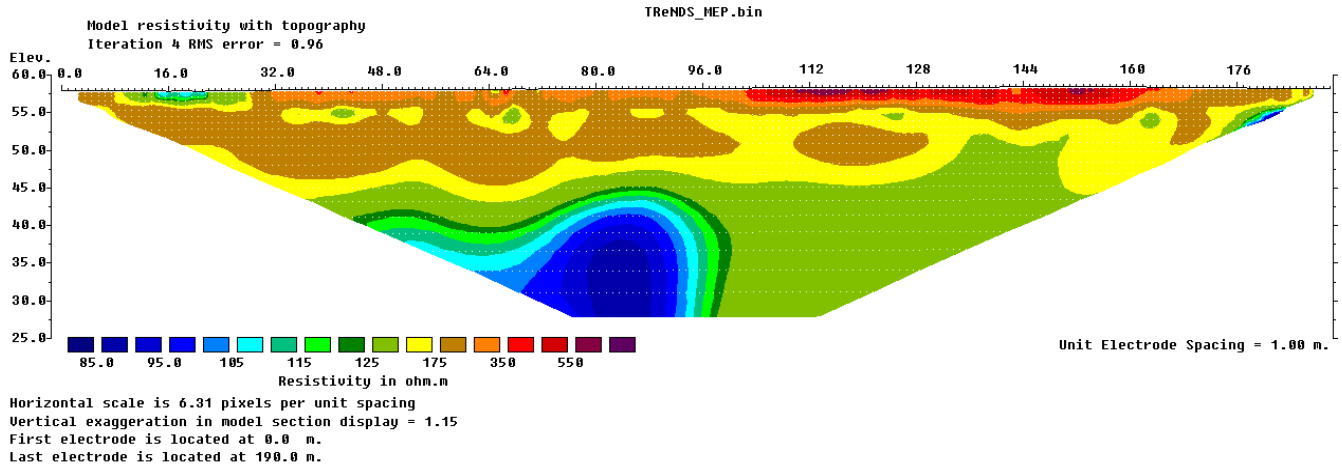

Figure 5.3: MEP profile 1, located along the stream at the bufferzone at EVI2 from west to east.

Profile 2 is located across the agricultural field at EVI2 from south to north, as a transect from the stream to the northern shoulder. In the northern part of the profile, areas with low resistivity values at 17 to 50 Ω*m is seen, which can be clay or very wet sandy material (figure 5.4). In the rest of the profile, the resistivity values varies between 50 and 500 Ω*m with indicates that the material is consisting of sand (figure 4.2). From 115 m to 155 m an area with higher resistivity values is found, which can indicate a sand lens with higher hydraulic conductivity because higher resistivity values is an indication of coarser material (figure 4.2).

During the field trips, a very wet area was observed at the surface above at the northern part of profile 2 with low resistivity values. This makes sense if a clay layer prevents the water to run away and causes formation of wet areas on the surface. A new well (TH5) was installed in this area down to 10 m.b.s. and the well did not give any water. This can be because the well is broken or perhaps the clay layer does not yield any water.

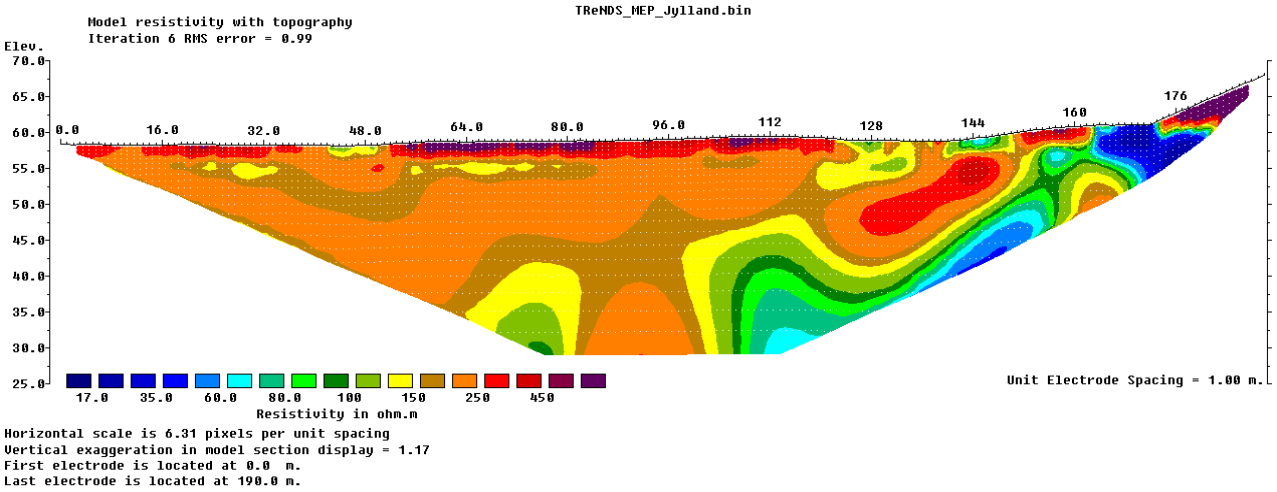

Figure 5.4: MEP profile 2, located across the agricultural field at EVI2 from south to north (as a transect from the stream to the northern shoulder.)

MEP profile 3, located along the northern shoulder at the agricultural field at EVI 2 from west to east, is presented in figure 5.5. It is seen that the resistivity values is in the range from 12 to 450 Ω*m. The material can be divided into four different layers. An upper layer with values around 400 Ω*m, can represent dry sand and the unsaturated zone. A layer with values around 50 Ω*m, which can represent a mix of sandy clay. A layer with high resistivity values from 100 to 450 Ω*m which indicates sand, is located from 55 to 45 m DVR90 in the western part of the profile to the surface in the eastern part of the profile. Underneath the sand layer in a depth at approximately 45 m DVR90 an area with low resistivity values between 12 to 50 Ω*m are found which indicates clay (figure 5.5 and figure 4.2).

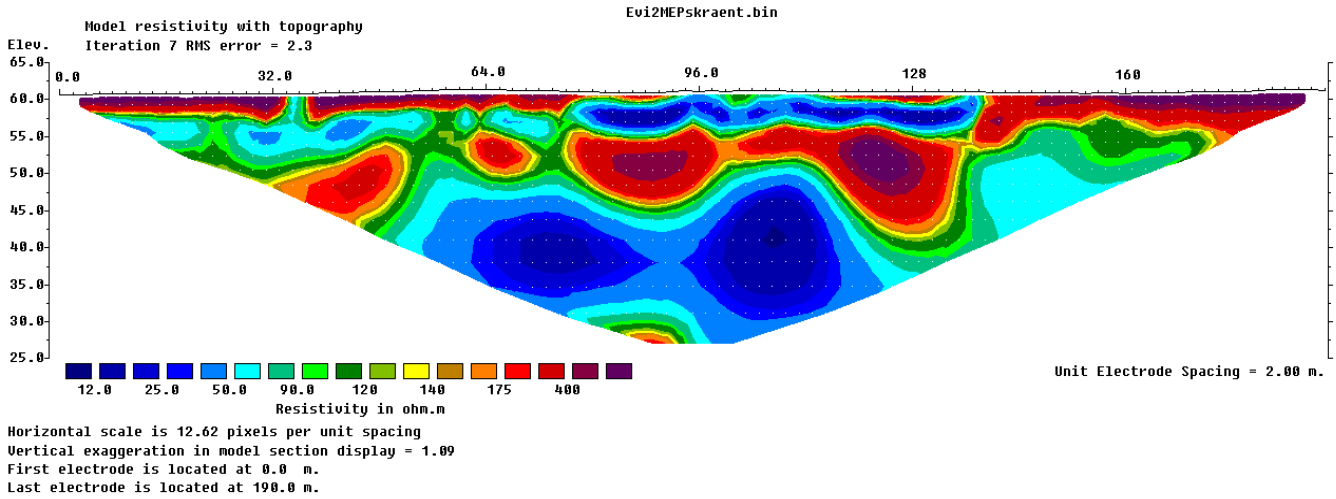

Figure 5.5: MEP profile 3, located along the northern shoulder at the agricultural field from west to east.

By comparing the MEP profile with the Jupiter borehole 96.1026, located close to the eastern part of the MEP profile 3, the geology is comparable. In both the MEP profile 3 and 96.1026 an upper sand layer is found down to approximately 8 m.b.s. This is followed by a clay layer down to approximately 15 m.b.s. followed by a sandy layer in the MEP profile that is defined as sand and clay in 96.1026. In addition, a lower clay layer is to be found from approximately 15 m.b.s. (figure 5.5 and 5.2)

5.1.2.3 Geoscene

A cross section covering EVI2 from the geology Geoscene model developed by Enemark (2015), is presented in figure 5.6, showing a conceptual model of the geology at EVI2.

From the conceptual model, it can be seen that the geology in EVI2 in the upper layers in south and north consisting of sandy material. At the northern part of the stream, an approximately 10 meter thick sand layer is present down to 50 meter DVR90. Underneath the sand layer, a clay layer is found from 10 to 45 m.b.s. (50 to approximately 12 m DVR90) (figure 5.6). Underneath the clay layer, a sand layer is present from 45 to approximately 100 m.b.s. (12 to -40 m DVR90) with an underlying clay layer present from approximately 100- 140 m.b.s. (-40 to -80 m DVR90) (figure 5.6).

The conceptual model of the geology in EVI2 is in relatively good agreement with the Jupiter boreholes and MEP profiles. An upper sandy layer is found, representing the aquifer at EVI2 and a lower clay layer from approximately 10 to 45 m.b.s. representing the bottom of the aquifer. However, the MEP profile 1 and 2 indicates that the upper clay layer is not present in 10 m.b.s. in the entire area, which can be due to the more heterogeneity geology in reality (figure 5.3 and 5.4). At the same time, the conceptual model does not show the upper clay layer, found in 96.2187 at the southern part of EVI2 (figure 5.6 and 5.2).

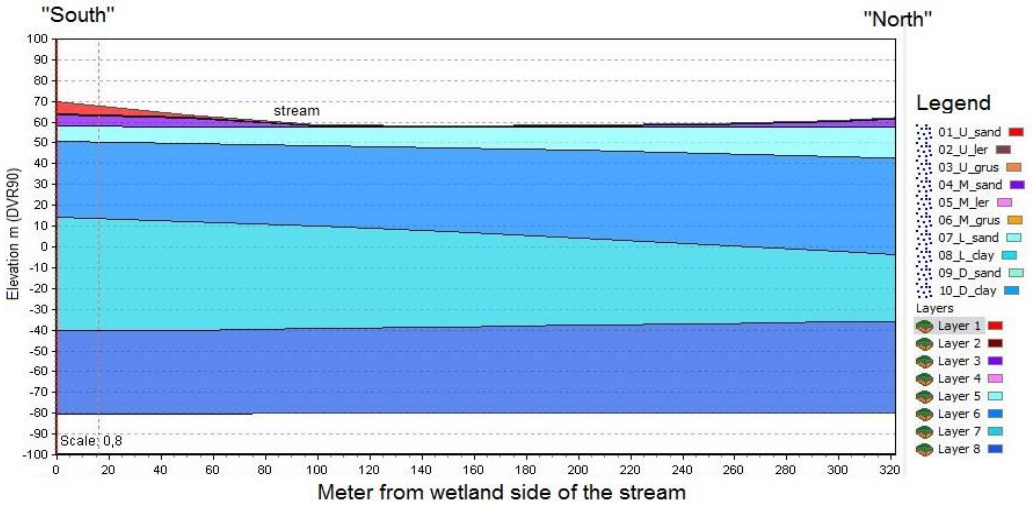

Figure 5.6: The geological layers in a transect covering EVI2 from the wetland side of the stream to the end of the agricultural field in north. Created in Geoscene from the model developed by (Enemark, 2015).

5.1.3 Hydraulic conductivity

The hydraulic conductivity measured in the wells at EVI2 varies between 0.1 and 50 m/day with only one measurement at 0.1 m/day (figure 5.7). This indicates that the geology in the area is dominated by sand, which often has a hydraulic conductivity from 1-100 m/day (Hendriks, 2010). TH2(6m) has a higher hydraulic conductivity at 50 m/day and the well TH4, located at the agriculture field have the lowest K values at 0.1 and 1 m/day in 3 and 8 m.b.s. which can mean that the material here is of lower permeable (figure 5.7).

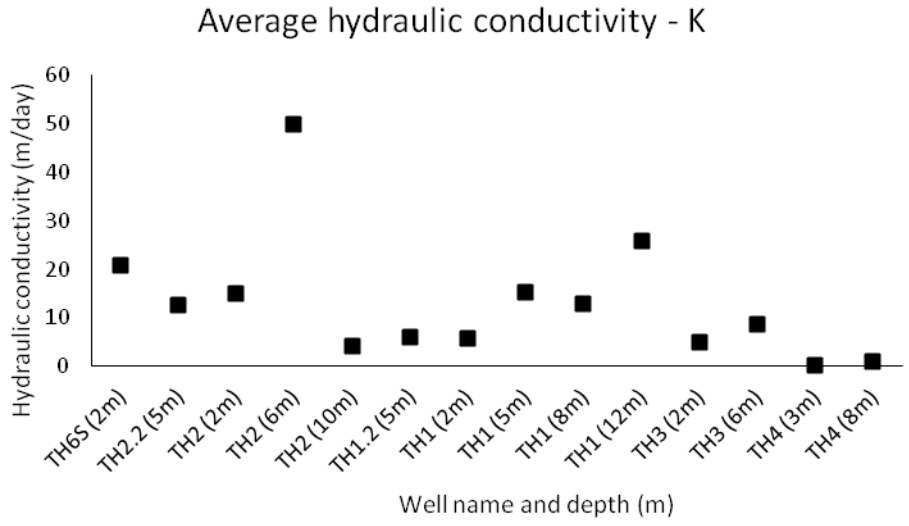

Figure 5.7: The average hydraulic conductivity measured by Slugtests in different wells at EVI2.

By comparing the hydraulic conductivities with the MEP profiles, a conceptual model of the geology at EVI2 in a depth down to 25 m DVR90 can be made (figure 5.8). If a relationship between the hydraulic conductivities and the resistivity of a material is assumed, like Karan et al, 2013 did, it can be seen from figure 5.8 that the material in the study area consist of material with a low hydraulic conductivity at 0.1 m/day, material with a hydraulic conductivity at 1-10 m/day and material with a high hydraulic conductivity at 20 – 50 m/day. Studies from the two study sites EVI1 and Hygild, also located in Holtum catchment, showed that the average horizontal hydraulic conductivity is around 10 m/day (Nørrevang and van't Veen, 2014) (Karan et al, 2013) which is also the average horizontal hydraulic conductivity found for EVI2.

By comparing figure 5.8 with the conceptual model of the geology at EVI2 (figure 5.6). The geology in EVI2 is with high probability consisting of sand in the upper layer with an underlying clay layer located in the elevation of approximately 50 m DVR90 in the northern part of the area. Profile 2 showed that the clay layer was only to be found in the northern part (figure 5.8, profil2). This means that conceptual model of the geology (figure 5.6) is a bit too simple and that the clay layer found in figure 5.6 is not present in 15 m.b.s. in the entire study site.

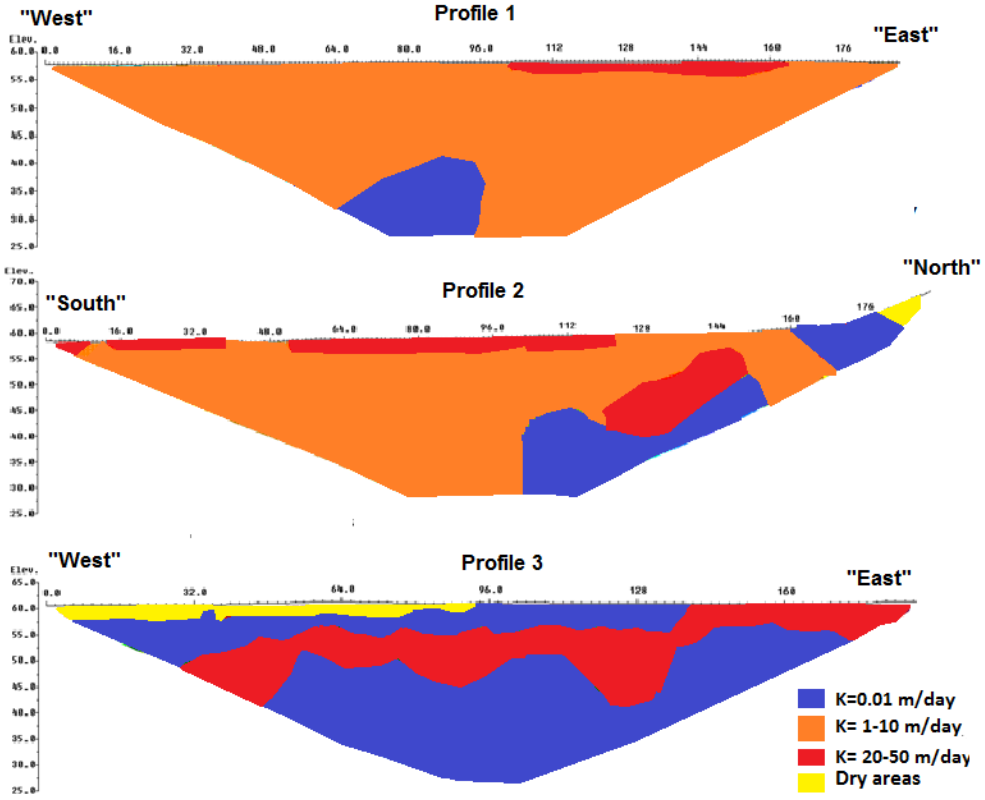

Figure 5.8: Conceptual model for the horizontal hydraulic conductivity based on the MEP analyses of the three MEP profiles and the measured K values by slugtests.

5.2 Isotopes

The $\delta^{18}O$ distribution in the wells at EVI2 measured in the winter season, are presented in figure 5.9. It is seen that the distribution follows the distribution of $\delta^{18}O$ down though the soil from the theory (figure 4.3). This means that the influence of the precipitation gets smaller with depth and the $\delta^{18}O$ signal gets closer to the bulk average for the precipitation with depth, due to the flow path length, residence time, mixing and physical characteristics of the soil (Clark and Fritz, 1997). Figure 5.9 then shows that the samples taken from the wells close to the surface can be more affected by the precipitation input and seasonal variations. Many of the measurements are smaller than the bulk average which means that they are depleted in ^{18}O and some of them are higher which means that they are enriched in ^{18}O (figure 5.9). The water in the wells at the agricultural side of the stream can therefore be divided into two groups: one that is enriched with ^{18}O and one that is depleted. The depletion can be because this water originates from precipitation in the winter with lower evapotranspiration or fall where a higher amount of water is infiltration the water, which means that the water flows faster though the soil and makes the evapotranspiration less.

The enrichment is found in many of the shallow wells, which can be due to the water originates from precipitation during the summer season, with higher evapotranspiration. The enrichment can also be because the water has been affected by the soil properties and therefore the water may be exposed to higher evapotranspiration.

In all the wells located at the wetland area, the $\delta^{18}O$ is enriched in ^{18}O. This can be due to the properties in the soil in the wetland area that makes the water infiltrating though the soil slower, which means that there is more time for evapotranspiration (figure 5.9). It is at the same time also possible that the water flow is more upward in the wetland area which means that the water can be enriched by ^{18}O due to mixing with other water that has been exposed to evapotranspiration during the summer season.

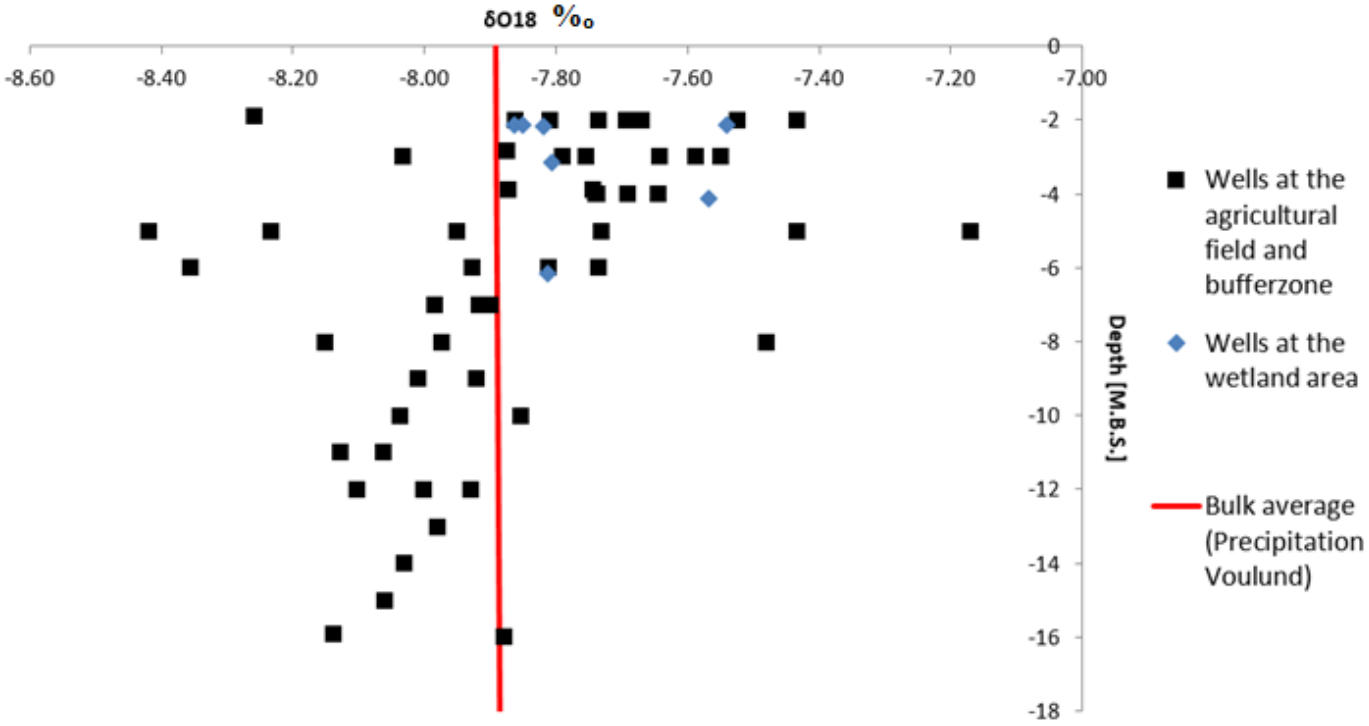

Figure 5.9: The $\delta^{18}O$ vs. depth distribution for the wells located at EVI2 in winter season compared with the bulk average measured at Voulund by Müller 2016.

$\delta^{18}O$ vs. δD is seen in figure 5.10. It is found that the trend line for the wells located at the agricultural field side of the stream at EVI2 is matching the slope of the Local meteoric water line (LMWL) for the precipitation in Voulund, which represent the precipitation in the catchment (Müller, 2016). However, the trend line is located a bit above the LMWL in the winter season and a bit under in the summer season, which means that the water in the wells are affected by processes and not only the precipitation. It should be kept in mind that the summer trendline is only based on few measurements. The wells located at the wetland area is all found over the LMWL and by that enriched in ^{18}O, which means that the water is affected by evapotranspiration. From this figure, it is also seen that the water in the wells at the agricultural side of the stream can be divided into two groups. One that is enriched with ^{18}O and one that is depleted as described above.

In the winter season, the isotope signals in the springs are above the LMWL but in the summer season, the signals are around the LMWL (figure 5.10 and 5.11). This can be because the seasonal signal is disappeared from the summer measurements, which means that the water can be groundwater that has been exposed for a long travel path and by that mixing with other groundwater.

However, the farmer probably irrigates the agricultural field at EVI2 during the summer seasons. This means that the isotope values for the wells located at the agricultural field side of the stream can be affected by some groundwater with other isotopes. This gives the results some uncertainties.

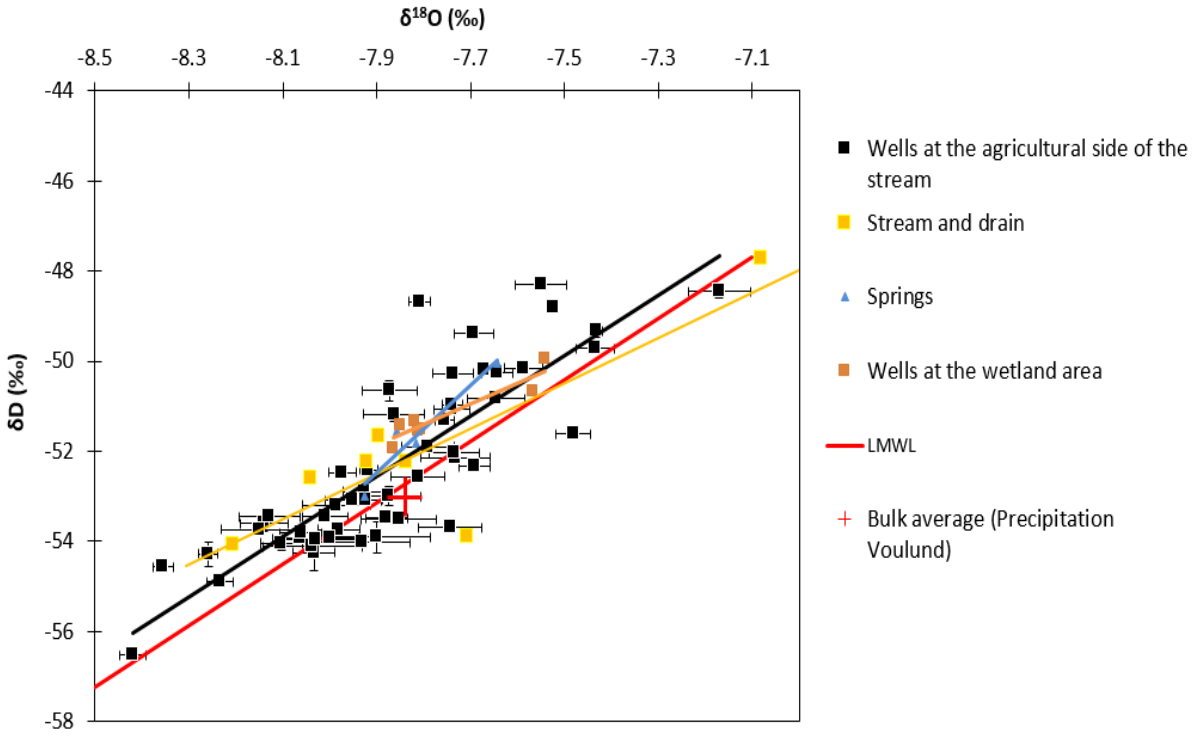

Figure 5.10: The $\delta^{18}O$ vs. $\delta^{18}D$ for the wells and the not wells measured at EVI2 in the winter season compared with the bulk average measured at Voulund and LMWL: Local meteoric water line from Müller, 2016.

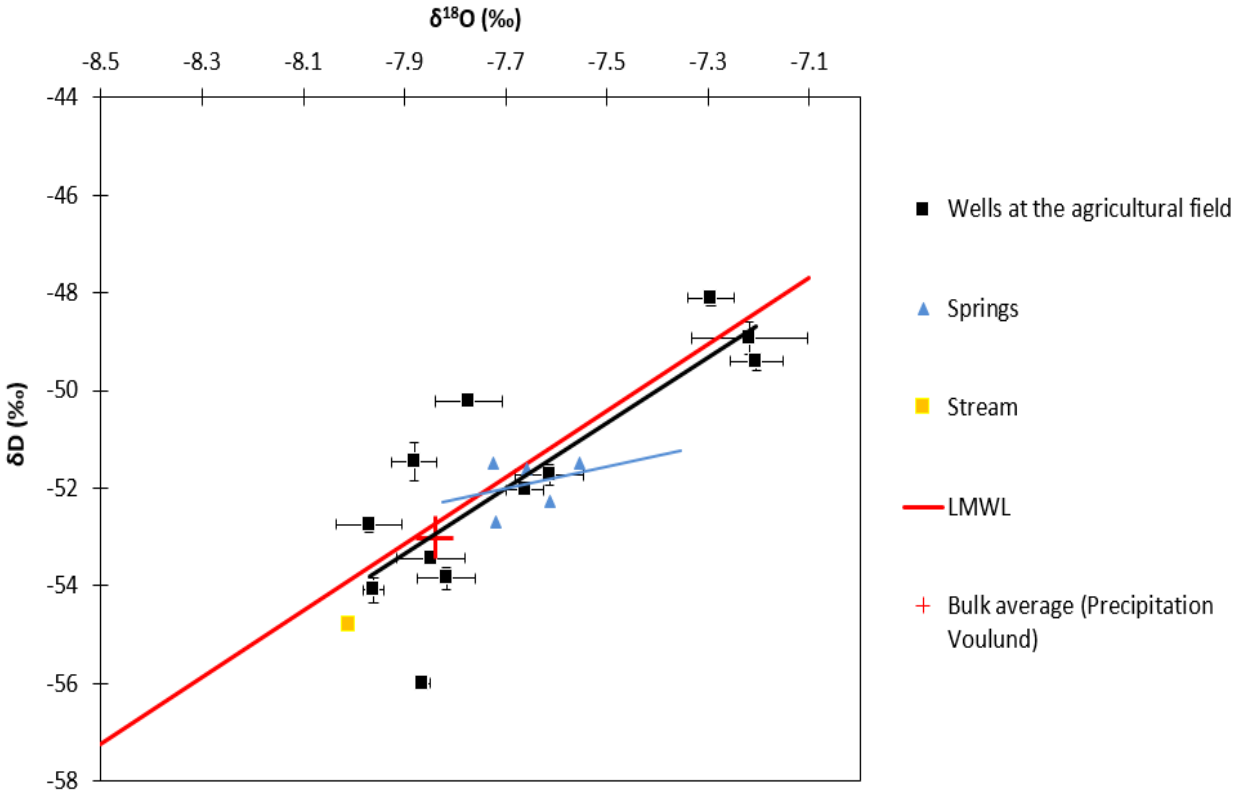

Figure 5.11: The $\delta^{18}O$ vs. $\delta^{18}D$ for the wells and the not wells measured at EVI2 in the summer season compared with the bulk average measured at Voulund and LMWL: Local meteoric water line from Müller, 2016.

5.3 Groundwater chemistry

The groundwater chemistry at EVI2 is in the following analyzed and described. First, analyses of three transects are performed in order to get an overall idea of the groundwater chemistry at EVI2 and secondly by analyzing the chemistry processes down though the soil in four wells (two installed in the winter season representing a winter snapshot and two installed in the summer season, representing a winter snapshot). This is done in order to investigate the controlling chemical processes going on at the agricultural field at EVI2.

The measurements at EVI2 from the winter season are divided into two different transects representing the winter measurements, Transect 1 and 2.

Transect 1 represents measurement from all wells at EVI2 in the winter season. Transect 2 represents measurements from the springs at the wetland area in EVI2, the stream and the drain. The

measurements from the summer season is all showed in the same figure which be that represents all measurements in both wells, stream etc.

In the transects and the figure showing the summer measurements, the stream is located in 0 m from the stream. Measurements collected at the wetland area are represented with negative distance from the stream. While measurements taken at the northern side of the stream, referred to as the agricultural side of the stream, are represented with positive meters from the stream in the figures.

5.3.1 Transect 1 – Wells in the winter season

By comparing the oxygen and Fe^{2+} results in transect 1, it is found that no wells contains both oxygen and Fe^{2+} (figure 5.12). This is impossible because Fe^{2+} cannot exist if oxygen is present because it will then precipitate as Fe^{3+} (Appelo and Postma, 2005). This also validates that the samples are performed correctly.

The oxygen concentrations are almost zero and the Fe^{2+} concentrations varies from 0.02 to 0.09 mM. This indicates an anoxic environment in all the wells (figure 5.12).

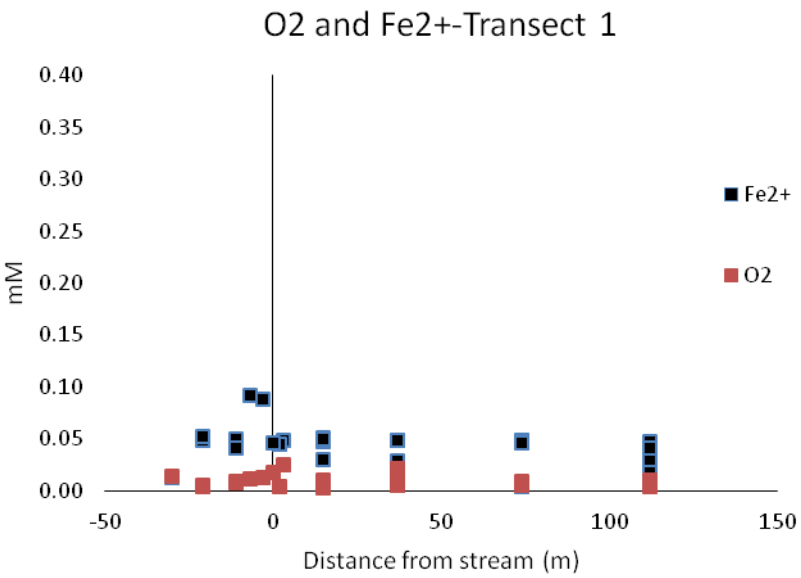

Figure 5.12. O_2 and Fe^{2+} concentrations in Transect 1 measured in the winter season.

The EC concentration is in all wells in transect 1 high, which can indicate an influence of agriculture and by that nitrate (Agriculture Solutions, 2016) (figure 5.13). At the agricultural side of the stream, the EC concentration varies from 200-450 µS/cm, which can indicate the background concentration in this environment. In the wetland area, the EC concentration is higher and varies from 250 to 600 µS/cm (figure 5.13).

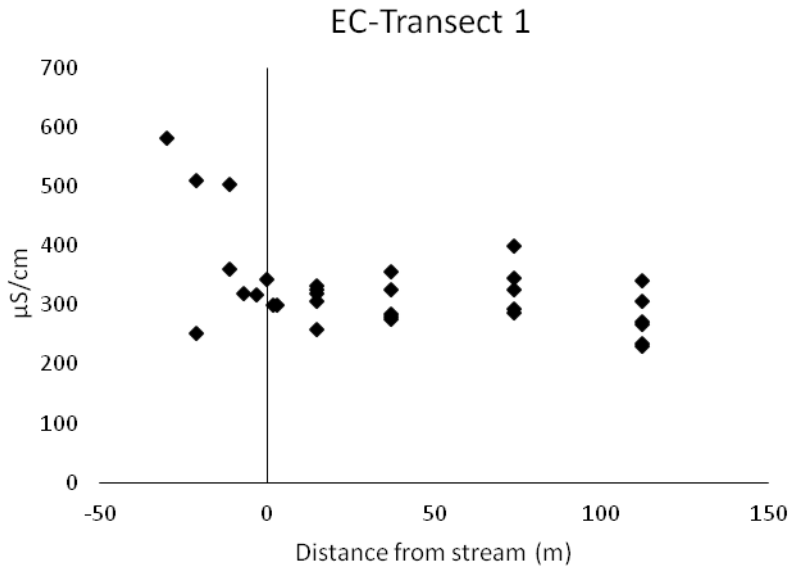

Figure 5.13. EC concentrations in Transect 1 measured in the winter season.

The sulfate concentrations in transect 1 show that the sulfate concentrations can be divided into two "groups". One that contains concentrations varying from 0.0 to 0.4 mM and one with concentrations from 0.7 to 1.3 mM (figure 5.14). It is possible that the first group represents the background concentrations of sulfate in the soil environment at EVI2 and the second group could represent an environment where denitrification of nitrate with pyrite as electron donor has taken place. This could explain the higher concentration of sulfate (section 3.2 Eq. 3).

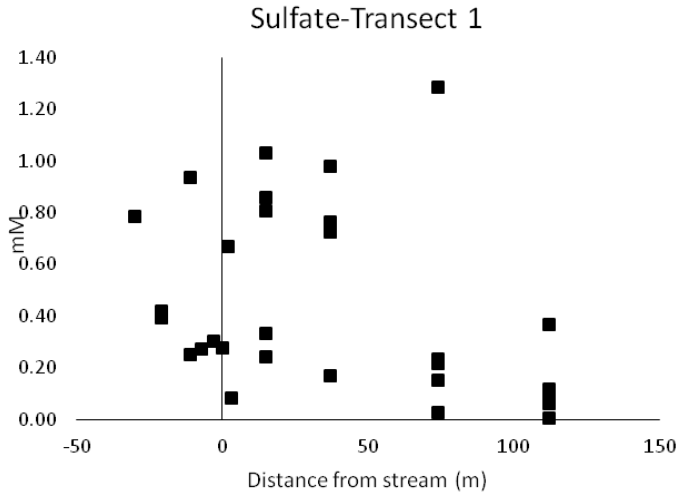

Figure 5.14: Sulfate concentrations in Transect 1 measured in the winter season.

The nitrate concentrations in transect 1 are illustrated in figure 5.15. It is found that nitrate is only present in one well, located at the agriculture field. This is TH3 in 2 and 3 m.b.s. (figure 5.15). In 2 m.b.s. the concentration is 1.2 mM which is higher than 0.8 mM that is the threshold value for nitrate in Denmark (Appelo and Postma, 2005). The absence of nitrate in the wells at the agriculture field indicates, that the nitrate from the fertilizer is reduced with can only happen with denitrification under anoxic condition (section 3.2). The oxygen concentration in transect 1 was almost nothing (figure 5.12), which makes the denitrification possible. At the same time, the high sulfate concentration in some of the wells can indicate that the nitrate is removed with pyrite as electron donor (figure 5.14). The fact that the wells in the wetlands area does not contain nitrate but high EC concentrations can mean that the nitrate in this wells are reduced before entering the wells, which means that the water flows though anoxic layers in the soil (figure 5.15 and 5.13).

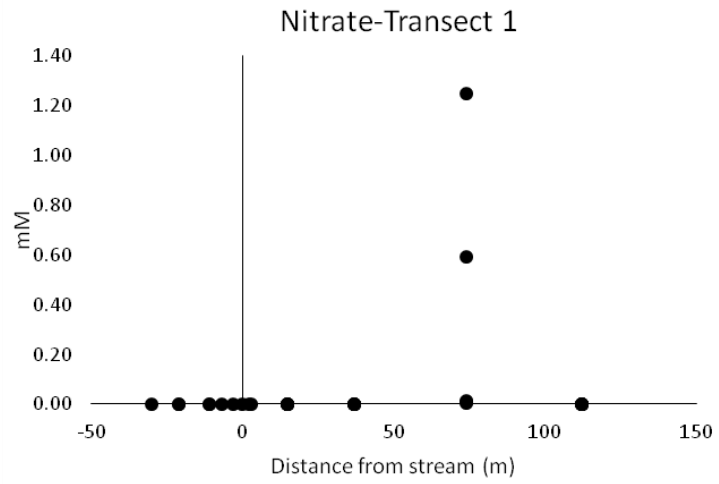

Figure 5.15. Nitrate concentrations in Transect 1 measured in the winter season.

5.3.2 Transect 2 – springs, stream and drain in the winter season

The opposite picture oxygen and Fe^{2+} concentrations are found in transect 2 compared to transect 1 (figure 5.16 and 5.12). In transect 2 the samples contains oxygen and no Fe^{2+} (figure 5.16). This validates, that the samples for transect 2 are performed correctly.

The Fe^{2+} concentrations are close to zero and the oxygen concentrations are between 0.15 and 0.4 mM, which indicates an oxygen rich environment (figure 5.16). This makes sense since the samples are collected in springs, the stream and drain that are in contact with the atmosphere.

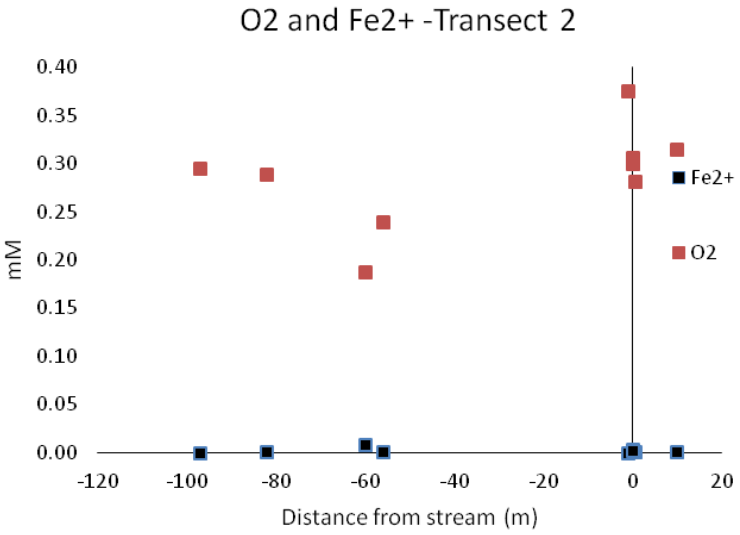

Figure 5.16. O_2 and Fe^{2+} concentrations in Transect 2 measured in the winter season.

The EC concentration in transect 2 is in the range of 300-600 µS/cm, which indicates an influence of agricultural and by that nitrate (figure 5.17). The EC concentrations found in transect 2 correspond to the concentrations found in the wells at the wetland area (figure 5.17 and 5.13). This indicates with high probability, that the water in the wells at the wetland area is the "same" as the water in the springs and in the stream and indicates a high background concentration in this environment.

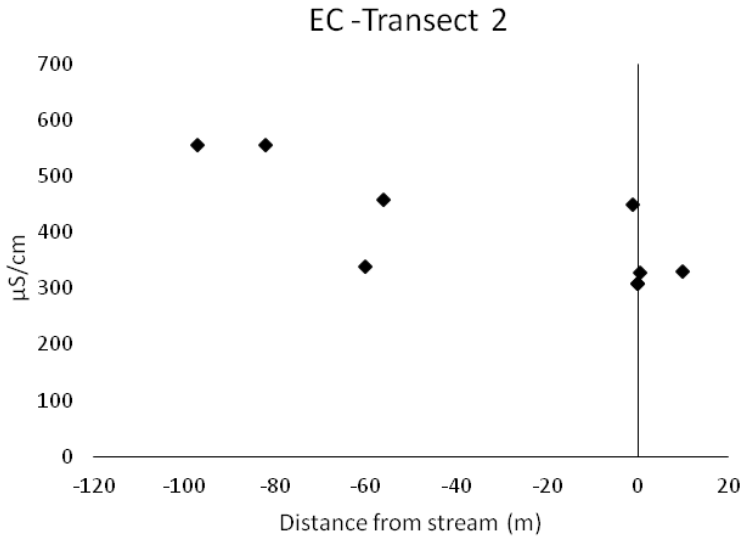

Figure 5.17: EC concentrations in Transect 2 measured in the winter season.

Transect 2 contains nitrate and two of the samples taken from two springs are above the threshold value for nitrate at 0.8 mM (figure 5.18). The nitrate concentration varies from 0.1 to 1.2 mM (figure

5.18). This indicates that the water in the springs in the wetland area side are affected by agriculture and that the water has not flowed though anoxic environment where the denitrification of nitrate is possible.

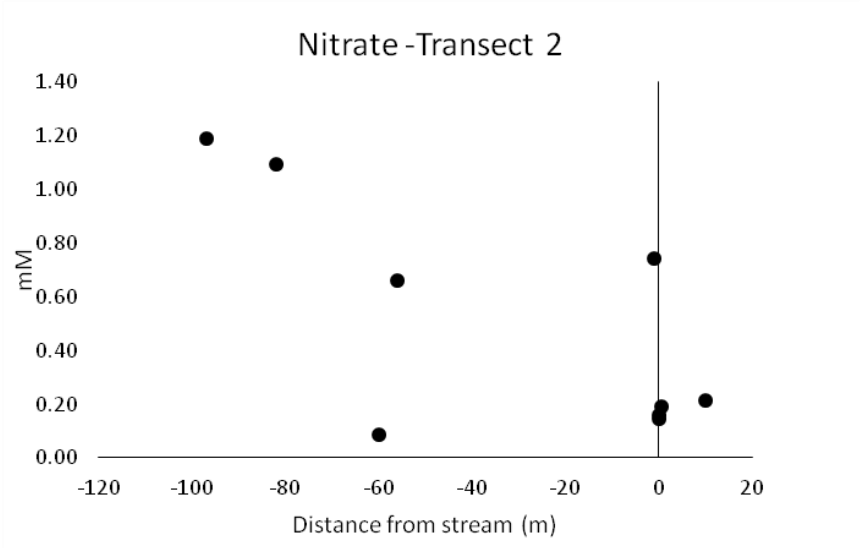

Figure 5.18: Nitrate concentrations in Transect 2 measured in the winter season.

The sulfate concentrations in transect 2 varies from 0.1 to 0.4 mM (figure 5.19). The sulfate concentrations in transect 2 are low compared to transect 1 and in the same range as the "group 1" representing the background concentration of sulfate. This makes sense since the samples contain nitrate and therefore the denitrification cannot take place. If it had been with pyrite as electron donor the results would be high concentrations of sulfate (figure 5.19 and 5.18).

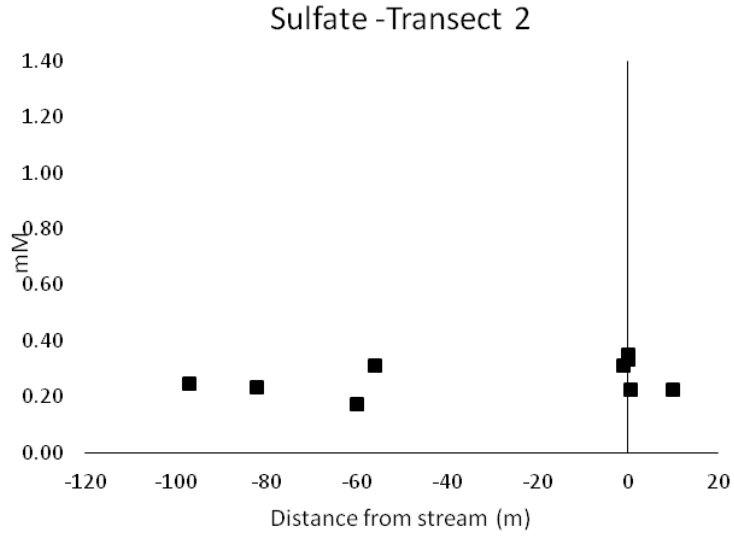

Figure 5.19: Sulfate concentrations in Transect 2 measured in the winter season.

5.3.3 Summer measurement – Wells and springs, stream, drain in the summer season

By comparing the oxygen and Fe^{2+} concentration in figure 5.20 which represents the summer season, the same tendency is found as for transect 1 and 2 representing the winter season (figure 5.12 and 5.16). The springs, stream and drain at the wetland side of the stream contains oxygen and no Fe^{2+} and the wells contain no oxygen and Fe^{2+} (figure 5.20).

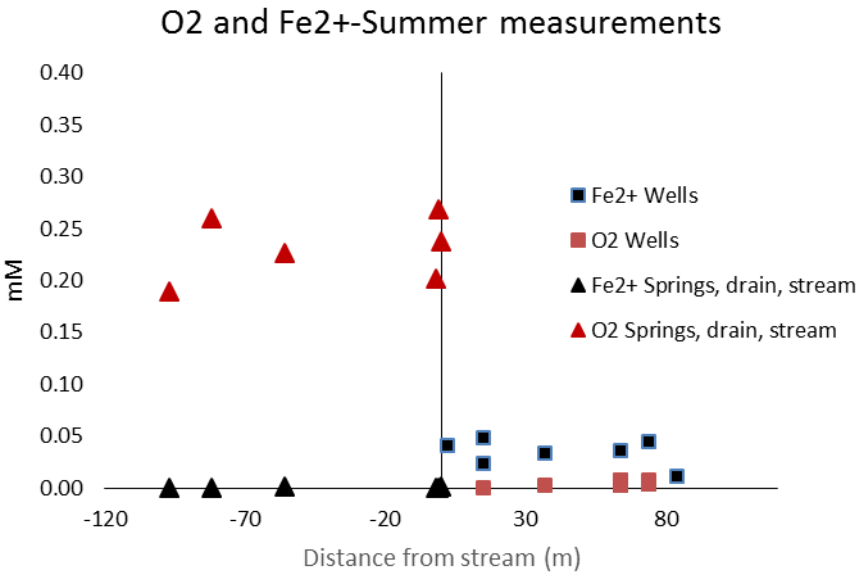

Figure 5.20: O_2 and Fe^{2+} concentrations measured in the summer season in wells, springs, stream and drain

The EC concentration in the summer season is in the same range as in the winter season from 200 – 500 µS/cm (figure 5.21, 5.13 and 5.17). The concentrations of EC are high in both of the wells and in the springs, stream and drain, which can indicate an influence of fertilizer (Agriculture Solutions, 2016) (figure 5.21). In the springs, stream and drain the EC varies from 350-600 µS/cm while the concentrations in the wells are a bit lower (between 200 and 400 µS/cm) which can indicate the background concentration in this environment (figure 5.21).

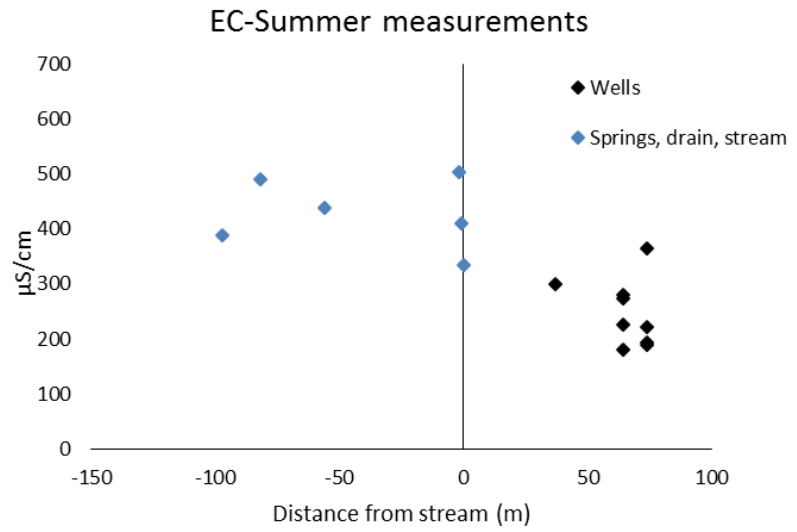

Figure 5.21: EC concentrations measured in the summer season in wells, springs, stream and drain

The nitrate concentration in the springs in the summer season varies from 0.1 to 1.3 mM (figure 5.12). By looking at the distribution of the nitrate concentration, the same pattern is found in the summer season, as in the winter season, with high nitrate concentration in the springs, stream and drain in the wetland area and no nitrate present in the wells under 3 m.b.s. (figure 5.22, 5.15 and 5.18). Nitrate is found in the wells at the agricultural field in the top of the three new installed wells (TH3.2, TH3-D and TH3-U). Two of the measurements are above the threshold value at 0.8 mM for nitrate (figure 5.22).

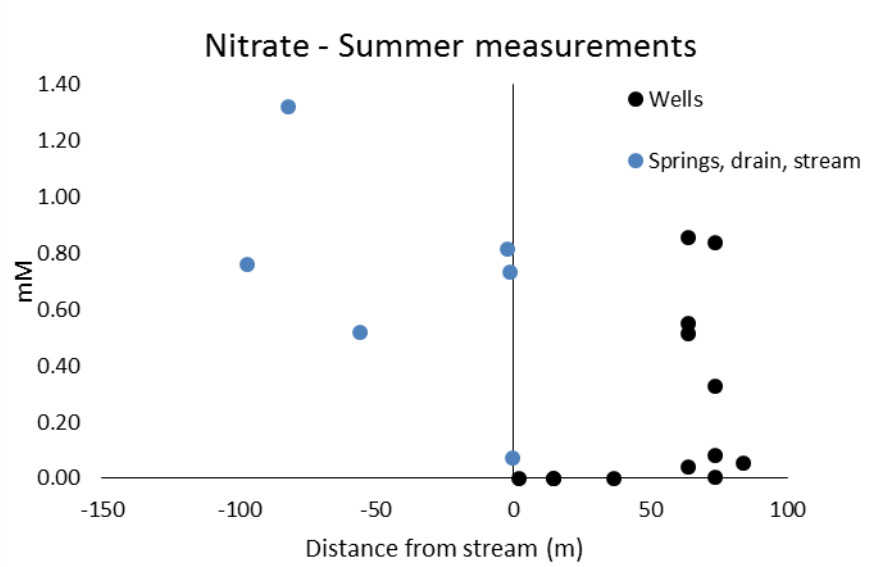

Figure 5.22: Nitrate concentrations measured in the summer season in wells, springs, stream and drain.

The sulfate concentrations in figure 5.23 illustrate the same pattern for the sulfate concentrations in the summer season as in the winter season (figure 5.14 and 5.19). The summer measurements also show that the sulfate concentrations can be divided into two "groups". One that contains concentrations from 0.0 to 0.6 mM and one with concentrations from 0.7 to 1.3 mM (figure 5.23). The first group represents the background concentration of sulfate in the environment at EVI2 and the second group represents that a denitrification of nitrate with pyrite as electron donor has been taken place which can explain the higher concentration of sulfate in this wells (section 3.2 Eq. 3).

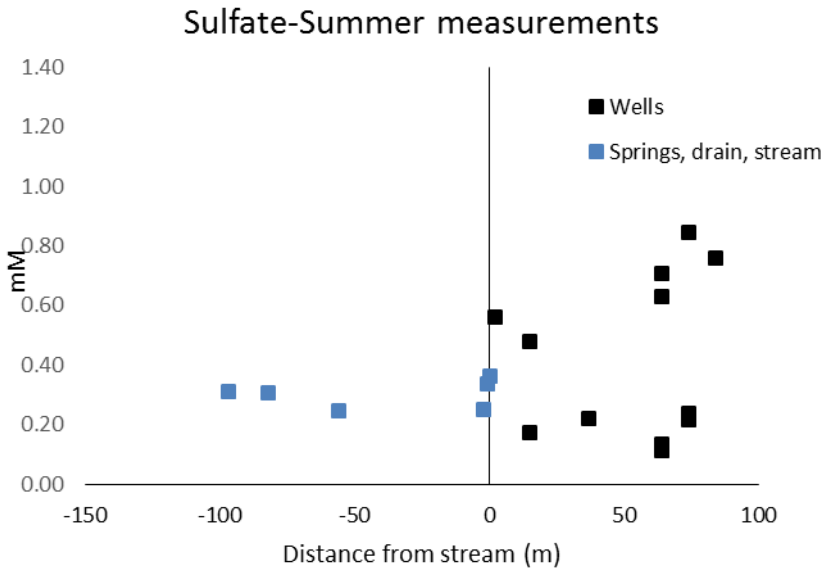

Figure 5.23: Sulfate concentrations measured in the summer season in wells, springs, stream and drain

5.3.4 Nitrate reduction in the riparian zone at the agriculture field

The absence of nitrate in the wells under 2.5 m.b.s. at the agricultural field means that the nitrate must be reduced at the agriculture side of the stream (figure 5.15). In the following, a winter and a summer snap shot of the water chemistry will be analyzed based on four wells located at the agricultural field. TH3 and TH4 will represent the winter season and TH3.2 and TH3-Dwill represent the summer season. The water chemistry in the wells is qualitatively analyzed in order to investigate which processes that control the groundwater chemistry at the agriculture field. Furthermore, the differences between the summer and winter season regarding the chemistry measurements will be analyzed.

5.3.4.1 Winter snapshot - TH3 and TH4

TH3

The pH in TH3 is around 6 while the alkalinity varies from 0.1 to 2 meq/L (figure 5.24. A). The same patterns are found for the pH and alkalinity because the pH and alkalinity is dependent on acid in the groundwater. It is seen that both components decreases in 3 m.b.s. and then increases in 4 m.b.s. (figure 5.24, A). The oxygen and Fe^{2+} concentration is illustrated in figure 5.24, B. It is seen that the concentration of oxygen is close to 0 in all depts. except in 2 m.b.s. where a small amount of 0.009 mM is present. The Fe^{2+} concentrations in TH3 are 0 in 2 and 3 m.b.s. and then they increase to around 0.05 mM. This makes sense because the Fe^{2+} cannot be present under oxygen rich conditions. The hydrogen sulfide is present in low concentrations. In 3 and 5 m.b.s. the highest concentration of 6 umol/L hydrogen sulfide is found (figure 5.24,C). This can indicate that a pyrite formation takes place.

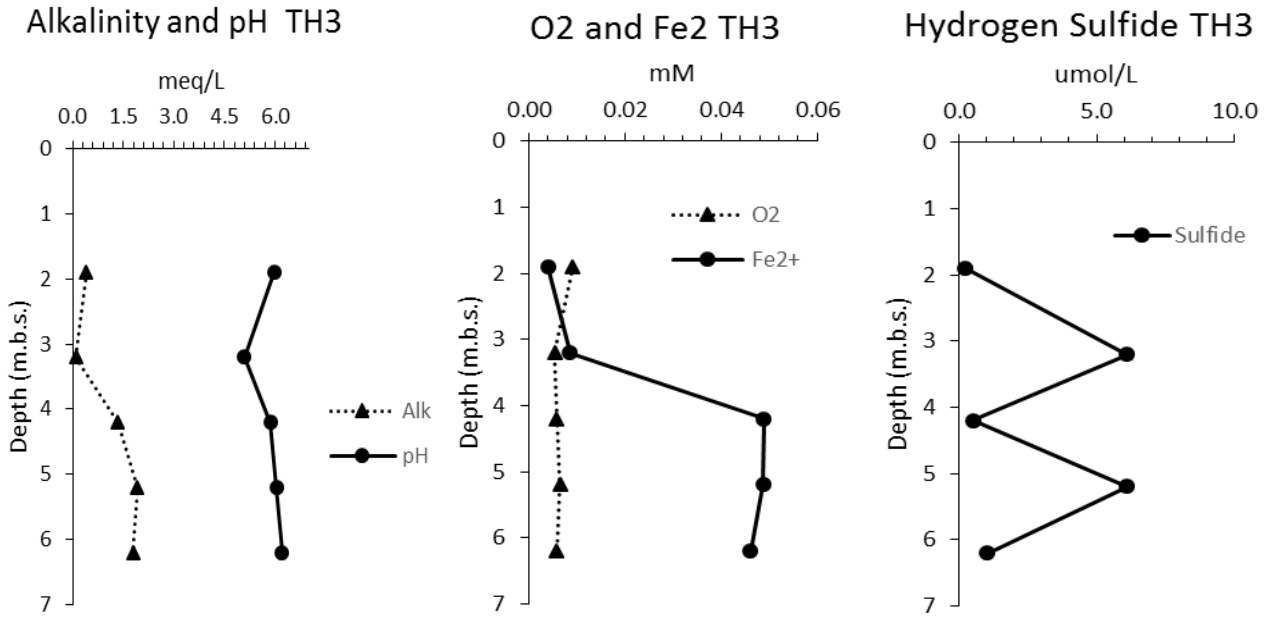

Figure 5.24: Chemical concentrations measured in TH3 in March 2016. A: measured O2. Fe2+ B: Measured alkalinity and pH and C: measured hydrogen sulfide.

The concentration of anions in TH3 is found in figure 5.25. It is seen that 1.23 mM nitrate is present in 2 m.b.s. and afterwards decreases down though the soil. At 3 m.b.s. the concentration is 0.6 mM and in the remaining depths the concentration is close to zero. This means that the nitrate must be reduced.

The sulfate concentration is increasing from 0.2 to 1.3 mM in 3 m.b.s. In 4 m.b.s. the concentration is decreasing and close to zero, in 4 and 5 m.b.s. and in 6 m.b.s. the concentration is 0.2 mM. The concentration of the alkalinity is decreasing from 2 to 3 m.b.s. and increasing from 3 to 5 m.b.s and then decreasing again in 6 m.b.s. The chloride concentration varies from 0.6 to 1 mM and the concentration of the rest of the anions is around 0 in all depths (figure 5.25). The cations concentrations are found in appendix 10.

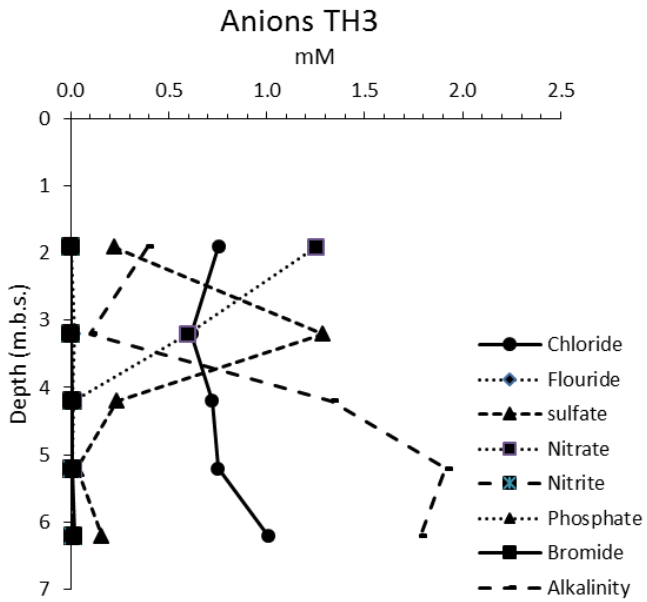

Figure 5.25: Chemical concentrations of anions measured in TH3 in March 2016.

From 2-3 m.b.s., a pyrite oxidation may take place because the small amount of oxygen is reduced and an increase in sulfate and Fe^{2+} is seen (figure 5.25). A reduction of nitrate is going on when the oxygen is used which can only be due to denitrification. The increase in the sulfate concentration means that this reduction probability is due to denitrification with pyrite as electron donor (Eq. 3). The denitrification cannot take place with organic matter or Fe^{2+} as electron donor because this would results in an increase in the alkalinity and a decrease in Fe^{2+} which is not found.

From 3-4 m.b.s. the nitrate is still decreasing which means that the denitrification is going on but now with organic material as the electron donor (Eq. 2) because an increase in the alkalinity is found and not with pyrite because a decrease in sulfate is found. The denitrification cannot explain the entire alkalinity increase and at the same time, the Fe^{2+} is increasing which with high probability, can be due to reductive dissolution of iron oxides. There are different sources of Fe2+ herby Fe-oxides and pyrite. Fe-oxides dissolve under reducing conditions while pyrite only dissolves under oxide conditions.

The decrease in the sulfate can be due to sulfate reduction, which results in increase in alkalinity and hydrogen sulfide (Eq. 8) (figure 5.25). An increase in hydrogen sulfide is not found (figure 5.24- C) and only low concentration appears. This can be explained by the fact that Fe^{2+} and hydrogen sulfide can form precipitation of pyrite.

From 4-5 m.b.s. there is no nitrate present. The sulfate is still decreasing and the alkalinity is increasing, which means that a sulfate reduction can still take place.
From 5-6 m.b.s. the chemical composition is quite different which means that it with high probability is other water that is present here. An increase in chloride was also found (figure 5.25).

TH4
The pH in TH4 from 4 to 9 m.b.s. is around 6 while the alkalinity varies from 1.3 to 2.1 meq/L (figure 5.26, A). The oxygen and Fe^{2+} concentration in TH4 is illustrated in figure 5.26, B. It is seen that the concentration of oxygen is close to 0 in all depths. The Fe^{2+} concentrations in TH4 vary between 0.02 and 0.05 mM. The hydrogen sulfide concentration varies from 0 to 5 umol/L in TH4 from 4 to 9 m.b.s. The highest concentration is found in 7 m.b.s. which can indicate a sulfate reduction (figure 5.26,C).

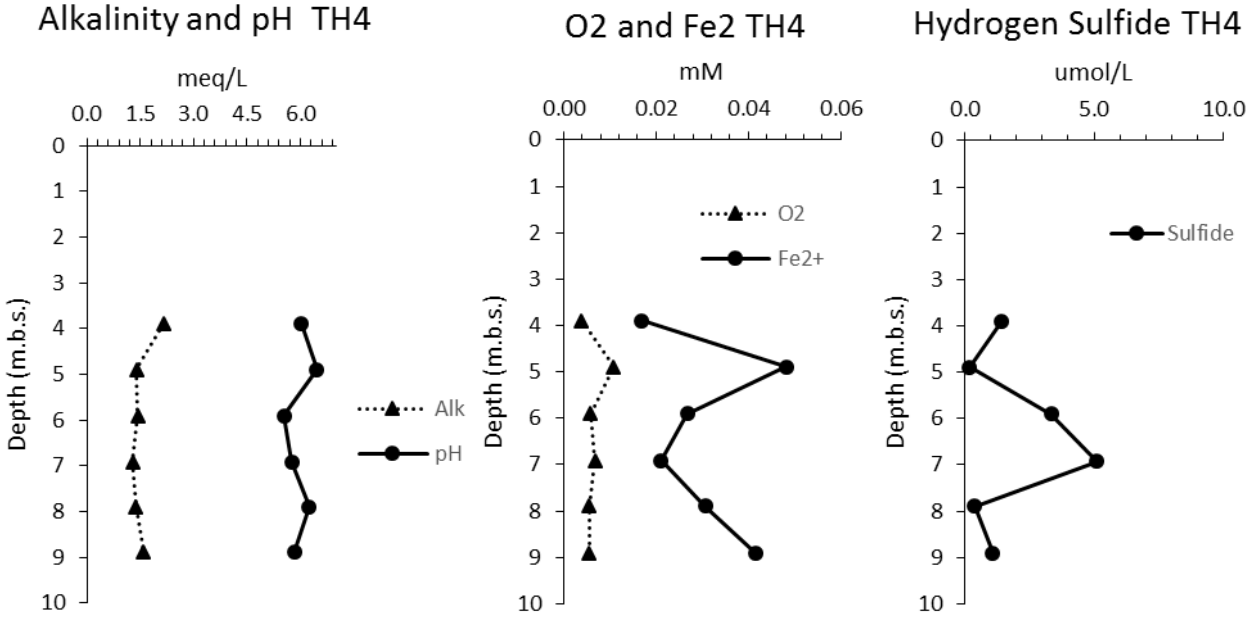

Figure 5.26: Chemical concentrations measured in TH4 in March 2016. A: measured O2. Fe2+ B: Measured alkalinity and pH and C: measured hydrogen sulfide.

The concentration of anions in TH4 from 4 to 9 m.b.s. is found in figure 5.27. It is seen that no nitrate is present in all depths. The sulfate concentration is increasing from 0.0 to 0.4 mM from 4 to 5 m.b.s. and decreasing to 0.1 mM in 6 m.b.s. where it stays stable around 0.1 in the rest of the depths. The

alkalinity concentrations in TH4 decrease from 2.1 to 1.3 meq/L from 4 to 5 m.b.s. From 5 to 8 m.b.s. the concentration is approximately 1.4 meq/L and increases to 1.6 meq/L in 9 m.b.s. The chloride concentration varies from 0.5 to 0.9 mM and the concentrations of the rest of the anions are around 0 in all depths in TH3 (figure 5.27).

The absence of nitrate in TH4 can be because the nitrate is already removed in 4 m.b.s., which was found in TH3 (figure 5.25).
From 4 - 5 m.b.s. an increase in the Fe^{2+} concentration is found which high probability can be due to reductive dissolution of iron oxides.
From 5 – 6 m.b.s. the sulfate concentration is decreasing, which can be due to sulfate reduction because an increase in alkalinity is found and an increase in the hydrogen sulfide (figure 5.27 and 5.26). Only low concentration of hydrogen sulfide appears which as explained earlier can be due to precipitation of pyrite.
From 6 - 9 m.b.s. the water chemistry is quite different which means that is with high probability is mixed water in this depth (figure 5.27). The concentration of cations is found in appendix 10.

From TH4, the same processes as in TH3 are found to be going on and it can be observed that the chemical processes are affected by nitrate in the infiltration water. In TH4 it seems like the water is flowing downwards until 6 m.b.s.

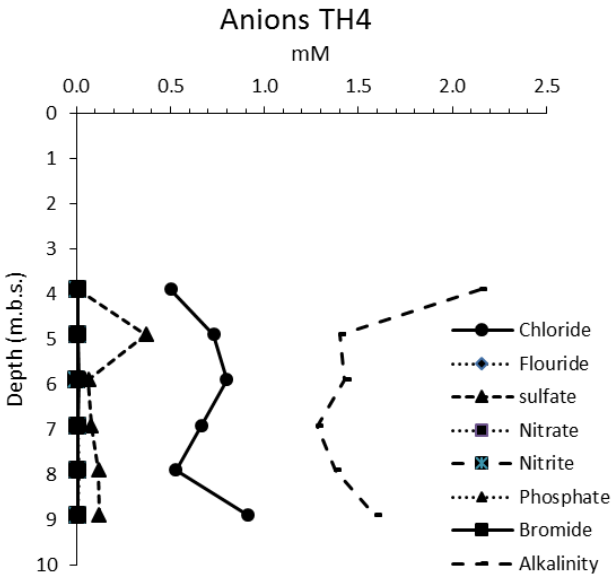

Figure 5.27: Chemical concentrations of anions measured in TH4 in March 2016

5.3.4.2 Summer snapshot - TH3-D and TH3.2

In order to investigate the groundwater chemistry in the summer season, snapshots of the chemistry measured in September 2016 in the two wells TH3-D and TH3.2 are analyzed in the following. The two wells are located respectively 8.7 and 1.5 m from TH3.

TH3.D

The pH in TH3.D from 1.5 to 4 m.b.s. is around 6 while the alkalinity varies from 0.1 to 1.3 meq/L and the concentrations are following the same shape (figure 5.28, A). The concentrations of oxygen are 0.1 mM in 1.5 m.b.s. and close to 0 in the rest of the depths (figure 5.28, B). The Fe^{2+} concentrations are close to 0 mM in 1.5 m.b.s. and varies between 0.01 and 0.05 mM from 2-4 m.b.s.. This means that the environment is anoxic from 2 m.b.s. (figure 5.28, B). The hydrogen sulfide concentration is low in all depths and varies from 0 to 0.3 umol/L (figure 5.28,C).

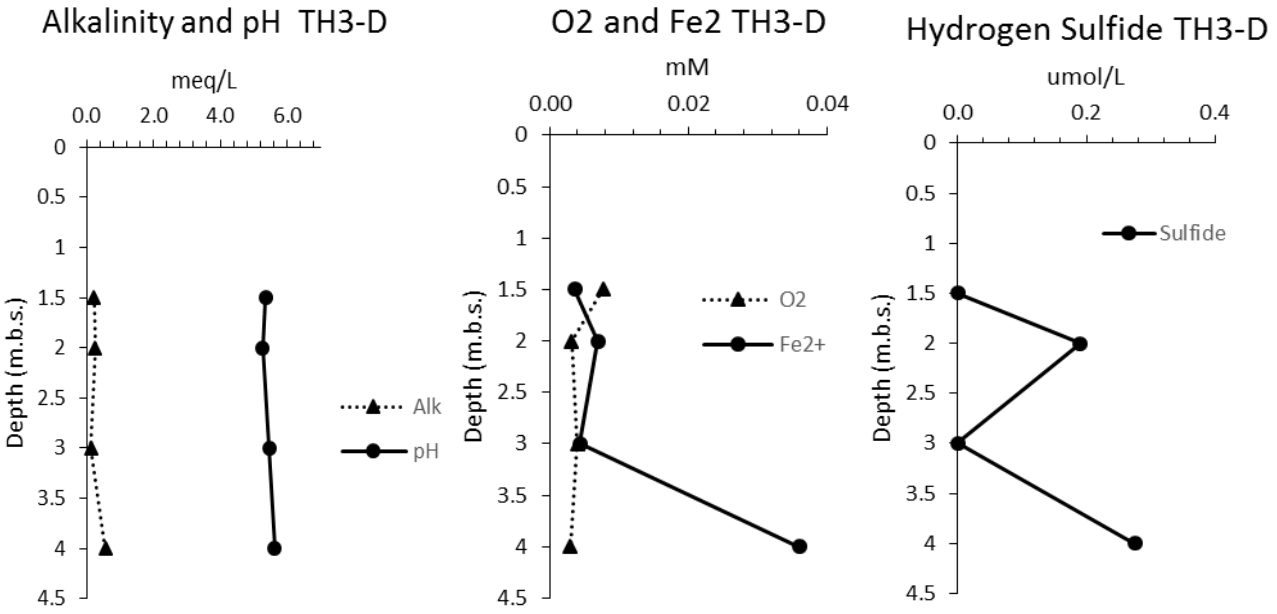

Figure 5.28: Chemical concentrations measured in TH3-D in September 2016. A: measured O2. Fe2+ B: Measured alkalinity and pH and C: measured hydrogen sulfide.

The concentration of anions in TH3-D is found in figure 5.29. It is seen that 0.9 mM nitrate is present in 1.5 m.b.s. and decreases stepwise to 0 mM in 4 m.b.s.. This indicates that a denitrification is going on. The sulfate concentration is increasing from 0.1 to 0.7 mM from 1.5 to 3 m.b.s. In 4 m.b.s. the concentration is increasing to 0.8 mM. The concentration of the alkalinity is decreasing from 1.5 to 3 m.b.s. and increasing from 3 to 4 m.b.s. The chloride concentration varies from 0.5 to 0.8 mM and the concentration of the rest of the anions is around zero in all depths (figure 5.29).

From 1.5 to 2 m.b.s. a pyrite oxidation can take place because the small amount of oxygen is removed and an increase in sulfate and Fe^{2+} is found (figure 5.29). After the oxygen is used, a reduction of nitrate is going on from 1.5 to 3 m.b.s. which with high probability, is generated by pyrite as electron donor due to increase in the sulfate and Fe^{2+} concentration and a decrease in the alkalinity.

From 3-4 m.b.s. the nitrate concentration is still decreasing which means that the denitrification is still going on, but now it can be with both pyrite and organic material as electron donor because an increase in the alkalinity and sulfate are found. The Fe^{2+} is simultaneously increasing, which with high probability is caused by reductive dissolution of iron oxides and denitrification with pyrite as electron donor (Eq. 3).

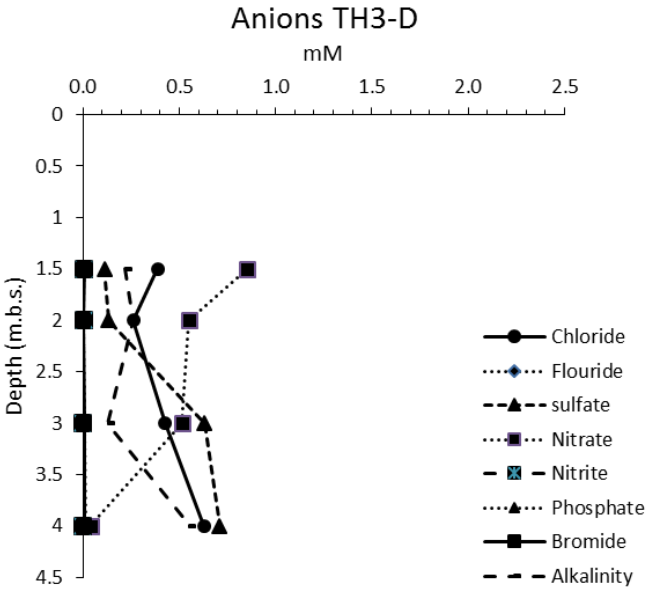

Figure 5.29: Chemical concentrations of anions measured in TH3-D in September 2016

TH3.2

The pH in TH3.2 from 1.5 to 3 m.b.s. is around 6 while the alkalinity varies from 0.1 to 0.5 meq/L (figure 5.30, A). The concentrations of oxygen are close to 0 in all depts. The Fe^{2+} concentrations varies between 0.01 and 0.05 mM, which validates that the samples are correctly performed (figure 5.30, B). The hydrogen sulfide concentrations are low in all depths and varies from 0 to 0.3 umol/L with the highest concentration in 2 m.b.s. (figure 5.30,C).

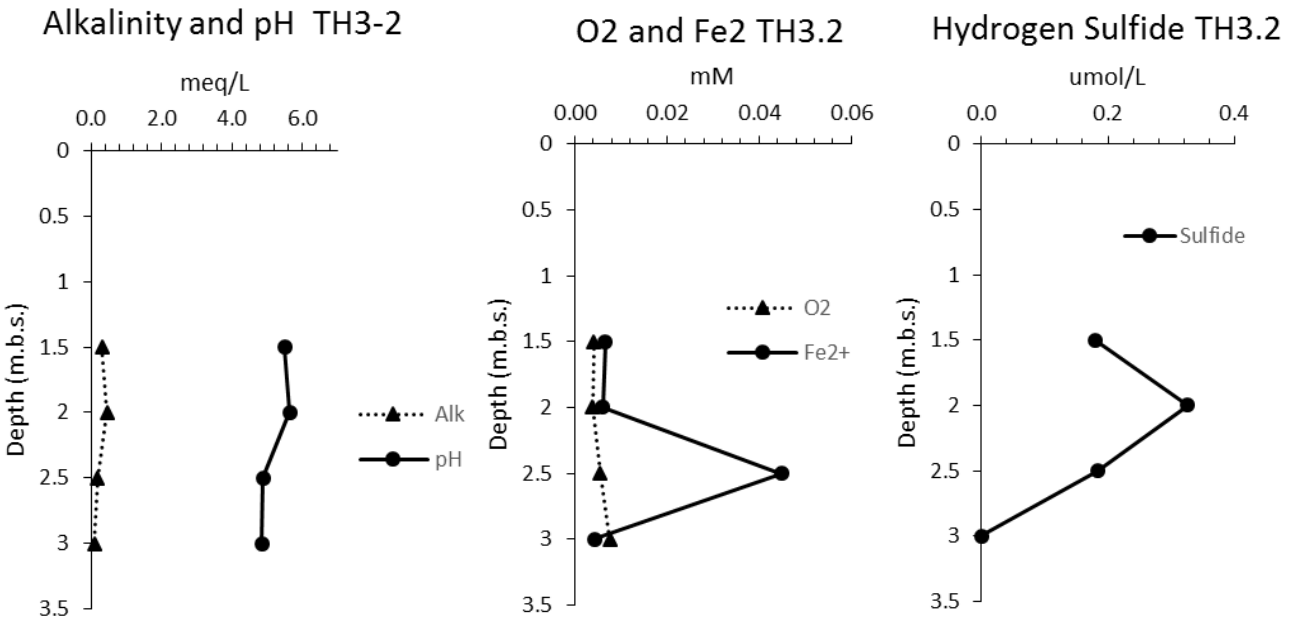

Figure 5.30: Chemical concentrations measured in TH3.2 in September 2016. A: measured O2. Fe2+ B: Measured alkalinity and pH and C: measured hydrogen sulfide.

The concentration of anions in TH3-2 is found in figure 5.31. It is seen that 0.9 mM nitrate is present in 1.5 m.b.s. and is decreasing down to 0 mM in 2.5 m.b.s. and then increasing a bit in 3 m.b.s. This indicates that a denitrification is going on. The small increase in 3 m.b.s. can be due to mixing with other water where the nitrate is not yet removed. The sulfate concentration is increasing from 0.2 to 2 mM from 1.5 m.b.s. to 3 m.b.s. The concentration of the alkalinity is increasing a bit from 1.5 to 2 m.b.s. and decreasing from 2 to 3 m.b.s. The chloride concentration varies from 0.4 to 0.5 mM and the concentration of the rest of the anions is around zero in all depths (figure 5.31).

The decrease in the nitrate concentration means that a denitrification is going on. From 2 to 3 m.b.s. is the denitrification with high probability, generated by pyrite as electron donor due to increase in the sulfate concentration and Fe^{2+}. At the same time, reductive dissolution of iron oxides can take place because a small increase in alkalinity is found and an increase in the Fe^{2+}.

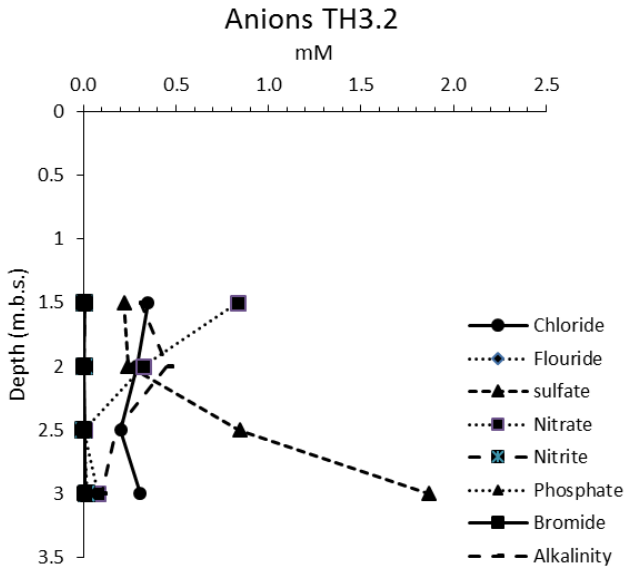

Figure 5.31: Chemical concentrations of anions measured in TH3.2 in September 2016

From the winter and summer snapshots of the water chemistry based on a qualitative analyzes, it is seen that the water infiltrates at the agricultural field and flows downward until around 5 m.b.s. where it is diluted with other water. However, the chemistry composition in the summer season also showed that the water is affected by nitrate input from the fertilizer and that the following chemistry processes is controlling at the agricultural field at EVI2: denitrification with pyrite and organic material as electron donors, reductive dissolution of iron oxides and sulfate reduction. The distribution of the processes is summarized in table 5.1.

Table 5.1: The result of processes from the qualitative analyze of measurements from TH3 representing a winter snap shot and TH3-D representing a summer snap shot.

Meters below surface	From the qualitative analysis of TH3, TH4, TH3.2 and TH3-D
2-3	- Denitrification of nitrate with pyrite as electron donor
3-4	- Denitrification of nitrate with organic material as electron donor. - Reductive dissolution of iron oxides - Sulfate reduction with organic material
4-5	- Sulfate reduction with organic material
5-6	- Mix of water

The fact that there is organic material present in the area makes sense because the study area is located at a subglacial stream trench (figure 2.2). However, the same controlling chemical processes were found in the winter and summer season, some differences is seen in the chemistry composition. These differences will be investigated in section 5.3.5.

5.3.5 Pyrite at EVI2

If pyrite is used as electron donor for the denitrification at EVI2, it requires some pyrite to be present in the soil. Therefore, the content of pyrite is investigated which will be analyzed in the following.
The pyrite extraction experiment shows that there is no pyrite present at EVI2 in 1.6 m.b.s. but from 1.7 m.b.s. to 3 m.b.s. there are (figure 5.32). The amounts ranges from 1.4 to 2.9 mmol/kg dry sediment (see appendix 7 for a table with the concentrations in other units).
The highest amount of pyrite is 2.9 mmol/kg dry sediment which was found in the mixed samples from 2-3 m.b.s. before crushing (figure 5.32). The higher amount in the mixed sample before crushing can be due to oxidation of pyrite at the crushing process or maybe the soil sample represents soil from different places between 2 and 3 m.b.s. The found pyrite concentrations indicate that a denitrification with pyrite as electron donor is possible in the area.

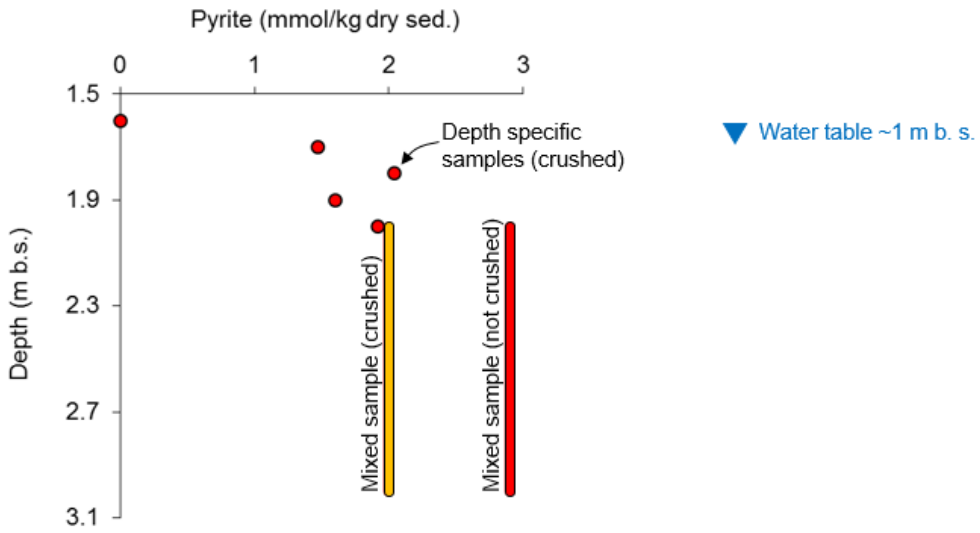

Figure 5.32. The pyrite content in the soil close to the well TH3. The unit is in mmol/kg dry sediment by assuming a porosity at 0.3 and that the rest of the sediments are quarts with a mole weight of 2.65.

The redox front progression as a function of groundwater nitrate concentration and the measured pyrite contents of the sediment at EVI2 is illustrated in figure 5.33. The figure is based on a downward water flow velocity at 0.45 m/yr (based on results from the 2D PHAST model), a porosity of 0.3,

varying nitrate infiltration concentration, a constant oxygen concentration and the pyrite concentration measured in the mixed soil sample from 2 to 3 m.b.s. before crushing. This is because this concentration is highest and assessed as more representative than the sample after crushing (appendix 8 for the calculations). It is seen that the pyrite content of the sediments is a controlling factor as it is found that the nitrate may have significant effects on the downward migration of the redox front (figure 5.33).

By assuming that the nitrate is infiltrating the agriculture field with 1.5 mM as found in the PHAST models, it can be seen that the pyrite front is progression with 1.3 cm/year (figure 5.33). This means that the profile from 0 to 3 m.b.s. has developed during the last 213 years (see appendix 8 for the calculations).

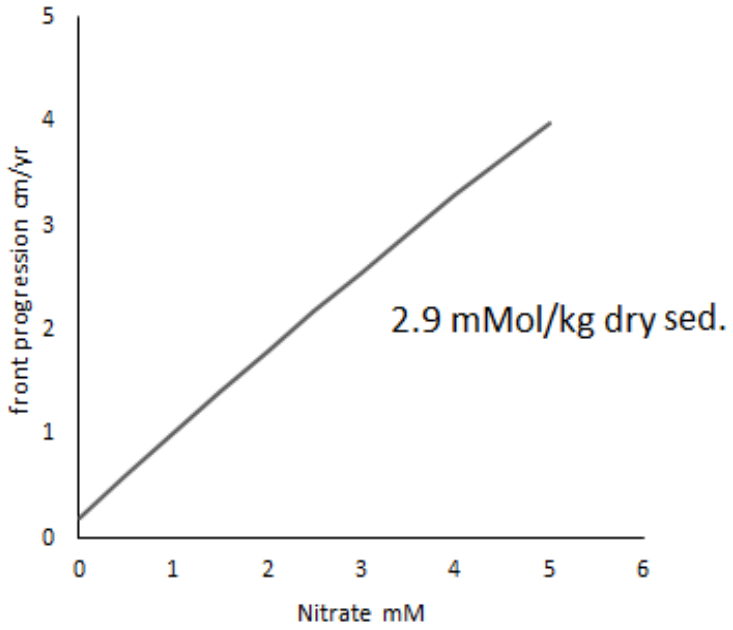

Figure 5.33: Redox front progression as a function of groundwater nitrate concentration and the measured pyrite contents of the sediment at EVI2 in 2-3 m.b.s. The following are assumed: a porosity of 0.3 representing sand and a vertical groundwater flow rate of 0.45 m/yr and a background O2 concentration of 0.33 mM.

5.3.6 Seasonal variations in the water chemistry

In order to investigate the seasonal variations in the water chemistry, the nitrate, sulfate and temperature are plotted for TH3 which represents the chemistry in the winter season, and for TH3.2 and TH3-D representing the summer season.

5.3.6.1 Seasonal variations at the agricultural field

The nitrate concentrations is different between the summer and winter season. In 2 m.b.s. a higher concentration is found in the winter season (figure 3.34). In all three wells, the nitrate is removed due to denitrification. In TH3 and TH3-D the nitrate is totally removed in 4 m.b.s.. For TH3.2, the nitrate is already removed in 3 m.b.s. (figure 5.34). The sulfate is increasing in 2-3 m.b.s. in all three wells, which can indicate denitrification with pyrite as electron donor (figure 5.34).

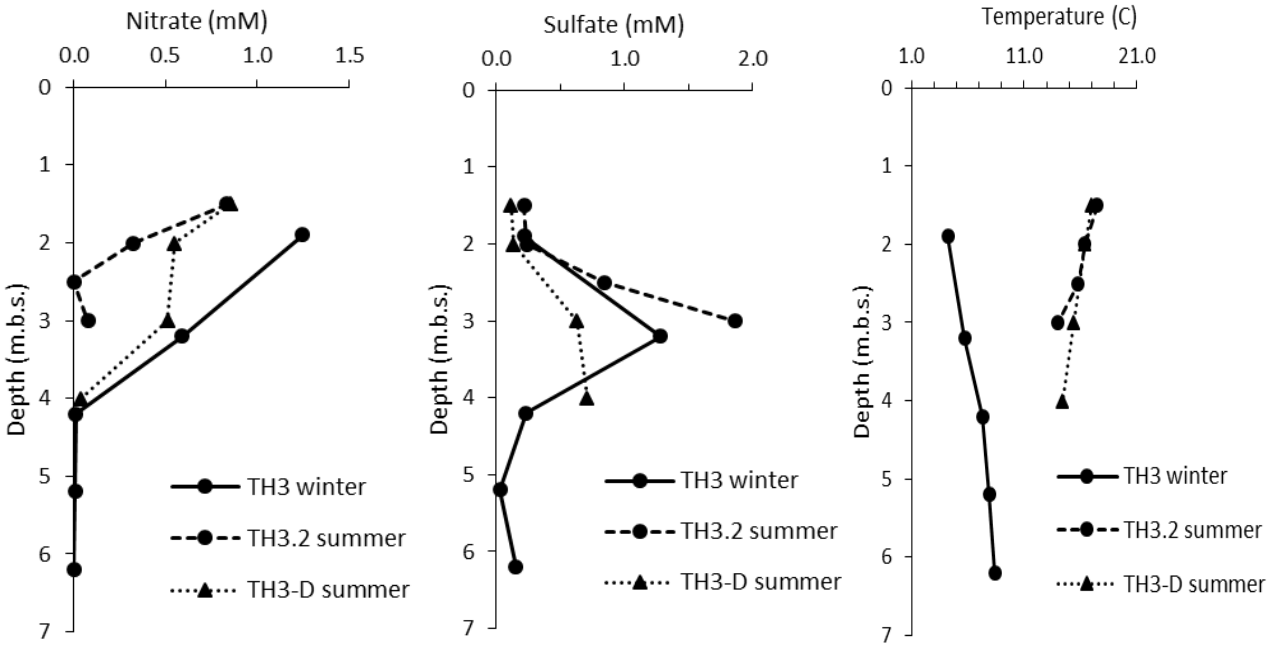

Figure 5.34: The seasonal variation in nitrate, sulfate and temperature at the agricultural field, EVI2. The winter measurement is from February 2016 and the summer measurement is from September 2016.

The chemistry measurements in the summer and winter season, show that the nitrate is removed due to denitrification with pyrite as electron donor in the summer season but also with organic material as electron donor in the winter season. The summer measurements only go down to 3 m.b.s. and an increase in the sulfate was found in that depth (figure 5.34). Therefore, it is unknown if the sulfate is reduced with organic material in the summer season, as it was seen in TH3 and TH4 in the winter season, but it is probable also going on in the summer season.

The composition of chemistry is similar in TH3 and TH3-D located 8.7 m from each other and different between TH3 and TH3.2, which is, located 1.5 meter from each other.

The different chemistry concentration in TH3.2 compared to TH3 and TH3-D is with high probability due to heterogeneity. However, the differences in the nitrate concentration in 2 m.b.s. between summer and winter (figure 3.34), can be due to a higher rate of denitrification in the summer with is

causes by higher temperatures (figure 5.34 and section 3.2). However, the differences can also be because the wells are not located at the same location or leaching. It should be kept in mind that the temperature measurements are indicative because they are measured in the flow cell and by that affected by the temperature in the atmosphere.

Figure 5.35 shows the isotope distribution in TH3, TH3.2 and TH3-D. If the same water flows in TH3.2 as in TH3, only small differences in the $\delta_{18}O$ should be found, due to higher evapotranspiration in the summer season, which can result in higher amount of $\delta_{18}O$ due to a higher amount of the heavy isotope $_{18}O$ in the water (Fitts, 2013). However, by looking at the isotope distribution in figure 5.35, it can be observed that the concentration in TH3.2 is different from TH3 but that the concentration in TH3-D is similar to TH3. This indicates that there is heterogeneity in the area.

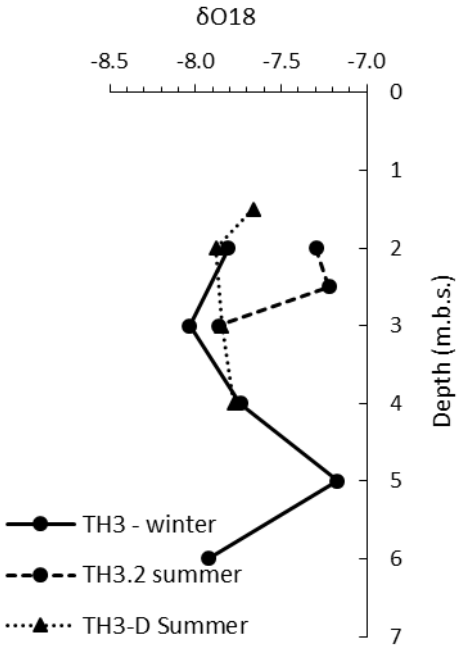

Figure 5.35: The seasonal isotope O18 variations between summer and winter at the agricultural filed, EVI2. The winter measurement is from February 2016 and the summer measurement is from September 2016.

5.3.6.2 Seasonal variation in the springs at the wetland area at EVI2

Figure 5.36 shows how the nitrate concentrations measured in the springs at the wetland area at EVI2 change over time. It is seen that the concentration of nitrate in the spring near the stream is around 0.75 mM both in the winter and summer measurement but the spring at the drainage shaft is a bit higher in the summer measurement compared to the winter measurement. This spring is the spring where the highest concentration of nitrate is measured (figure 5.36). The nitrate concentration in the

stream and in the drain is close. In the summer season, the drain was dry due to less precipitation, which is illustrated in the figure with a nitrate concentration of 0. In addition, it is seen that the stream contains less nitrate in the summer season compared to the winter season (figure 5.36). This makes sense since the plants at the agricultural fields in the winter season are gone due to harvest. Therefore the nitrate is not used by the plants and by that, a higher nitrate leaching can occur. At the same time, the precipitation is higher in the winter season, which also generates higher nitrate leaching to the stream.

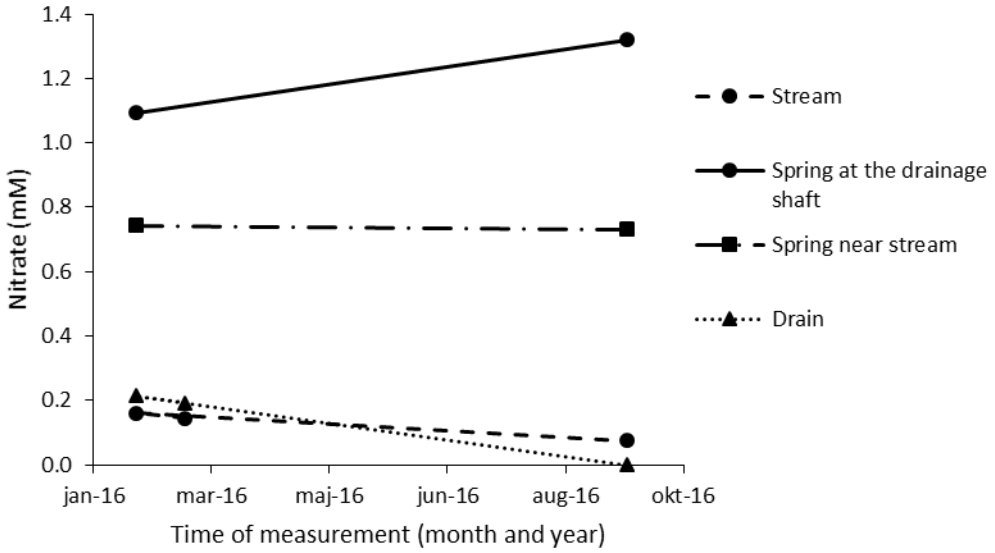

Figure 5.36: The seasonal variations in the nitrate concentration in the springs at the wetland area

5.4 3D groundwater modeling at catchment scale

In the following, the results from the 3D GMS model is presented and analyzed. This includes investigation of the groundwater flow at EVI2, the origins and ages of the water in the stream and in the wetland area.

5.4.1 Groundwater flow in Holtum catchment

The groundwater flow in Holtum catchment without drain is illustrated in figure 5.37. It is seen that the water flows from the eastern part of the catchment toward the outlet of Holtum stream in the western part of the catchment (figure 5.37).

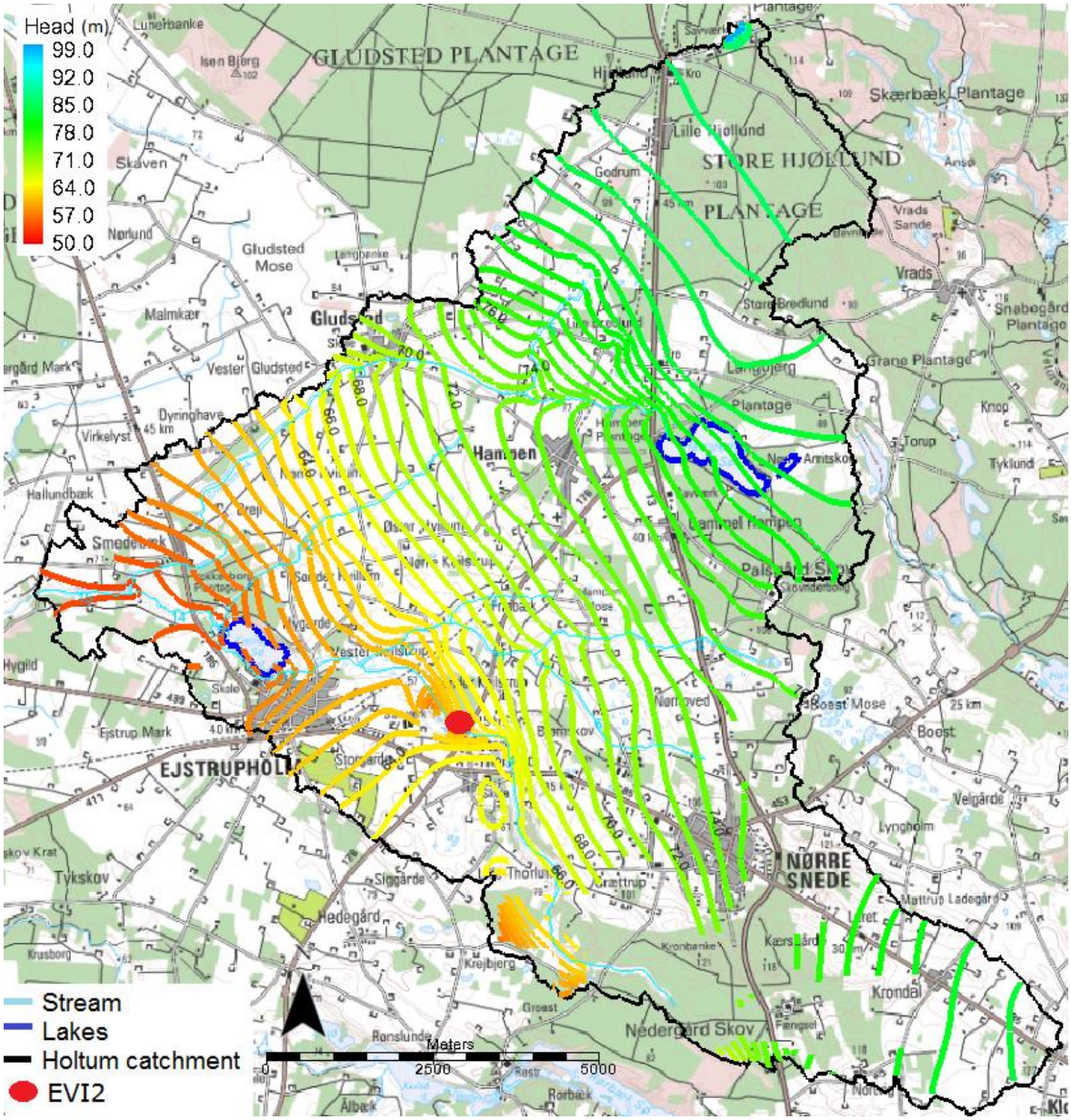

Figure 5.37: The groundwater flow in the 3D model without drain for Holtum catchment.

The including of the drain in the Holtum catchment does not affect the general groundwater flow in Holtum catchment that looks the same as without drains included. The location of the drains can be seen in figure 4.6.

The recharge is the main source of water input in both models and represents over 99% of the incoming water. However, a small amount of water from the stream network is recharging to the aquifer in the model including drain (appendix 16).

The sinks in the water balance for the models with and without including drainage are presented in figure 5.38. The drains influence can be seen at the sinks in the water budget for the two models (figure 5.38). It is found that the drain removes 13% of the water in the model, which otherwise would have entered the stream as stream leakage. This is seen by the sinks in the model without drain (figure 5.38).

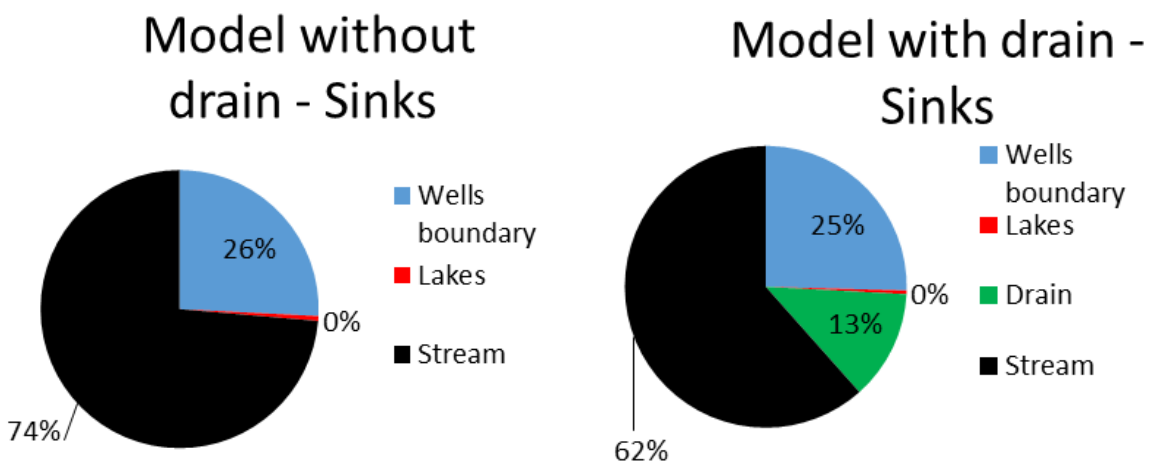

Figure 5.38: The distribution of the different sinks in the water budget for the two 3D groundwater models with and without drain included.

The RMSE calculated for the simulated and observed head in the model without drain is 4.13 m while the RMSE for the GMS model with drain is 3.84 m. This means that the model including drain gives a better output of the model compared to reality. The 1-1 lines of the observed vs. simulated heads is found in appendix 11.

5.4.2 Groundwater flow at EVI2 - from catchment scale to local scale

The groundwater flow in EVI2 generated by the 3D GMS model is seen from figure 5.39. This means that the groundwater flow in the study area is based on boundary conditions from the entire catchment with eight geological layers included in the model.

It can be observed that the water flows from the northern part of the study area towards Holtum stream and that some of the water actually flows from the stream towards the southern part of EVI2 (figure 5.39). The flow paths at the northern part of the stream corresponds to the flow paths that was found based on an isopotential map of the measured hydraulic heads at EVI2 (figure 5.1). The flow arrow

from the stream towards the southern part of EVI2 can represent that water flows under the stream and enters the wetland.

It can be observed that the calibration targets are yellow and green (figure 5.39). The yellow represents 3 meter to high water level. This can be because of some scale problems by going from catchment scale to investigating the groundwater flow at local scale. The smallest grid size the model could run with in EVI2 was 25x25m. This means that along the stream the same hydraulic head is simulated for one cell representing both the stream and the wells located close to the stream. The method used to represent the springs at the wetland side of the stream as a drain polygon can perhaps be too simple. The conductance was sat as high as possible in the simulation and still not enough water was removed to lower down the simulated hydraulic heads in the wells.

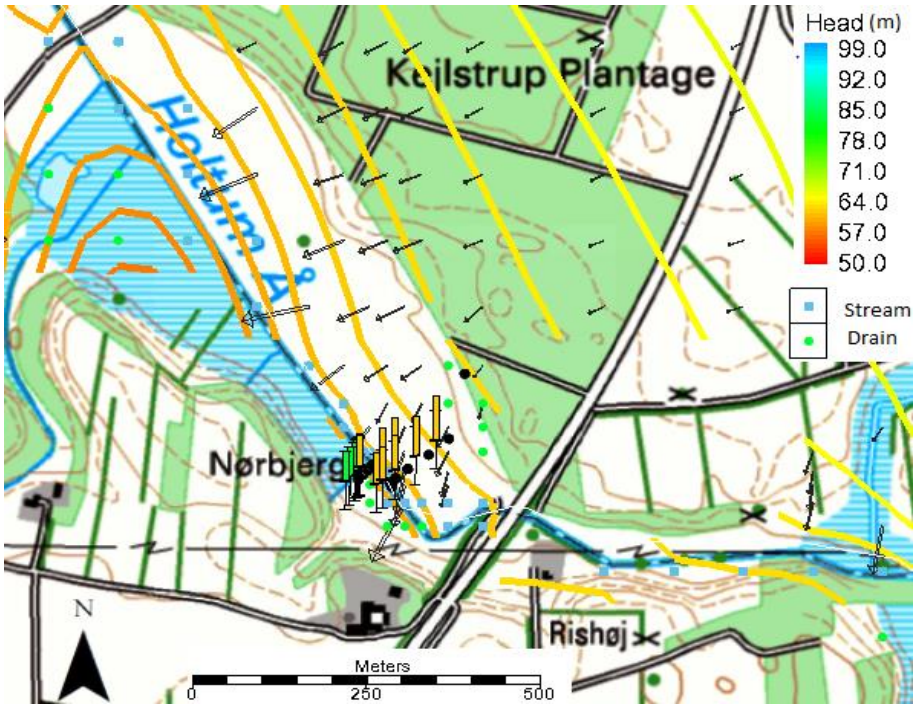

Figure 5.39: The groundwater flow in EVI2 in the 3D model for Holtum catchment. The observation targets for the wells located at EVI2 is showed.

The flow budget is investigated for the cells representing the wetland area at EVI2. It is found that the drains in the wetland area remove 1709.8 m^3/day (appendix 16), which by dividing the number with the number of springs in the wetland corresponds to a discharge of 342 m3/day for each spring. This number is high compared to the measurements of the discharge in the springs in September 2016 that was measured to 14.6, 56.3, 80.7, 22.0 and 29.4 m^3/day. In total 203.1 m^3/day (Steiness M., et al. 2016, unpublished). Given the simplicity of the 3D model and the approach, this is in good agreement with the measured discharges.

In order to investigate the incoming water at the aquifer at the agricultural field at EVI2, a flow budget for this area is explored (it is assumed that the extent of the aquifer is down to the underlying clay layer in the model which is layer 6, given the name budget zone 600 (appendix 16). It is found that the water is entering the agricultural field from the two top layers consisting and not from the underlying clay layer. This means that there is no leakage from the underlying clay layer (appendix 16) (figure 5.6).

5.4.3 The origins and age distribution of the groundwater in the wetland area and stream at EVI2

The particle tracking is used in order to investigate the origins of the particles going into the springs at the wetland area and into the stream at EVI2. This is done by exploring the pathways of the particle's travel before infiltration of the wetland area and the stream bed. Afterwards, the age distribution of the particles is investigated.

The pathways for the particles entering the wetland area at EVI2 are presented in figure 5.40 and 5.41. It is seen that the lengths of the pathways vary a lot. Some of the particles originate close to the stream and some originates from far away close to the catchment outlet (figure 5.40). The pathways are complex and dominated by both vertical and horizontal pathways due to the varying geology in the model (figure 5.41). Figure 5.41 shows that the particles entering the wetland flows in the deepest sand layer. This means that the nitrate that is measured in the springs in the wetland area at EVI2 based on this model can originate from agricultural field sites mainly located in the eastern part of the catchment.

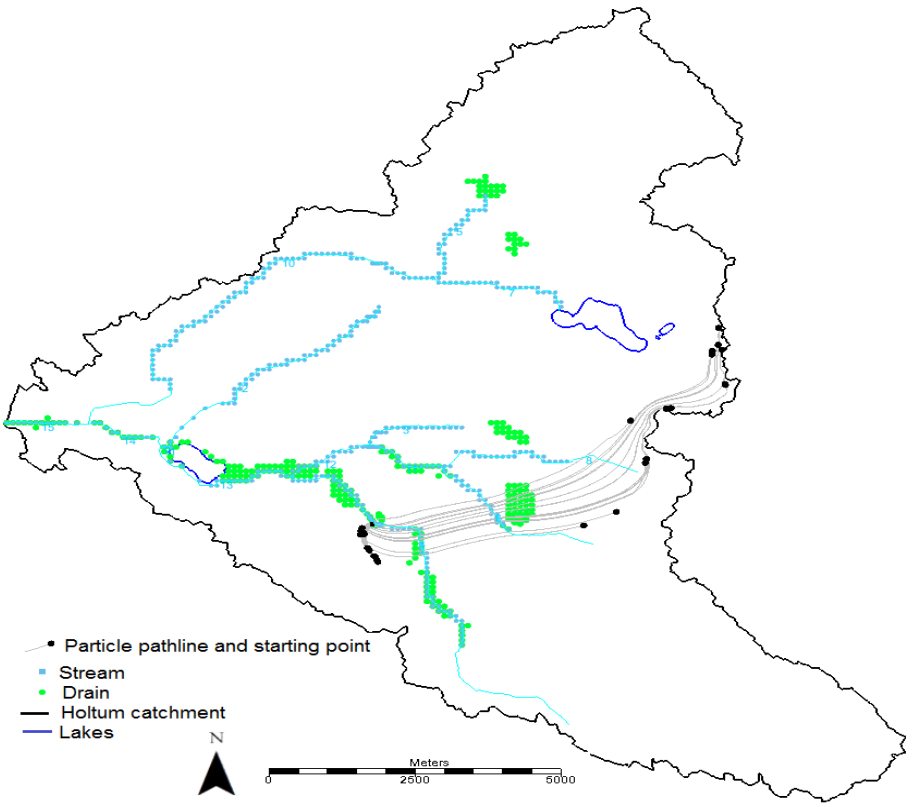

Figure 5.40: The pathlines of the 100 particles going into the wetland area at EVI2 showing the origins of the water particles in a spring at EVI2.

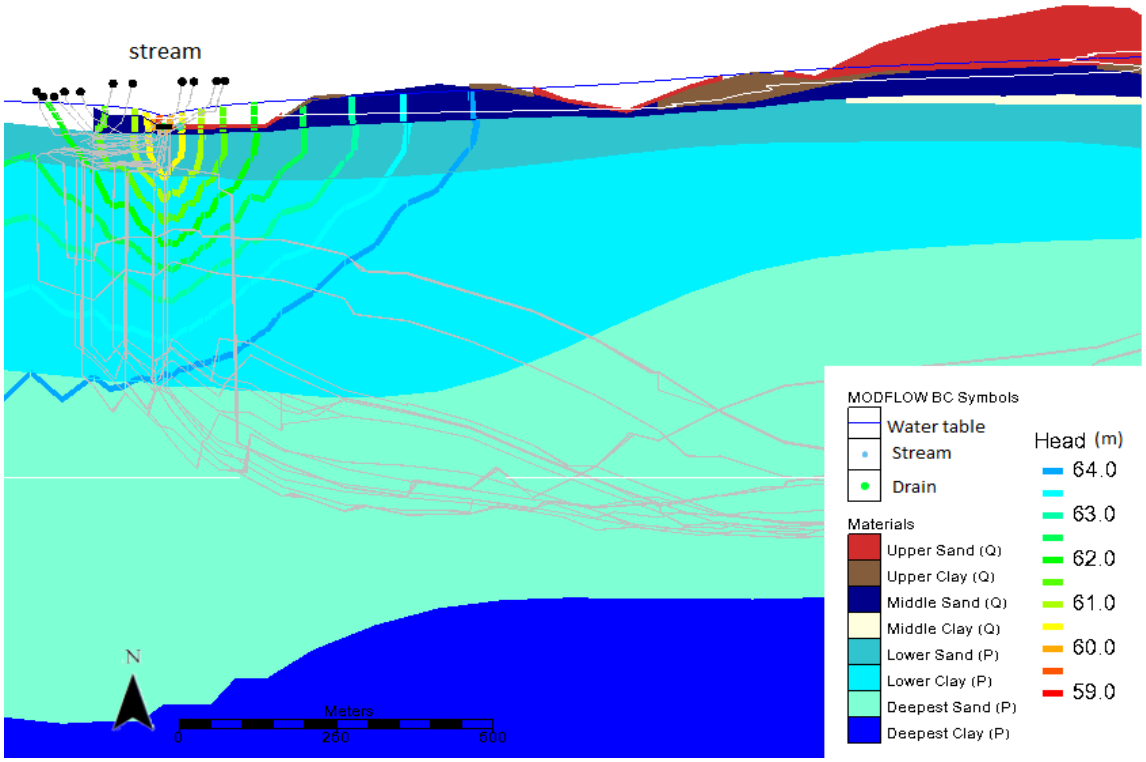

Figure 5.41: Crossection of the pathlines for the 100 particles entering the springs in the wetland area at EVI2 showing the origins of the water particles in the stream.

The pathways for the particles entering the stream at EVI2 are presented in figure 5.42 and 5.43. It is found that the path lengths are shorter compared to the particle entering the wetland area (figure 5.40). Some of the particles originate from the agricultural field at EVI2 and others from the wood plantation located right next to EVI2 (figure 5.42). At the same time, it is seen that the particles are only flowing in the upper sandy layers in the model (figure 5.43).

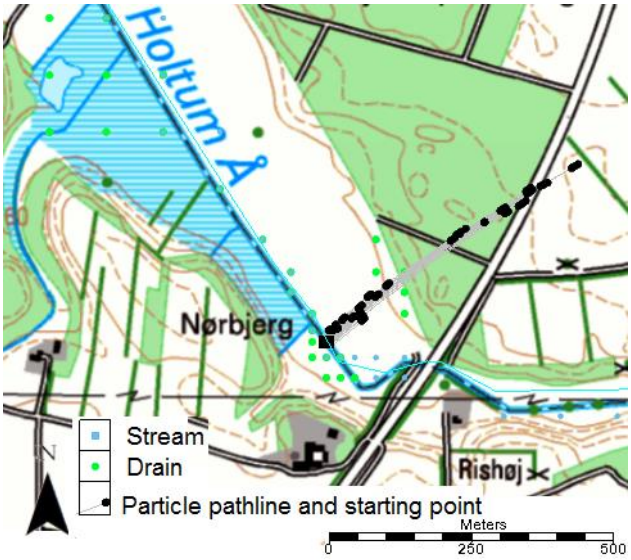

Figure 5.42: The pathlines of the 100 particles going into the steam at EVI2 showing the origins of the water particles in the stream.

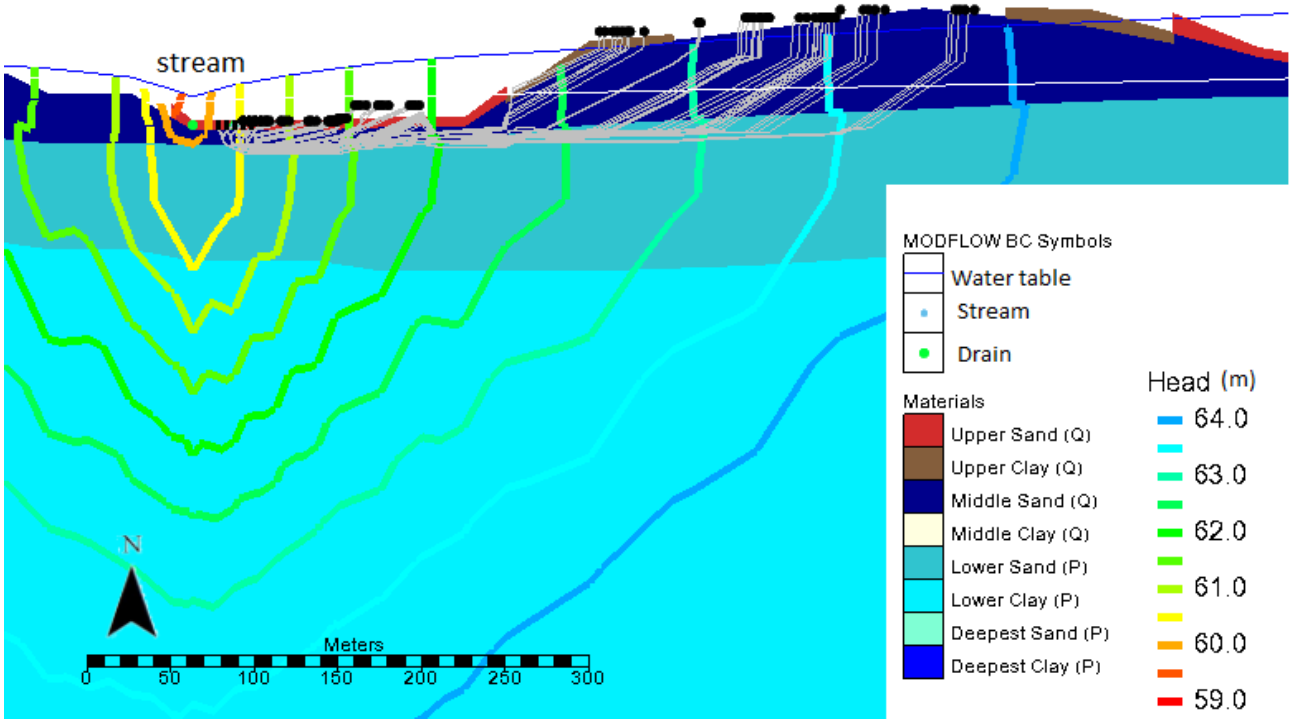

Figure 5.43: Crossection of the pathlines for the 100 particles entering the steam at EVI2 showing the origins of the water particles in the stream.

Comparing the isopotential lines for the hydraulic head in the 3D model (figure 5.41 and 5.43) with the isopotential map based on the measured hydraulic head in the wells at EVI2, it is seen that the measured head is lower than the simulated (figure 5.1). This illustrates the difficulties of match head in the riparian zone.

The age distribution of the particles entering the wetland area at EVI2 is presented in figure 5.44. It is found that most of the particles are either relatively young or old (figure 5.44). Several of the particles are relatively young between 1 and 20 years old and some of the particles are relatively old between 130 and 150 years old. This makes sense because the length of the pathways was different which is also seen from the maximum and minimum age (figure 5.40 and 5.44). Similarly, it is seen that 36% + 7 %= 43% of the particles are young, which is nearly half of the particles. This can explain the nitrate measured in the springs at the wetland because younger particles in general haves a lower opportunity for flowing though anoxic environments where denitrification is possible and also time is recurred for the denitrification to happen (section 3.2).

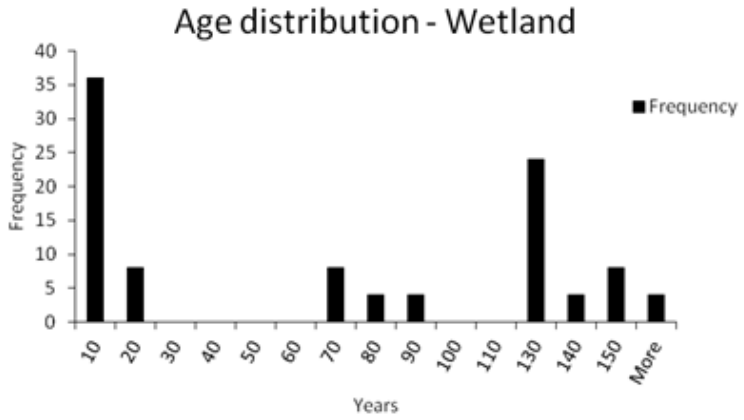

Age distribution	Years
Max	153.5
Min	2.4
Median	66.4
Average	67.3
Standard deviation	59.0

Figure 5.44: Age distribution of the 100 particles in a cell representing a spring at the wetland side of the stream at EVI2 divided into groups of 10 years and a table showing the max, min, median, average and standard deviation of the age distribution.

From figure 5.45 the age distribution of the particles entering the stream at EVI2 is seen. Compared to the particles entering the wetland, the particles entering the stream are younger which was also expected, due to the shorter pathways for the particles in the stream (figure 5.45 and 5.42). It can be seen that most of the particles in the stream has a low age because the median values are closer to the minimum value than the maximum (figure 5.45).

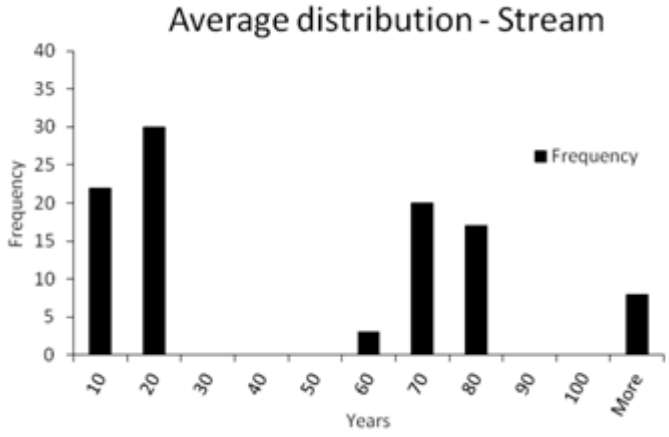

Age distribution	Years
Max	125.8
Min	4.7
Median	16.6
Average	42.6
Standard deviation	36.4

Figure 5.45: Age distribution of the 100 particles in the stream at EVI2 divided into groups of 10 years and a table showing the max, min, median, average and standard deviation of the age distribution.

5.5 Qualitative groundwater chemistry modeling at local scale

The chemistry processes at the agricultural field at EVI2 are in the following analyzed quantitatively by modeling. First by use of a simple 1D model and secondly by 2D models, by assuming no flow in y direction. The 2D modeling includes the groundwater flow and kinetic. It should be kept in mind that the chemistry modeling is based on the winter snapshot of the water chemistry.

5.5.1 1D chemistry modeling in PHREEQC

The results from the 1D PHREEQC model is found in figure 5.46 and 5.47. The figures show the simulated and measured chemical concentrations and in which m.b.s. the different processes are defined in the model. The locations of the chemical processes are based on the qualitative analyzes of the controlling chemistry processes at the agricultural field (section 5.3.4).

The simulated concentrations of Fe^{2+}, alkalinity, pH, nitrate and sulfate are following the measured concentrations in TH3 (figure 5.46 and 5.47). The poorest match is the sulfate simulations. The 1D model simulates the same shape in the distribution of sulfate concentrations but the peak seen in 3 m.b.s. in TH3 is simulated too low. Perhaps, this can be because the model is too simple or alternatively, that too much organic matter is available for sulfate reduction in the model.
The fact that the simulations are similar with the measurements in TH3 means with high possibility that it is the controlling chemistry processes at the agricultural field at EVI2 that are included in the simple 1D model for TH3.

A speciation of TH3 and TH4 based on the chemical measurements in the different depths was simulated by PHREEQC (appendix 9). It was found that mackinawite is supersaturated from 4.2 to 6.2 m.b.s. in TH3, which is a precursor to pyrite formation and means that precipitation of pyrite is possible here. Additionally, it is seen that precipitation of pyrite from 3.9 to 8.9 m.b.s. is possible in TH4 (appendix 9). This means that the pyrite present in the sediment underneath the agricultural field at EVI2 can be authigenic pyrite, which means that it is formed at the location (Hunger and Brenning, 2007).

Summarized the simple 1D model shows that the controlling processes at TH3 with high probability is distributed in the following depths: From 2- 3 m.b.s. denitrification with pyrite as electron donor. From 3-4 denitrification with organic material as electron donor, reductive dissolution of iron oxides (in the model represented as goethite) and sulfate reduction with organic material and from 4-5 m.b.s. sulfate reduction (figure 5.46 and 5.47).

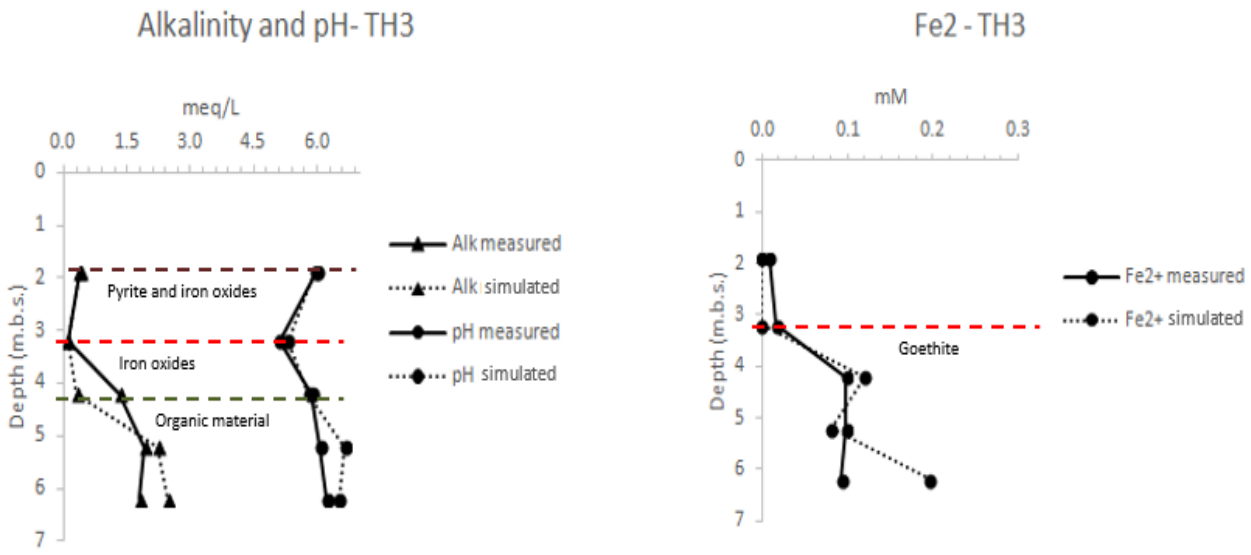

Figure 5.46: A: The observed and simulated alkalinity and pH in TH3 from the 1D PHREEQC model. B: The observed and simulated Fe2+ in TH3 from the 1D PHREEQC model.

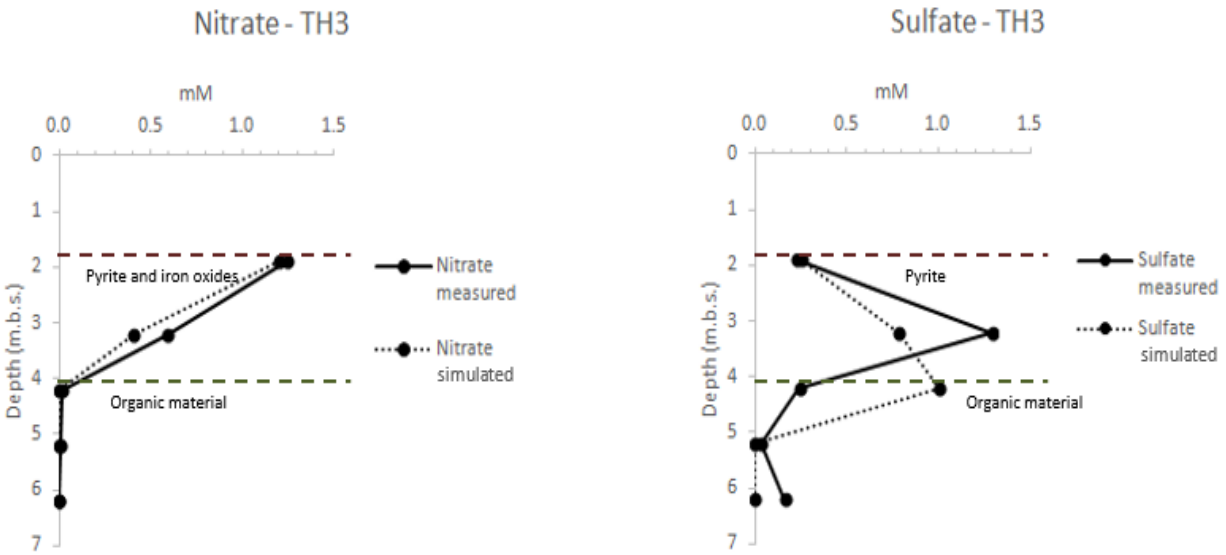

Figure 5.47: The observed and simulated nitrate (A) and sulfate (B) concentration in TH3 from the 1D PHREEQC model.

5.5.2 2D groundwater and chemistry modeling in PHAST

In the following, the results from the 2D PHAST models are analyzed. First, the groundwater flow pattern is analyzed. Second, the nitrate and sulfate distribution in the 2D models is analyzed. Third, the rate transferred pyrite and organic material are investigated followed by a analyze of the simulated chemical concentrations in the cells in the models corresponding to the location of the wells TH3, TH4, TH1 and TH2 is similar to the measurements in the wells. The models are created in order to investigate if 2D modeling can simulate the measured chemistry at EVI 2. The flow paths found by the measured hydraulic head and the 3D GMS model for EVI2 shows that the water in EVI2 flows from north towards the stream in south. Therefore, the models are in 2D with a neglect of groundwater flow in y direction.

5.5.2.1 2D groundwater flow in EVI2

Figure 5.48, 5.49 and 5.50 show the groundwater flow in the three 2D PHAST models. In all models, the water is entering the model by incoming recharge and from the northern boundary, which makes the water to flow towards the stream in the southern part of the model.

The same flow velocities are to be found in the model A, due to homogeneous conditions. For model B, which is also homogeneous but included drain, it is seen that the water flows towards the stream but also towards the drain. The drain takes away some of the water, which means that the flow velocities are affected around the drain. For model C with heterogeneous conditions, the water also

flows towards the stream and drain but for this model, the water velocities are affected by the properties of the different geology in the model. This means that the water prefer to flow in the cells with high hydraulic conductivity (figurer 5.48, 5.49 and 5.50).

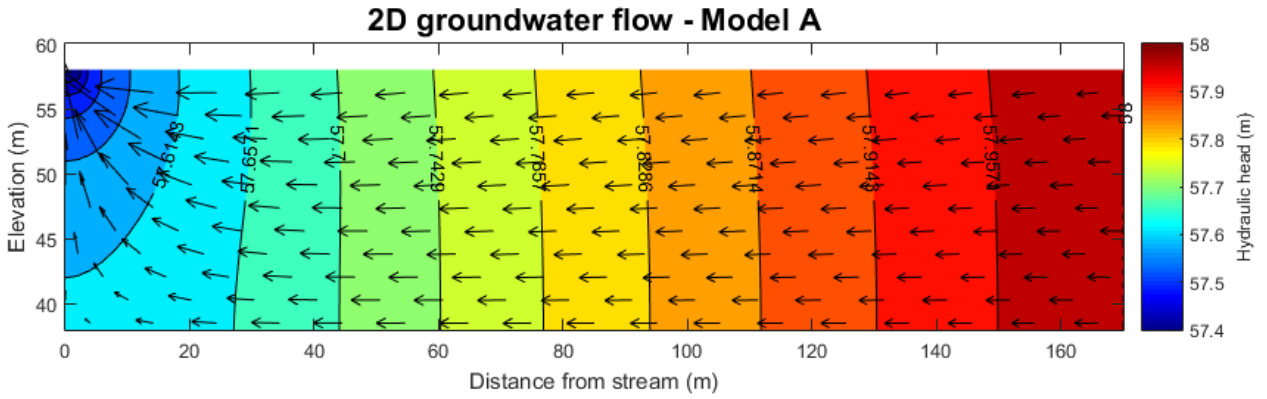

Figure 5.48: The flow pattern in the homogeneous 2D PHAST Model A.

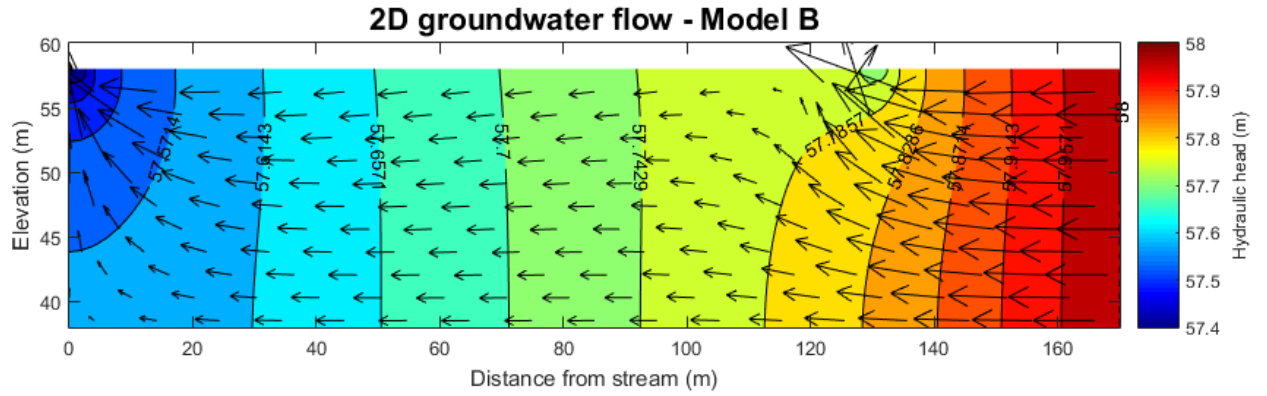

Figure 4.49: The flow pattern in the homogeneous 2D PHAST Model B with drain

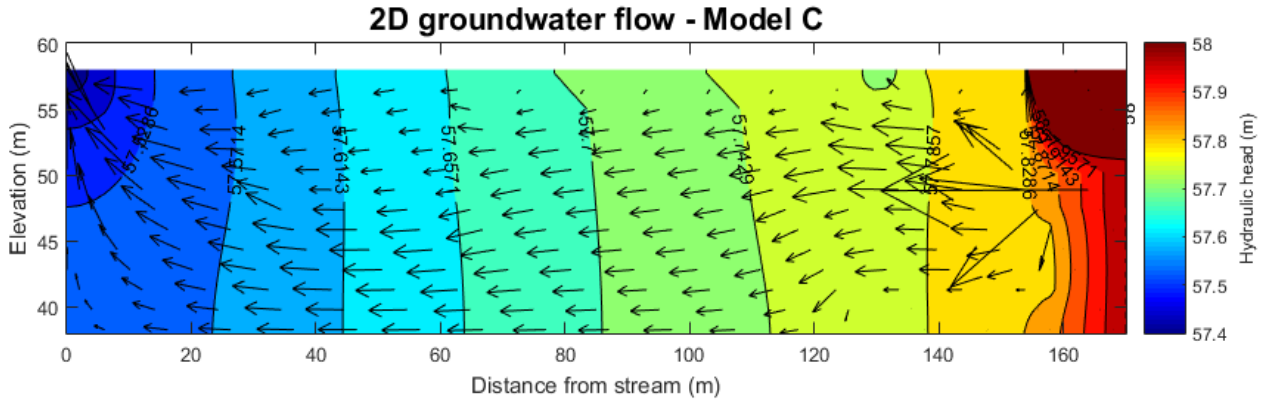

Figure 5.50: The flow pattern in the heterogeneous 2D PHAST Model C

The RMSE for all three models are calculated in MATLAB (appendix 13). The RMSE is for model A, B and C respectively 0.12 m, 0.08 m and 0.08 m (table 5.2). From this, it can be assumed that the simulated hydraulic head is in good agreement with the measured and the best fit is found for model B and C that are equally good. However, it should be kept in mind that the RMSE is only calculated based on nine measurements.

In model B, the drain removes to high amounts of water compared to the measured. In model C the drain removes too little (table 5.2). This means that the 2D model can be too simple. The Darcy flux in the stream for the different models is seen in table 5.2. It is found that all three models simulates to high fluxes compared to the observed flux at 0.06 m/day (table 5.2) (Steiness et al, 2016). This can be because the 2D models are too simple to simulate the reality and that maybe some of the recharging water is flowing from the agricultural field and northern part of EVI2 underneath the stream. This water can then enter the wetland area at EV2 by upwelling. This can explain the springs at the wetland area. If this is the case, the water entering the wetland area must be mixed with some water from somewhere else because it is containing nitrate and the chemistry measurements from the agricultural field shows that no nitrate is present under 3 m.b.s. at the agricultural field (figure 5.15 and 5.22).

Table 5.2: The differences in RMSE, Drain, stream q and which nitrate concentration that infiltrates the area in the different PHAST models. The q was measured in September 2016 by Steiness et al.

	RMSE (m)	Drain (m^3/day)	Nitrate con. in solution 1 (mM)	Stream q (m/day)
Observed		0.295		0.05
Model A: Homogeneous	0.12	-	1.3	0.31
Model B: Homogeneous with drain	0.08	0.67	1.5	0.25
Model C: Heterogeneous with drain	0.08	0.07	1.3	0.21

5.5.2.2. Solute transport of a conservative tracer Chloride in the different PHAST model simulations

The chloride distribution in the 2D models is presented in figure 5.51, 5.52 and 5.53, which represents solute transport of a conservative tracer at EVI2. It is found that chloride is transported with the water flow towards the stream due to advection. In model A, the chloride is present in the upper 8 m.b.s. and afterwards diluted with water without chloride that enters the model from the northern boundary. In model B and C it is seen that chloride poor water is entering the model from the northern boundary and flows upwards due to the drain, where it is diluted with the chloride rich water, before it flows downward again (figure 5.49, 5.50, 5.52 and 5.53). The largest amount of chloride is found in model C where the heterogeneity in the geology has an influence (figure 5.53 – C).

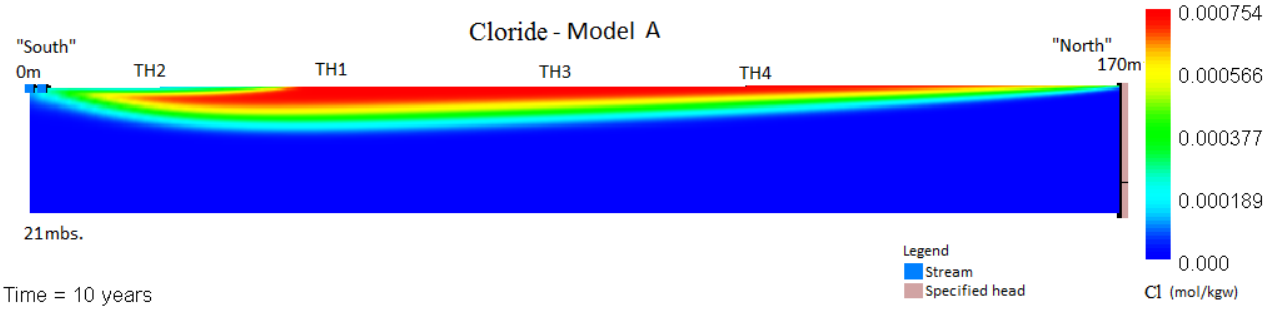

Figure 5.51: The chloride distribution in the homogeneous Model A after 10 years, simulated in PHAST.

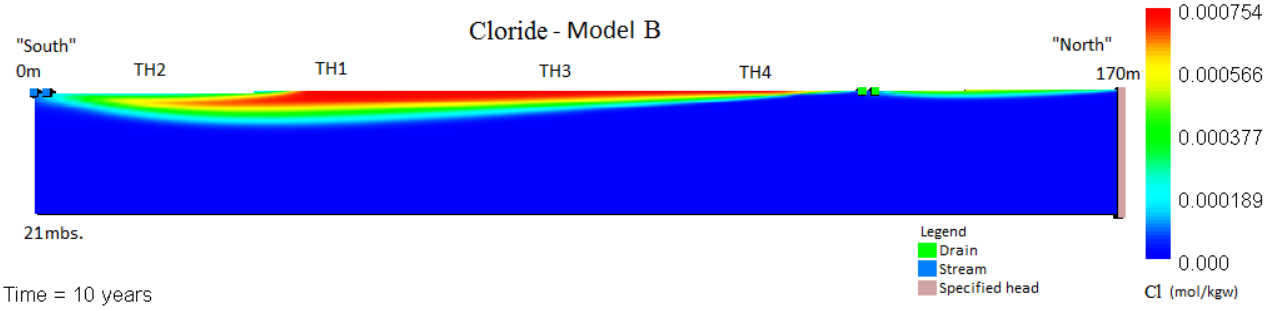

Figure 5.52: The chloride distribution in the homogeneous Model B with drain after 10 years, simulated in PHAST.

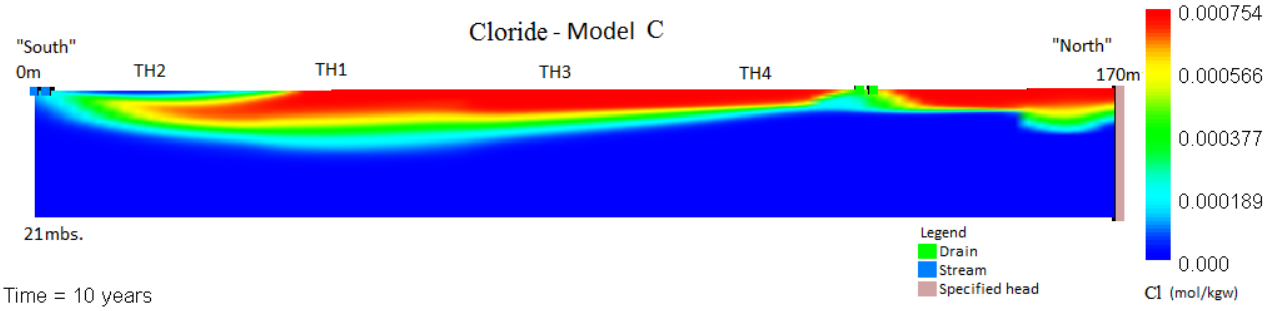

Figure 5.53: The chloride distribution in the heterogeneous Model C with drain after 10 years, simulated in PHAST.

5.5.2.3. The nitrate distribution in the different PHAST model simulations

The nitrate distribution in the 2D models is presented in figure 5.54, 5.55 and 5.56. It is found that nitrate is present in the upper 3 m.b.s. and afterwards removed which is due to denitrification with pyrite and organic material as electron donors and also dilution with water without nitrate that enters the model from the northern boundary. In model B and C, it is seen that nitrate poor water is entering the model from the northern boundary and flows upwards due to the drain, where it is diluted with the nitrate rich water before it flows downward again (figure 5.49, 5.50, 5.55 and 5.56).

Model B simulates higher concentration of nitrate compared to model A and C which is due to the higher amount of nitrate in the recharge. The nitrate distribution in model C is more complex due to the heterogeneity and because of that, the influence of the geology and drain can be observed from this model C compared to model A and B (figure 5.54, 5.55 and 5.56).

In all models, the nitrate is transported towards the stream due to advection and dispersion and the nitrate is also present in the buffer zone close to the stream (figure 5.54, 5.55 and 5.56). No nitrate was found in the wells located at the buffer zone (figure 5.15). This can be because the organic material present in the sediment at the buffer zone in reality is younger than the organic material at the agricultural field. By that, the nitrate can be removed at the buffer zone with a higher reaction rate (Postma et al. 2012). It should also be remembered that the model is only a simplification of natural varying condition and do not include seasonal variation in the nitrate inputs to the aquifer. It is also assumed that pyrite and organic matter is present equally at the agricultural field and buffer zone but there could be areas in the anaerobic zone without or with lower concentrations of pyrite or organic matter.

Compared to solute transport of chloride in the models it is seen from the nitrate distribution that the present of pyrite and organic material has a high impact due to the capability of removing nitrate by denitrification (figure 5.54, 5.55, 5.56, 5.51, 5.52 and 5.53)

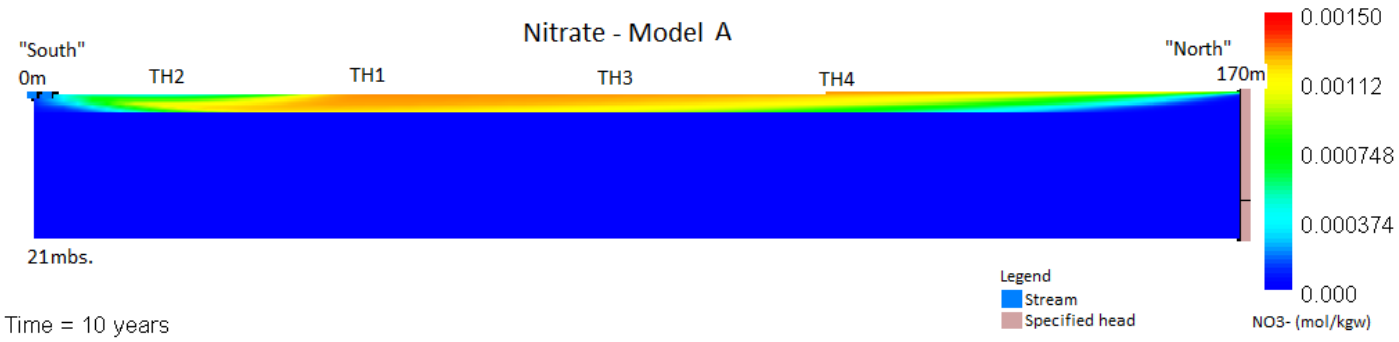

Figure 5.54: The nitrate distribution in the homogeneous Model A after 10 years, simulated in PHAST.

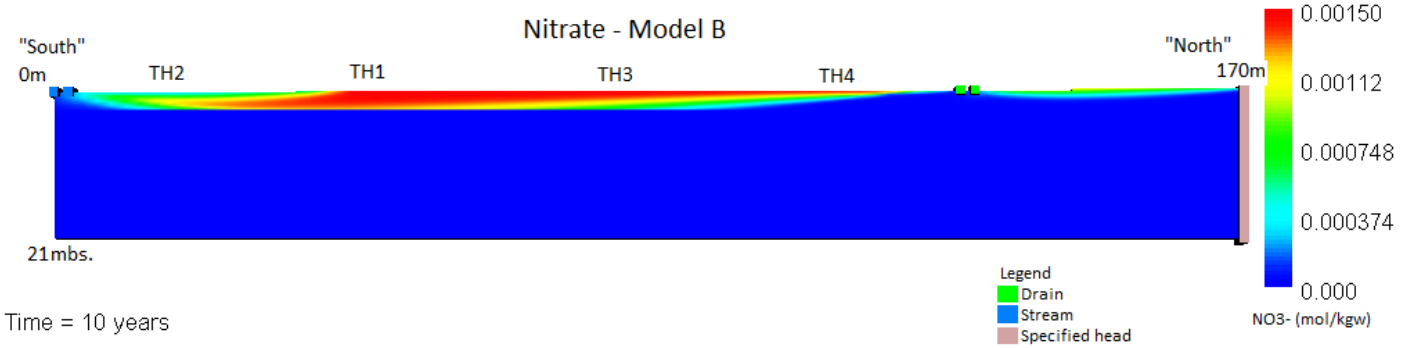

Figure 5.55: The nitrate distribution in the homogeneous Model B with drain after 10 years, simulated in PHAST.

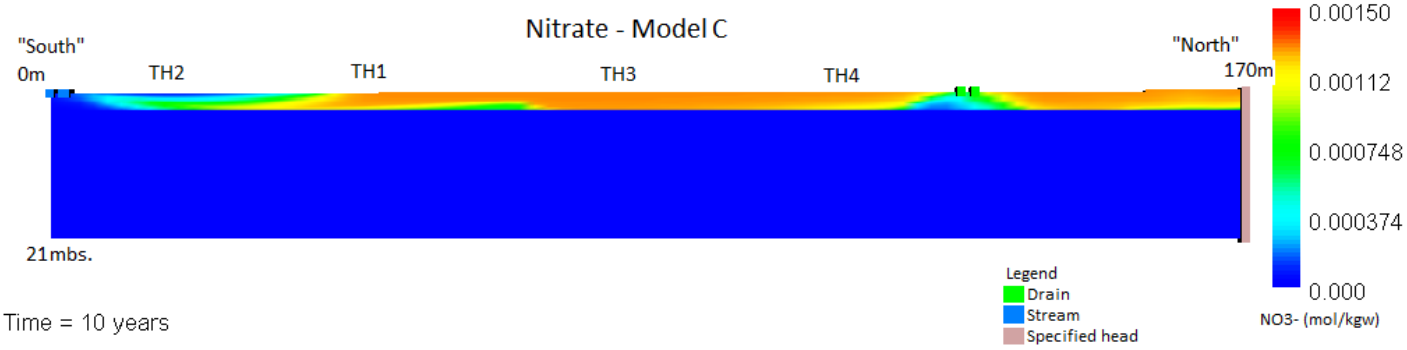

Figure 5.56: The nitrate distribution in the heterogeneous Model C with drain after 10 years, simulated in PHAST.

5.5.2.4. The sulfate distribution in the different PHAST model simulations

The sulfate concentrations in the three different models are found in figure 5.57. 5.58 and 5.59. It is evident that the sulfate is formed in the model which is due to denitrification with pyrite as electron donor. This means that the sulfate is formed in the depths where nitrate is reduced. At the same time the present of Fe^{2+} and hydrogen sulfide (hydrogen sulfides is generated due to sulfate reduction) can form pyrite which by that also can be a sink for the sulfate in the model.

The drains influence at the chemistry concentrations is seen in model B and C. It is found that the drain removes nitrate contaminated water from the system, which means that the denitrification is not taken place around the drain due to higher velocity vectors or the absent of nitrate, which means that the sulfate is not formed here (figure 5.58 and 5.59). It is illustrated that the highest amount of sulfate is 1.07 mM, which is formed by the heterogenic model C and the lowest amount is formed in model B, which means that the heterogeneity has a great impact at the sulfate distribution (figure 5.58 and 5.59).

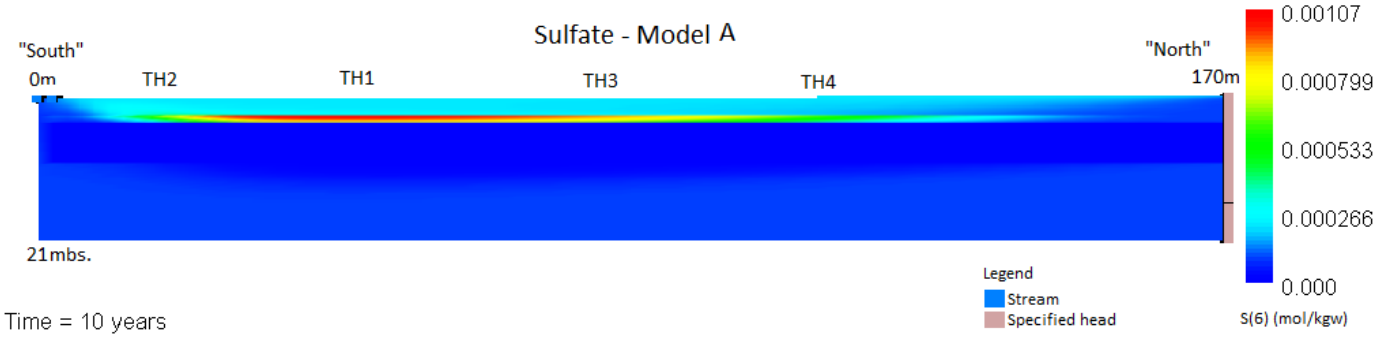

Figure 5.57: The sulfate distribution in the homogeneous Model A after 10 years, simulated in PHAST.

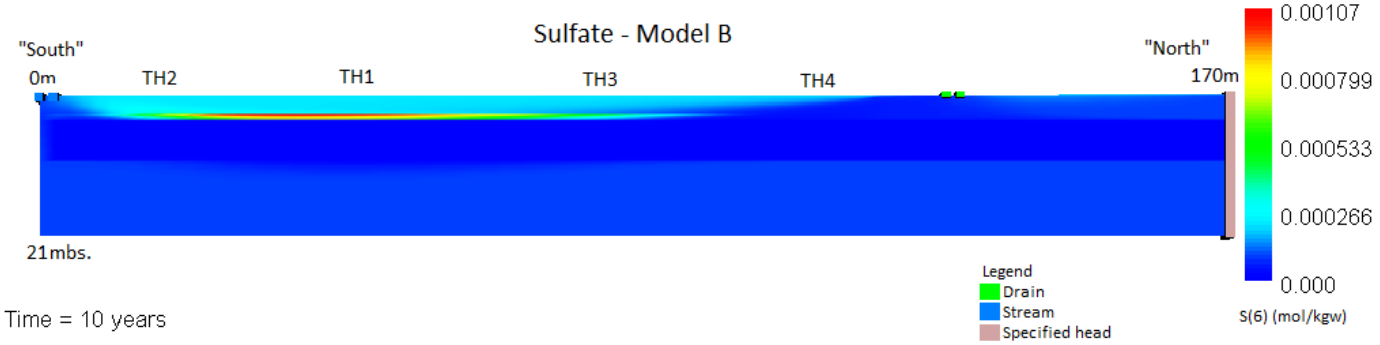

Figure 5.58: The sulfate distribution in the homogeneous Model B with drain after 10 years, simulated in PHAST.

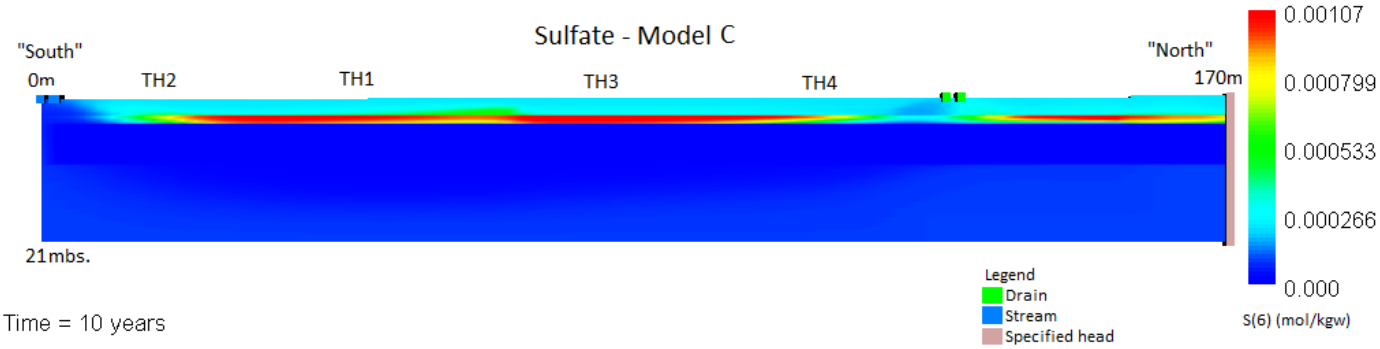

Figure 5.59: The sulfate distribution in the heterogeneous Model C with drain after 10 years, simulated in PHAST.

5.5.2.5. The denitrification rate in the different PHAST model simulations

In the following, the denitrification rates based on pyrite and organic material in the 2D PHAST models will be presented and analyzed.

Pyrite

The moles of transferred pyrite/year is illustrated in figure 5.60 simulated by the different PHAST models. The pyrite in the models are used for pyrite oxidation both with oxygen and after the oxygen is used then nitrate (section 3.3). It is seen that up to 0.1 mM/year is transferred in every model in approximately 2 m.b.s. where the pyrite kinetic is defined in the model (figure 5.60). The front of the pyrite remove is soft and the kinetic controls that not all the pyrite present in every cell is transferred.

Figure 5.60 also shows that the heterogeneous model C transfers most pyrite compared to model A and B. At the same time, the differences between model A and B is due to the drain. This means that the drain has an influence in how much pyrite that is used for pyrite oxidation which makes sense since the drain takes away some of the oxygen and nitrate rich water. The influence of the entering nitrate-free water from the northern boundary is also to be seen. Since the nitrate-polluted water is diluted with the entering nitrate-free water from the northern boundary, a lower concentration of nitrate is to be found in the northern part of the model which of cause affects the amount of used for pyrite oxidation (figure 5.60).

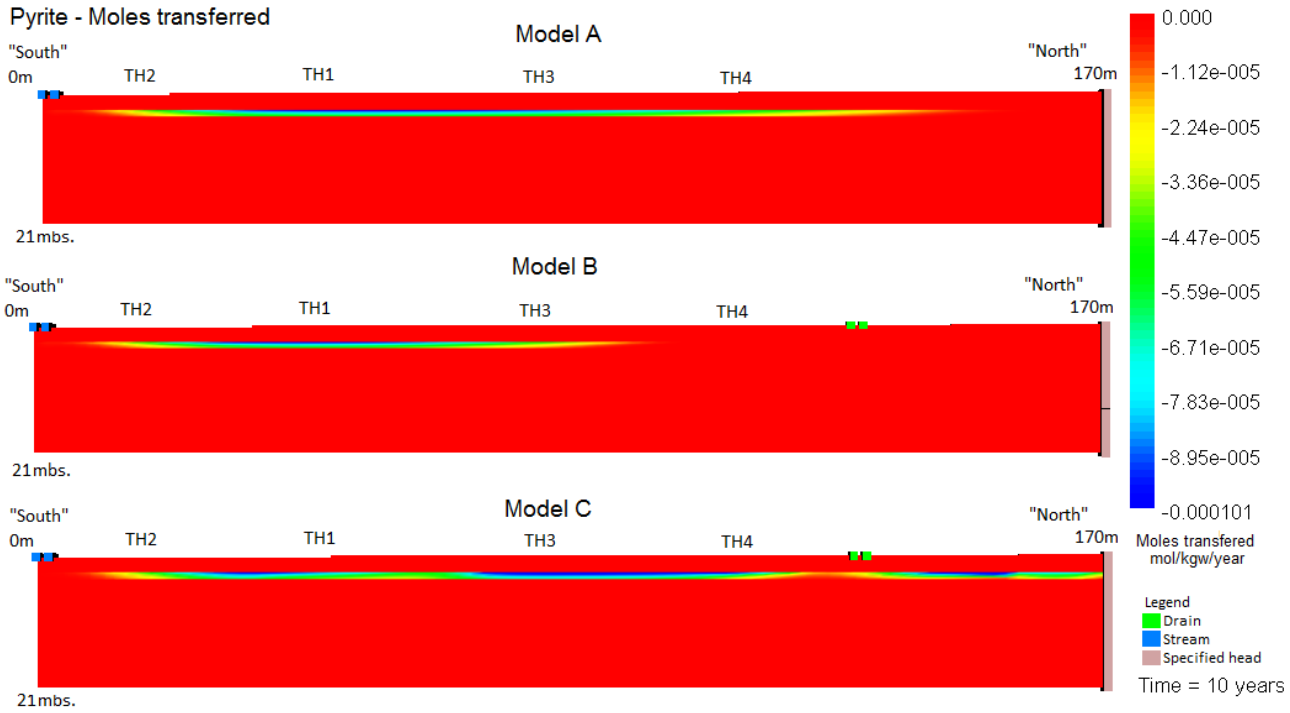

Figure 5.60: The moles of pyrite that are transferred after 10 years in the PHAST model A, B and C.

For model A -0.076 mM/year pyrite is transferred in the cell that represent TH3 in 4 m.b.s. due to denitrification. This can be assumed because no oxygen is present in this elevation and therefore it

must be due to pyrite oxidation with nitrate (figure 5.61). For model B and C, the amount of transferred pyrite is -0.049 mM/year and -0.089 mM/year in the cell that represent TH3 in 4 m.b.s. (figure 5.61). This means that for TH3 most pyrite was transferred in model C.

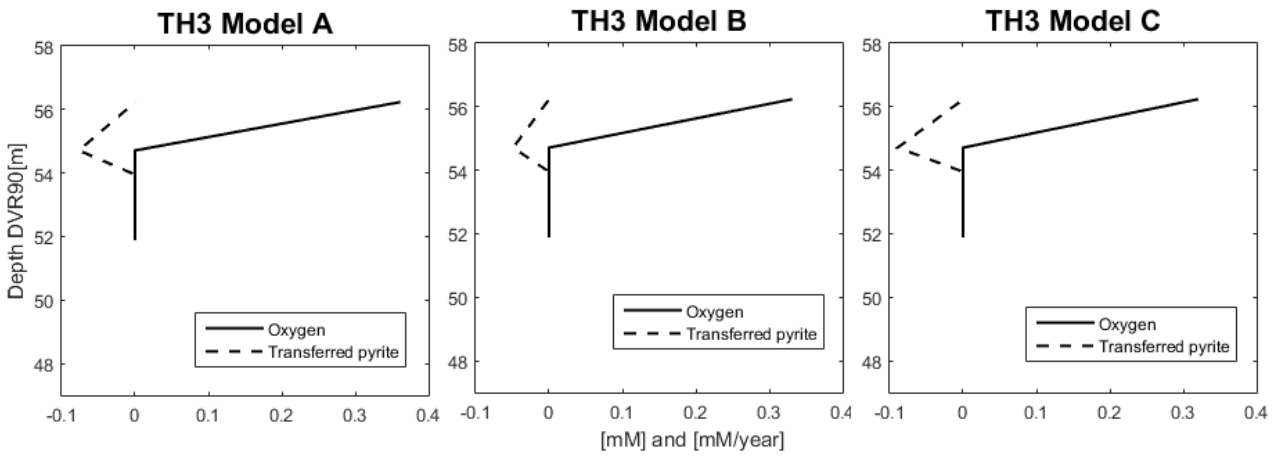

Figure 5.61: The simulated oxygen content and transferred pyrite in the different 2D PHAST models. The negative amount of the transferred pyrite means that the pyrite is removed from the model and not formed.

Organic material

The moles of transferred organic material/year are illustrated in figure 5.62, simulated by the different PHAST models. The organic material is in the models used as electron donor in the denitrification of nitrate and for sulfate reduction. It is seen that up to 0.5 mM/year is transferred in every model in approximately 4 m.b.s. where the organic material kinetic is defined in the model (figure 5.62).

Figure 5.62 also shows that the heterogeneous model C transfers most organic material compared to model A and B. At the same time, the differences between model A and B is due to the drain (figure 5.62). This means that the drain has an influence in how much organic material that is used for denitrification and sulfate reduction, which makes sense since the drain takes away some of the nitrate rich water that affects the amount of sulfate in the water because the denitrification with pyrite is the source of sulfate to the model.

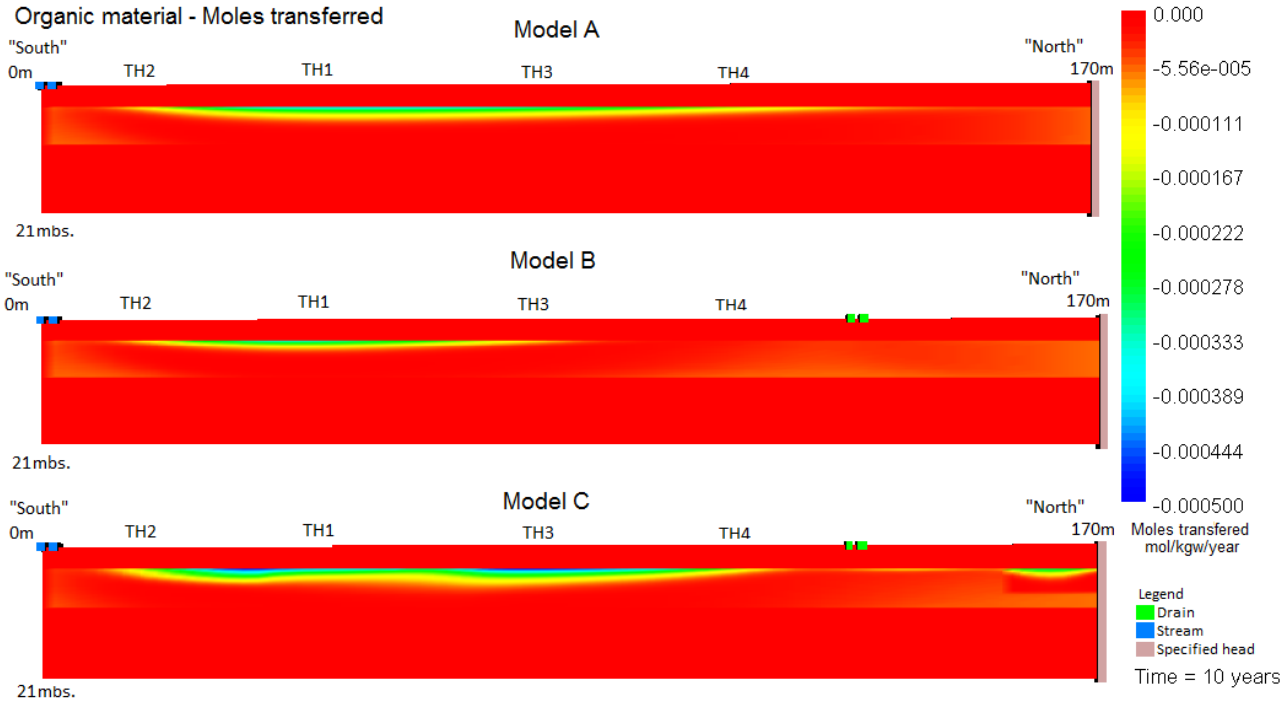

Figure 5.62: The moles of organic material that are transferred after 10 years in the PHAST model A, B and C.

5.5.2.6 Chemical results simulated by Model A compared to measurements

The simulated chemical concentrations from model A is following the measurements in TH3 (figure 5.63) which is located in the middle of the agricultural field at EVI2 (figure 2.3). This indicates that the controlling chemical processes with high probability are included in the model (table 4.4). It is seen that the nitrate is totally removed in 55 m elevation, which is 0.5 meter earlier than what was measured (figure 5.63). This means that maybe the model is a bit too simple and the denitrification rate with pyrite can be defined with a to low rate or the organic material can in reality be present closer to the surface, but this was not possible to simulate with the PHAST model. At the same time, it is seen that the sulfate concentration is a bit lower in the simulation compared to the measurement in 55 m DVR90.

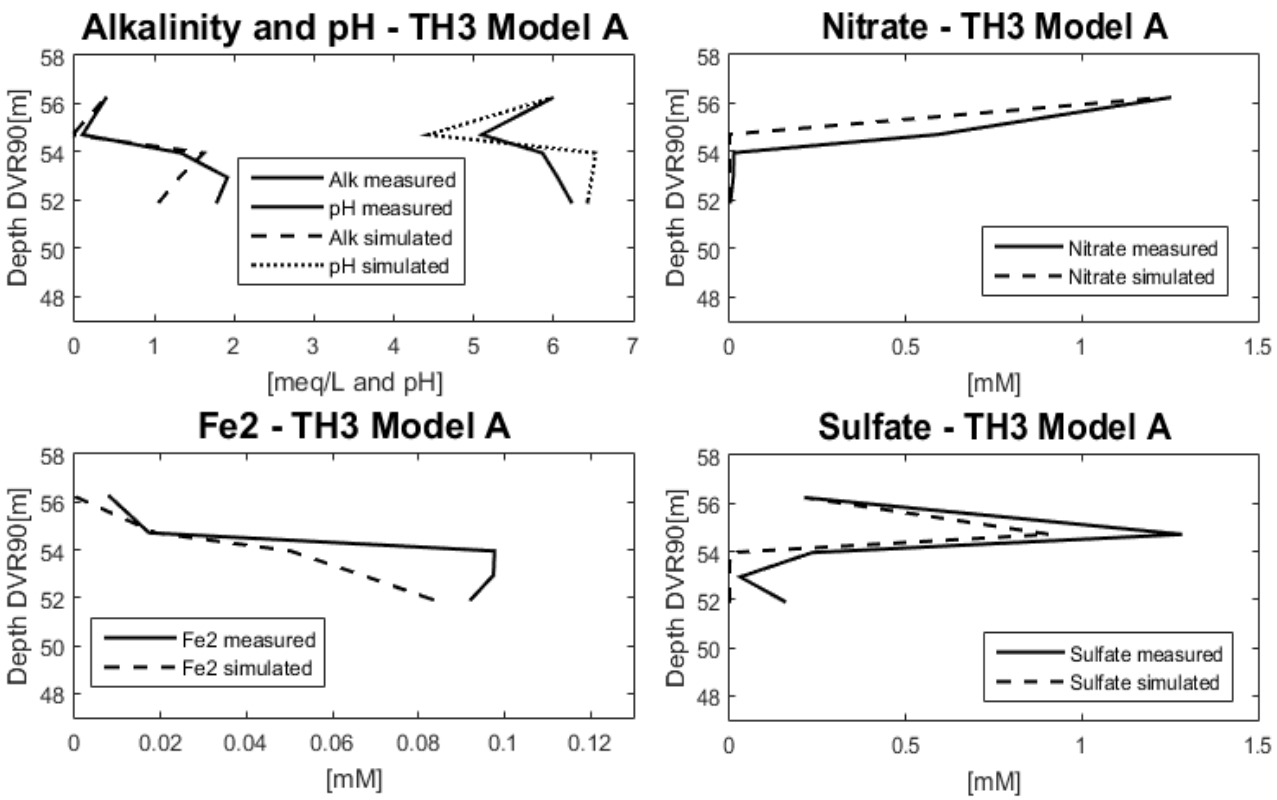

Figure 5.63: The chemical results for TH3 in the PHAST Model A compared with the observations in TH3. The surface is located at 59 m DVR90.

The simulated and measured chemical concentrations in TH4, located at the northern part of the agricultural field at EVI2, are seen in figure 5.64. It is, as for TH3, found that the simulated concentrations are similar to the measurements but with some differences (figure 5.64). The model A does not simulate nitrate in TH4, which is also what is measured. This can be the result of a denitrification that has already taken place in 54 m DVR90 or a dilution of the nitrate rich water that is diluted with the water without nitrate that is entering the model from the northern boundary. The sulfate concentration is peaking too early but in the same range as measured. The Fe^{2+} simulations are matching the measurements in 55 and 54 m DVR90 but not in the rest of the depths and the simulated alkalinity are too low (figure 5.64).

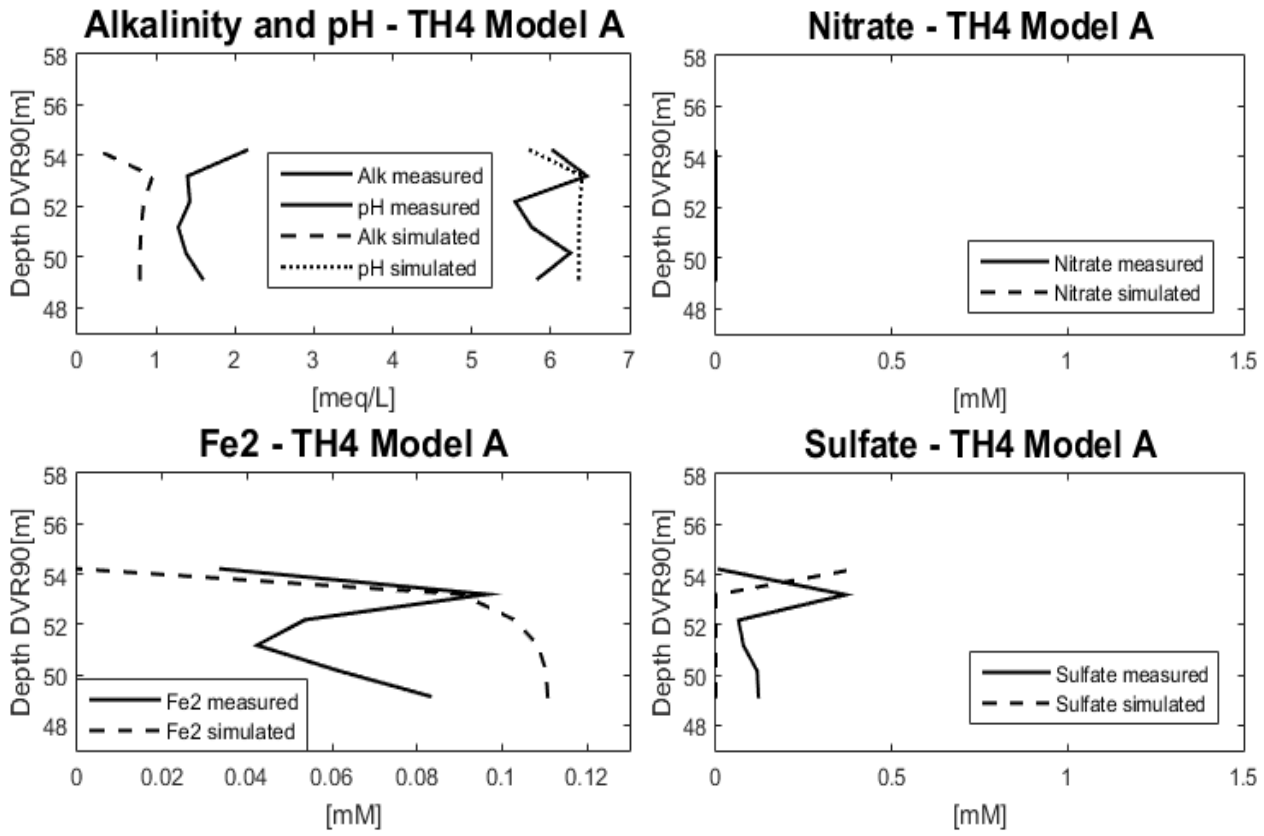

Figure 5.64: The chemical results for TH4 in the PHAST Model A compared with the observations in TH4. The surface is located at 59 m DVR90.

The simulated and measured nitrate and sulfate concentrations from model A in TH1 and TH2 located in the buffer zone at EVI2, are seen in figure 5.65. It is found that the model simulates nitrate to be present at the buffer zone. This can as earlier described be because the model is too simple and that the organic material present in the sediment at the buffer zone in reality is younger which can cause a higher rate for the nitrate denitrification (Postma et al. 2012).

From the simulated sulfate concentration in TH1 and TH2, a comparable shape is found by looking at the measurement with a peak around 55 m DVR90, followed by a decrease and then an increase around 50 m DVR90. It is observed that the model simulates a sulfate reduction too early compared with the measurements (figure 5.65).

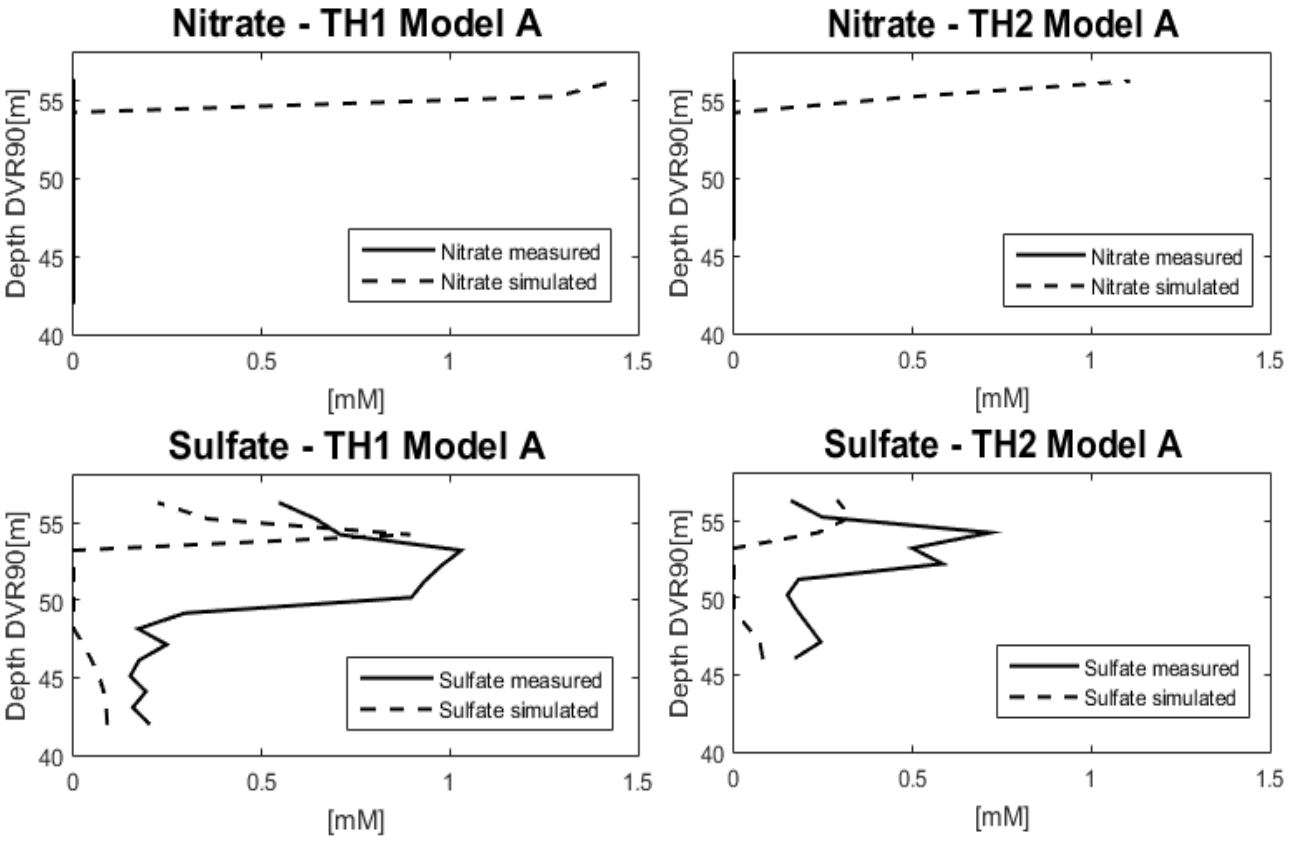

Figure 5.65: The nitrate and sulfate results for TH1 and TH2 in the PHAST Model A compared with the observations. The surface is located at 59 m DVR90.

5.5.2.7 Chemical results simulated by Model B compared to measurements

The simulated chemical concentrations in model B are following the measured concentrations in TH3 as for model A. It is seen that the nitrate in model B is also removed in 55 m depth (figure 5.66). The simulated Fe^{2+} concentrations in TH3 follow the measured even better in model B compared to model A but the sulfate peak is in model B even lower than in model A (figure 5.66 and 5.63). This can be due to a too high kinetic of the organic material which causes the sulfate reduction. In addition, the concentration of alkalinity is lower in 54 m DVR90 compared to the measurement and the simulated alkalinity in model A.

This means that the drain has an influence at the chemistry composition at EVI2 because it removes some nitrate containing water from the system. The nitrate concentration in the recharge is therefore higher for model B, in order to match the chemical measurements in the best way. This higher concentration of nitrate can especially have an impact at the areas where the drain does not have an influence.

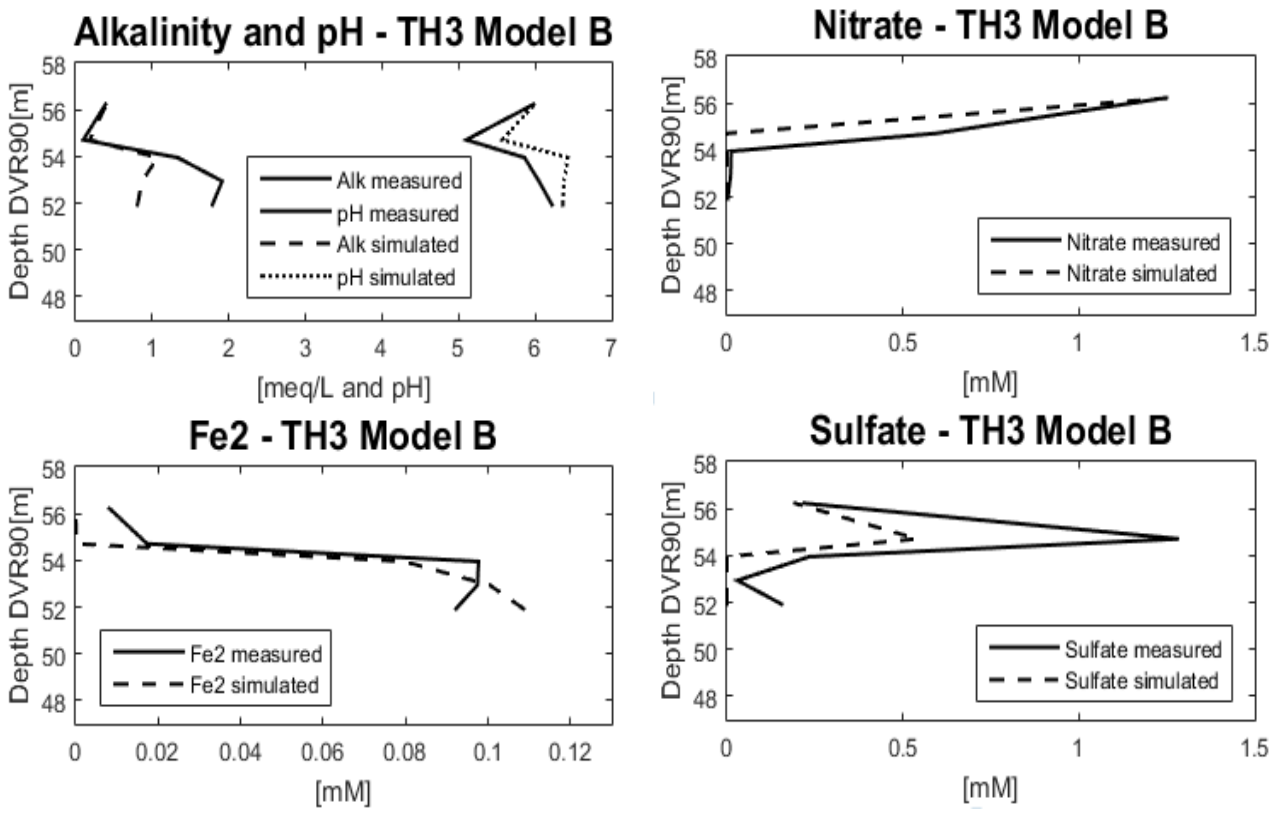

Figure 5.66: The chemical results for TH3 in the PHAST Model B compared with the observations in TH3. The surface is located at 59 m DVR90.

By looking at the simulated chemical composition in TH4 based on model B, it is seen that the chemical composition is affected by the drain in the model and the higher nitrate concentration in the recharge (figure 5.67). The simulated Fe^{2+} concentration is higher in 55 m DVR90 compared to model A and constant from 54 to 50 m DVR90 and the sulfate in almost not present (figure 5.67 and 5.64). This absence of sulfate can be due to the removal of nitrate contaminated water by the drain which means that the denitrification does not take place and due to that no sulfate can be formed.

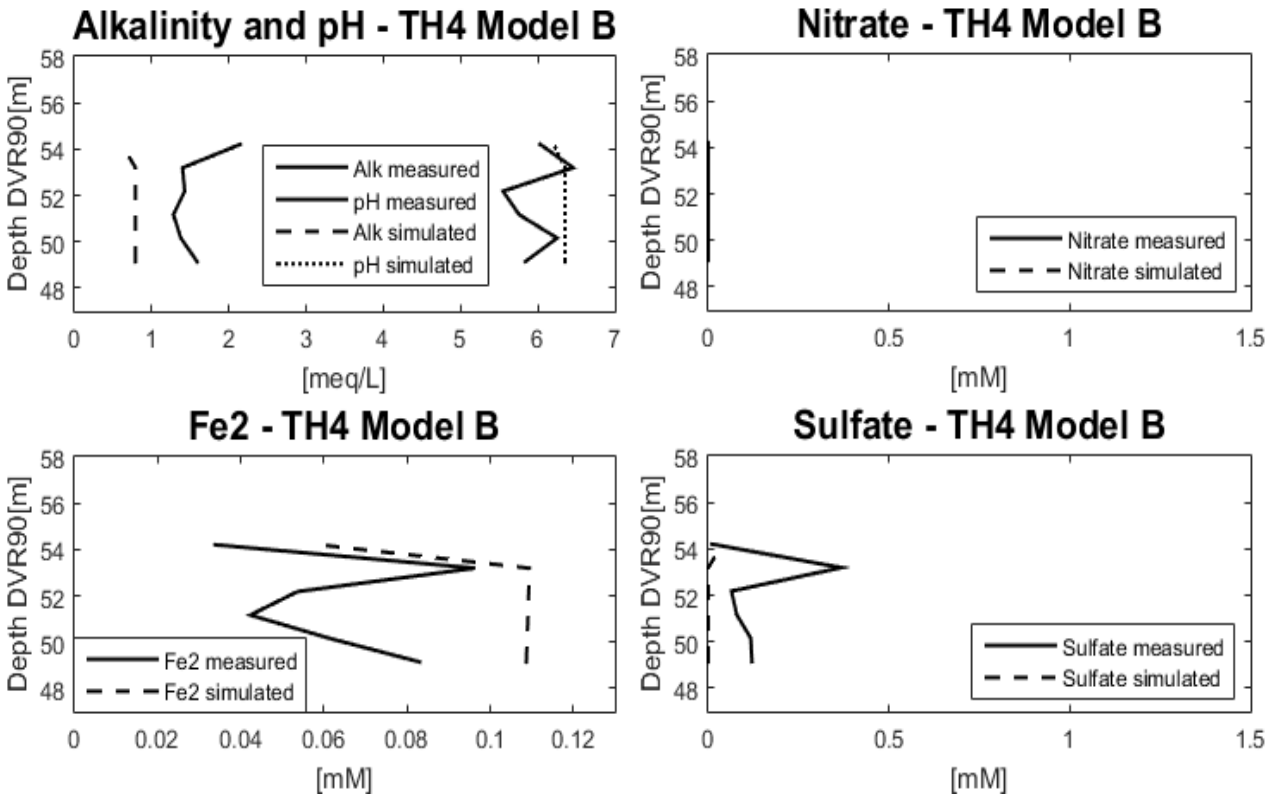

Figure 5.67: The chemical results for TH4 in the PHAST Model B compared with the observations in TH4. The surface is located at 59 m DVR90.

The simulated and measured nitrate and sulfate concentrations from model B in TH1 and TH2, located in the buffer zone at EVI2, are seen in figure 5.68. The simulated measurements are similar to the concentrations simulated by model A. Model B also simulates nitrate to be present at the buffer zone. From the simulated sulfate concentrations in TH1 and TH2, a comparable shape is also found by model B, with a peak around 55 m DVR90 followed by a decrease around 53 m DVR90 and an increase around 50 m DVR90. Despite the fact that the model is simulating a sulfate decrease too early and in too low concentrations compared to the measurement, it is still following the same shape, which indicates that the controlling processes are included in the PHAST model (figure 5.68).

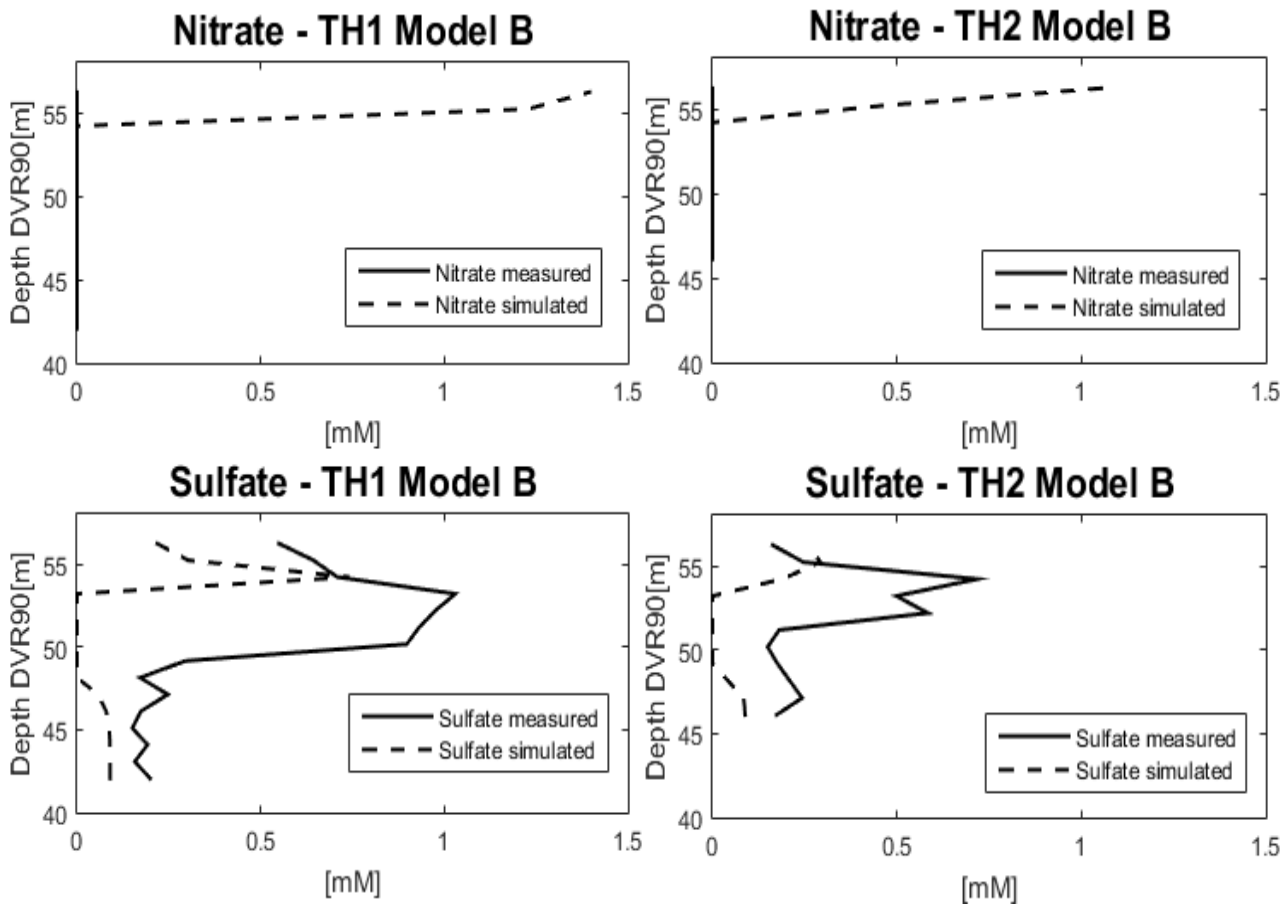

Figure 5.68: The nitrate and sulfate results for TH1 and TH2 in the PHAST Model B compared with the observations. The surface is located at 59 m DVR90.

5.5.2.8. Chemical results simulated by Model C compared to measurements

The simulated chemical concentrations from model C are following the measured concentrations in TH3, as for model A and B (figure 5.69). It is seen that the heterogeneity of the model has an impact on the chemical concentrations because it affects the water flow and by that also the dispersion and diffusion, which together with the chemical processes control the transport of the chemical components.

The simulated nitrate in TH3 in model C is still removed too early in 55 m depth, as in model A and B (figure 5.69, 5.63 and 5.66). The simulated sulfate concentrations are almost perfectly matching the measured in model C (figure 5.69). The simulated alkalinity and pH are matching the measured concentrations but the simulated Fe^{2+} concentrations is not following the measured shape but can still be found in the same range as the measured concentrations (figure 5.69).

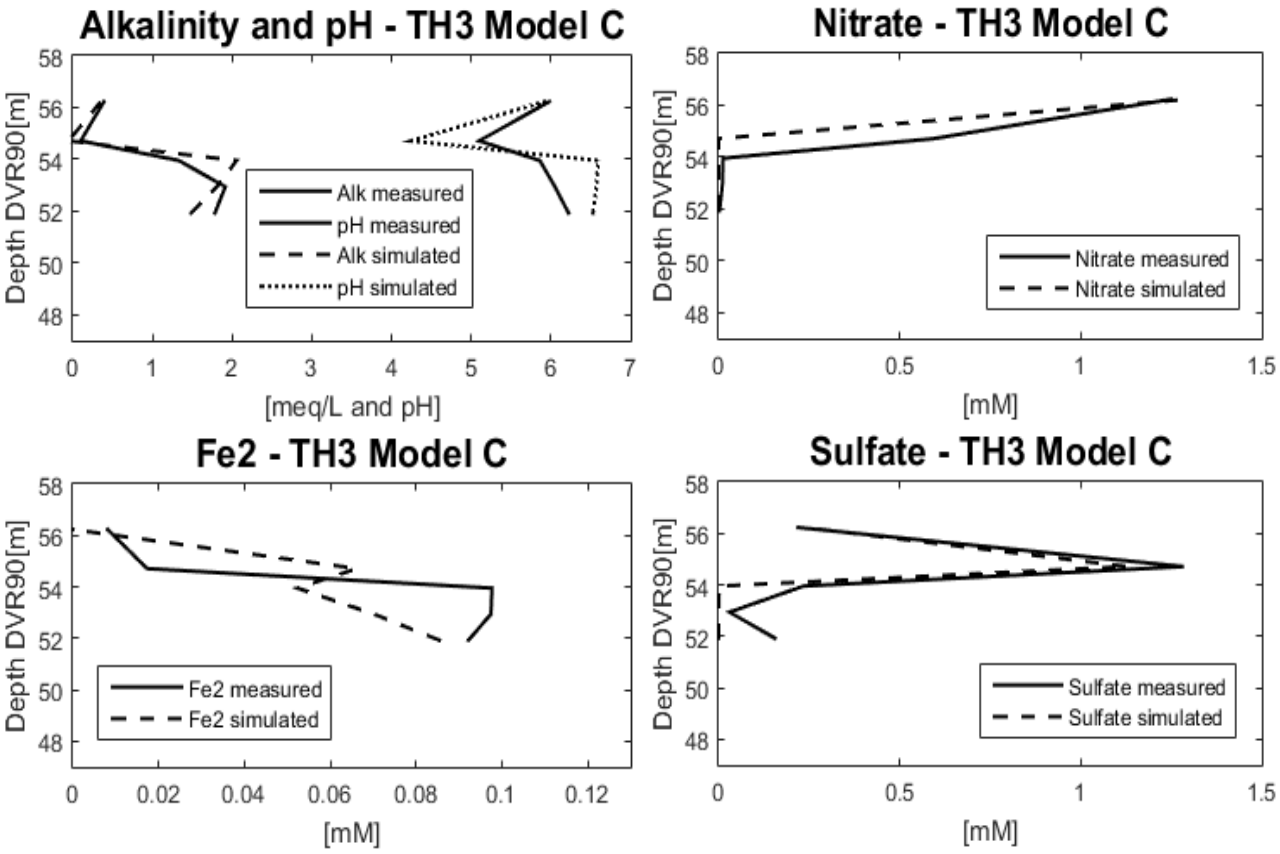

Figure 5.69: The chemical results for TH3 in the PHAST Model C compared with the observations in TH3. The surface is located at 59 m DVR90.

The simulated chemical composition in TH4 based on model C is seen in figure 5.70. It is seen that the chemical composition is affected by the heterogeneity in the model and that the sulfate is now present in TH4 despite the influence of the drain (figure 5.70). Overall, the simulated concentrations found by model C is looking a lot like the simulated concentrations from model A which means that the drains influence is minimized due to the heterogeneity in the model (figure 5.69, 5.70, 5.71, 5.63, 5.64 and 5.65).

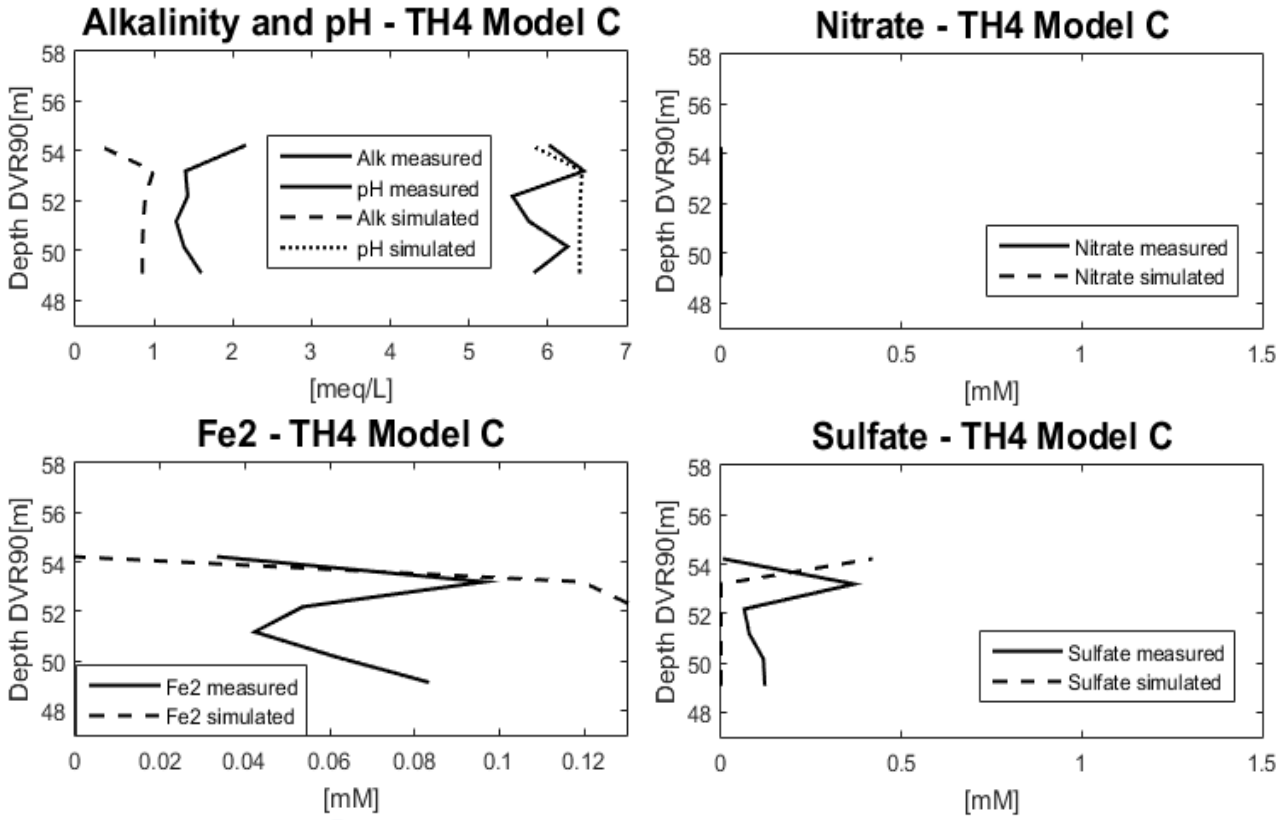

Figure 5.70: The chemical results for TH4 in the PHAST Model C compared with the observations in TH4. The surface is located at 59 m DVR90.

The simulated and measured chemical concentrations from model C in TH1 and TH2 located in the buffer zone at EVI2 are seen in figure 5.71. The simulated measurements are still to low compared to the measured and similar to the concentrations simulated by model A and B and Model C also simulates nitrate to be present at the buffer zone.

The simulated sulfate concentrations in TH1 and TH2, are still following the same shape as the measured with a peak to early around 55 m DVR90 followed by a decrease around 53 m DVR90 and a small increase around 50 m DVR90 (figure 5.71). Model C simulates a higher sulfate peak in 55 m DVR90 in TH1 compared to model B but the same amount as the measured which was also simulated by model A (figure 5.71, 5.65 and 5.68).

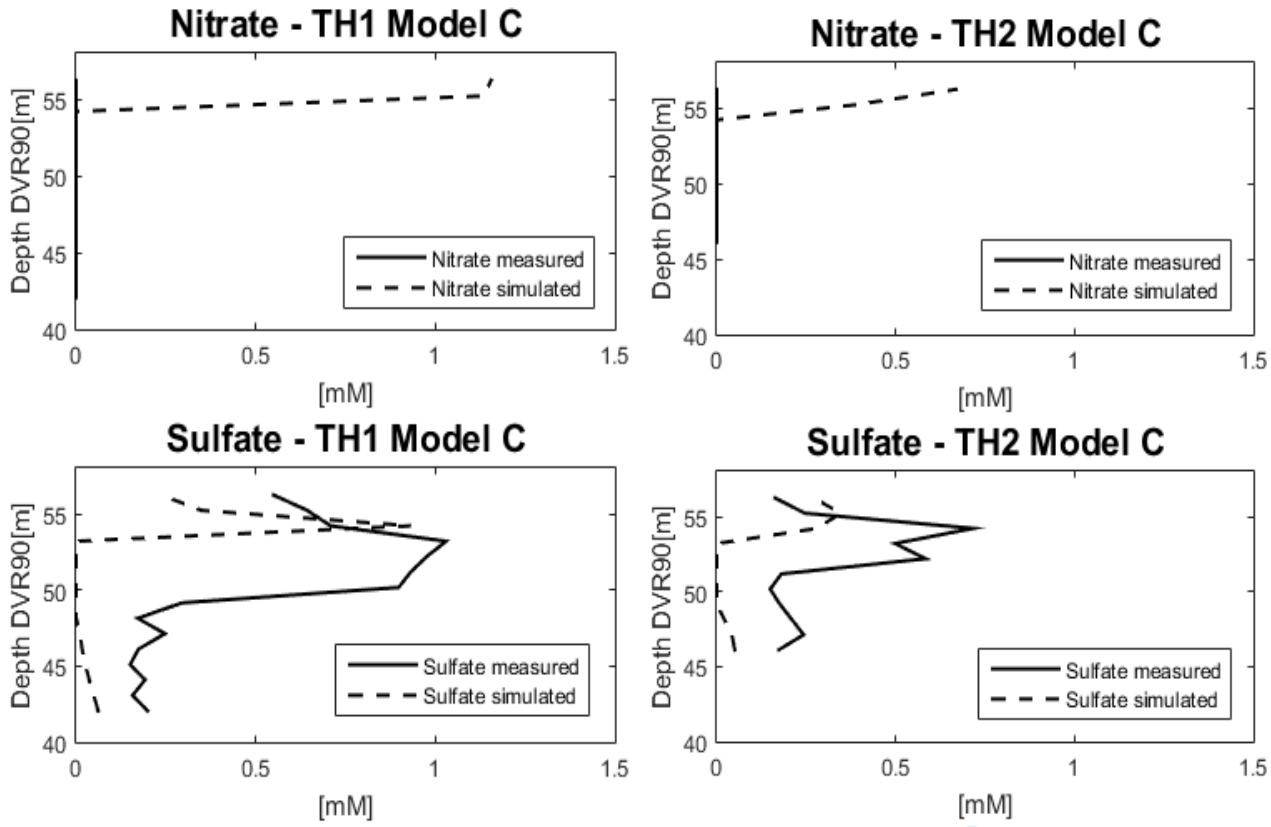

Figure 5.71: The nitrate and sulfate results for TH1 and TH2 in the PHAST Model C compared with the observations. The surface is located at 59 m DVR90.

The fit between the simulated and observed chemical concentrations in the three simple 2D models shows that it is with high probability that the controlling chemical processes that are included in the model. This means that the qualitative analysis of the chemical processes at the agricultural field at EVI2 also can be explained by a quantitative analysis in 2D where the groundwater flow, the influence of the drain and heterogeneity and kinetics are included. Therefore, it is with even higher probability that included chemical processes are controlling the water chemistry at EVI2.

6. Discussion

In the following, a conceptual model of EVI2 is conducted based on the geological, hydrogeological and groundwater chemistry investigations at EVI2. Afterwards the groundwater flow, chemistry processes and denitrification rate at EVI2 are discussed based on the different results and methods used in this thesis. In addition, the results are compared to relevant studies.

6.1 Conceptual model of the groundwater flow and nitrate distribution at EVI2

A conceptual model for EVI2 based on the geological, hydrogeological and groundwater chemistry investigations for the area is seen in figure 6.1.

The figure illustrates that the geology in the study site primarily consists of sand with clay sediments in the southern and northern part of EVI2 and in approximately 37 m elevation, a clay layer is deposited which may act as a bottom for the sandy aquifer. The distribution of the geology at the southern part is only based on one Jupiter borehole while the agricultural field at EVI2 was also investigated with MEP profiles. Based on the MEP profiles it is assumed that a sandy layer is present in the clay deposits at the northern part, which may act as a "window" for the water to enter the study site. The assumption about a lower clay layer that acts as a bottom for the aquifer is based on the MEP profiles together with the Jupiter Boreholes and the Geoscene model, but the exact position is unknown. The assumption about a uniform lower clay layer is a simplification of reality. As Petersen (2016), and Enemark (2015), points out, the clay layer may be deposited horizontally but the landscape processes may also have affected the deposition of the different materials, which means that there can be underlying sandy deposits in the clay layer and heterogeneity.

The conceptual model shows that the water flows from the northern part of EVI2 towards the stream and that the recharge to the agricultural field with high possibility flows downwards to approximately 5 m.b.s. (figure 6.1). In this depth, the water is most likely diluted with other water containing a different chemical composition.
This downward flow affects the water chemistry because the water that recharges at the agricultural field is nitrate-polluted due to fertilization. The conceptual model also illustrates where pyrite and organic material may be present in the soil at EVI2, which is affecting the controlling chemical process in the area as earlier discussed (figure 6.1).

However, it should be kept in mind that only the location of one drain at the agricultural field is known and included in the conceptual model (figure 6.1) as well as in the 3D and 2D models. In reality, more drains can be installed at the agricultural field, which can affect the water chemistry and flow, as it was observed in the 2D PHAST models (figure 5.55 and 5.56).

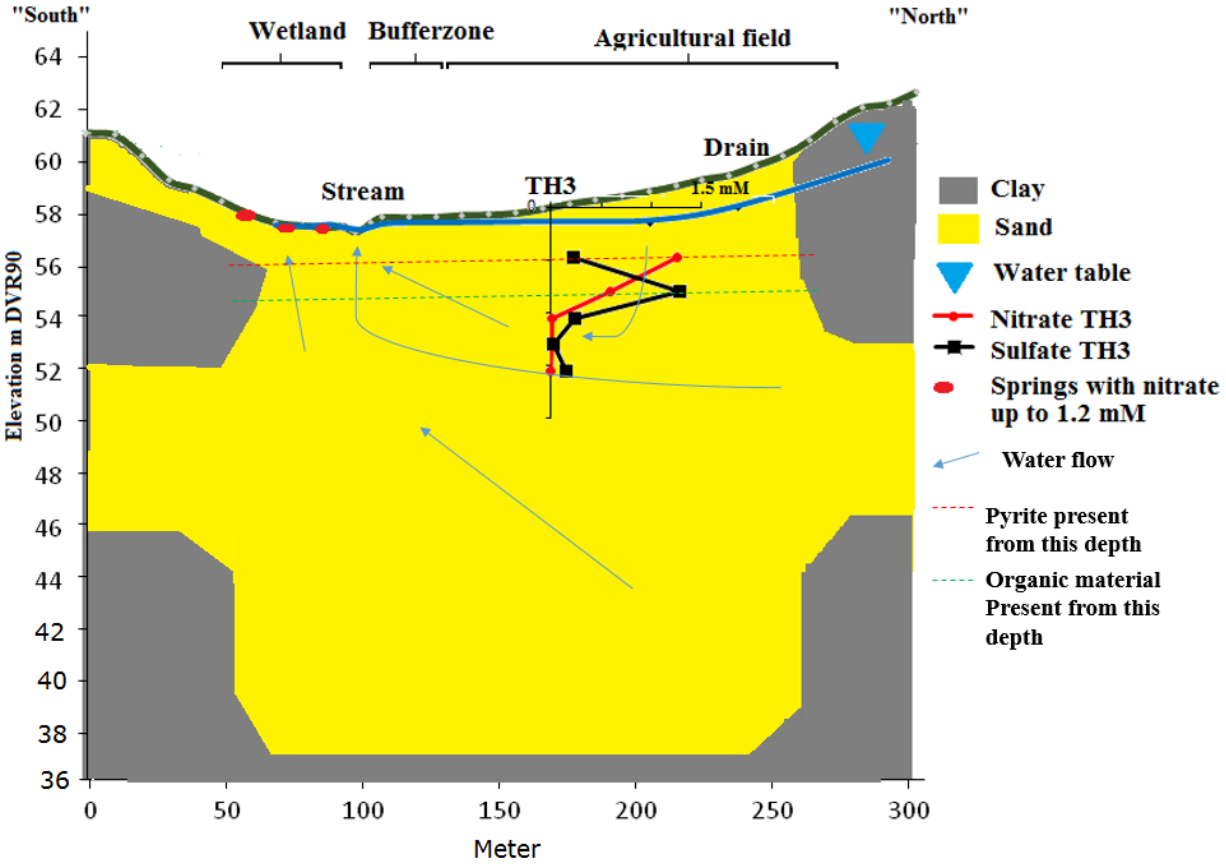

Figure 6.1: Conceptual model for EVI2.

6.2 Groundwater flow at EVI2

The groundwater in EVI2 flows from the northern part of the study site towards the stream and under the stream. This flow pattern is based on the isopotential map of the average measured hydraulic heads at the study site, the 3D model of Holtum catchment and the 2D models. The fact that the 3D MODFLOW model shows the same flow pattern as the isopotential map and 2D models means that the model at catchment scale can be used to investigate the flow pattern at local scale, despite scale issues and the fact that models always are simplifications of reality (Sonnenborg and Henriksen, 2005).

The average hydraulic heads measured in the wells at the wetland show that the water may also flow from the wetland area towards the stream, but the 3D model shows that the amount of water flowing from the southern part towards the stream is minimal. The model actually simulates some dry cells in the upper layers at the wetland area generated by the drain that represents the springs in the wetland area (figure 5.39). Similarly, the 3D model illustrates that the groundwater particles in the stream at EVI2 originate from the northern part of Holtum catchment (figure 5.40 and 5.42).

The Darcy fluxes in the 2D PHAST models in the stream are simulated too high compared to the observed flux in the stream. This shows that the 2D models may be too simple and that the water with high probability not only flows towards the stream but also under the stream. This means that the model domain with advantage could have included the wetland area.
A 2D model developed by Petersen (2016), for the study site, conducted the same flow pattern. This 2D model domain included the wetland area at EVI2 and too high amounts of water was simulated which resulted in an upwelling at the wetland area (Petersen, 2016).

The investigation of the particles entering the wetland area at EVI2 shows that this explanation may be possible. It is observed that the particles entering the wetland area at EVI2 originates from the northern part of Holtum catchment and that the main part of the particles flow under the agricultural field in a lower sand layer (figure 5.41). In addition, the isotope measurements from September 2016, show that the groundwater in the springs may have been exposed to a long travel path because the seasonal influence is not to be seen (figure 5.11).

Many different assumptions were taken regarding the modeling of EVI2. The northern boundary condition in the 2D models is defined as a specific head at 58 m which in principal is unknown due to a broken well (TH5). The neglecting of the flow in y direction also affects the flow in the model and gives the model some uncertainty because the water in reality not only flows in two dimensions.

6.3 Distribution of nitrate in the riparian area EVI2

The chemical measurements show that nitrate is present at the agricultural field at EVI2 in the upper sediments down to 2.5 m.b.s. and only in the springs at the wetland area (figure 5.15, 5.18 and 5.22).

This is not what was expected in the area due to high use of fertilizer at the agricultural field and the common assumption about wetlands capability to remove nitrate (SVANA, 2016). However, the absence of nitrate in the wells at the wetland area and the presence of high amounts of sulfate, indicate that nitrate may be removed in the wetland (figure 5.14 and 5.15). The nitrate-polluted water in the springs means that not all the nitrate entering the wetland area is reduced, which can be due to upwelling. Upwelling can results in high water velocities in an area where the water would normally flow diffuse, which means that there is no time for a nitrate reduction to take place (Hill, 1996).

The fact that the springs contain high concentrations of nitrate mean that nitrate-polluted water with high probability enters the stream as surface flow. This is observed in the spring located close to the stream where water flows as surface water directly into the stream. Exactly how much nitrate-polluted water that enters the stream because of the presence of springs and how much nitrate that is reduced at the wetland area is currently unknown and more investigations are needed.

An investigation of the study site EVI1, located downstream in Holtum catchment found that upwelling happens in the wetland area, which affects the wetlands capability for reducing the nitrate (Nørrevang and van't Veen, 2014). In addition, Karan et al. 2013 investigated the study site Hygild, located in the outlet of Holtum catchment, and found that the upper part of the wetland area receives most of the nitrate from the surrounding agricultural fields and the wetland does not remove the nitrate.

This means that the hydrogeological conditions and especially geological versatility affect the nitrate reduction and shows that small-scale investigations of riparian areas are important for the implementing of a more spatially nitrate regulation.

At the agricultural field at EVI2, the absence of nitrate in the wells under 2.5 m.b.s. both in the winter and summer season and the complete absence of nitrate in the wells located at the buffer zone (figure 5.15 and 5.22) means that nitrate must be reduced.

This means that no nitrate-polluted water with high probability reaches the stream naturally from the agricultural field. Therefore, it is interesting to investigate the chemical processes which are going on at the agricultural field at EVI2 to understand small-scale nitrate removal processes and parameters.

6.4 The chemical processes at the agricultural field at EVI2

The analyzes of the chemistry processes at the agricultural field at EVI2, show that the water is highly affected by nitrate input from fertilizer and that some few chemistry processes with probably are controlling the water chemistry. These processes are seen in table 6.1.

Table 6.1: The most likely chemical processes at the agricultural field at EVI2

Meters below surface	Chemical processes at the agricultural field at EVI2
2-3	- Denitrification of nitrate with pyrite as electron donor
3-4	- Denitrification of nitrate with organic material as electron donor. - Reductive dissolution of iron oxides - Sulfate reduction with organic material
4-5	- Sulfate reduction with organic material

If the nitrate were not present, the chemical processes would have been different which means that the fertilizer has a great impact on the chemical processes in the soil. The fact that the results from the relatively simple 1D model and the 2D models are in agreement with the measured chemical concentrations, means that the few chemical processes are most likely to be the controlling processes for the agricultural field at EVI2. This is taken into account even though the water chemistry is affected by a complex soil environment with different microorganisms and chemical processes though many years.

General measured nitrate concentrations under agricultural field sites are reported to be less than 3 mM (Postma et al, 1991). The highest nitrate concentrations measured in the wells at EVI2 are 1.2 mM (figure 5.25) and the simulated concentrations are up to 1.2 mM (figure 5.54, 5.55 and 5.56). This is in agreement with the measured nitrate concentrations in the water entering Lake Hampen located in Holtum catchment (Kidmose et al., 2014). Kidmose (et al., 2014) found in a study of nitrate

concentrations up to maximum 2.4 mM in the Lake Hampen which also measured concentrations around 1.6 mM.

A study of sulfate sources and sinks in an anoxic river recharged sandy aquifer in Germany (Massmann et al, 2003) showed that sulfate concentrations were absent close to the surface and high in the upper part of the sediments. This means that the source of sulfate was located in the upper sediment layers and that the sulfate originated from dissolution of pyrite. This is also the case for the sulfate concentrations at EVI2 (figure 5.34) and what the 2D models simulated (figure 5.5, 5.58 and 5.59). The absence of oxygen in the wells means that the sulfate can originates from denitrification with nitrate.

Similarly, the pyrite investigation shows that denitrification with pyrite as the electron donor is possible at the agricultural field. The pyrite content in the sediment at EVI2 was investigated but only down to 3 m.b.s. and only at one location. The ideal would have been to take sediment samples below 3 m.b.s. and also at other locations at the agricultural field. This was not possible due to a broken instrument.

A study of nitrate reduction in an unconfined sandy aquifer at Rabis Creek, located 50 km from EVI1, showed that pyrite was the main electron donor for denitrification in a sandy outwash aquifer (Postma et al, 1991). They measured pyrite to be present in the range of 1-10 mmol/kg, which is also, what other studies generally report for pyrite contents in sandy aquifers (Postma et al, 1991). The measured pyrite concentrations at EVI2 are in the range of 1.4-2.9 mmol/kg dry sediment (figure 5.32), which compared to the study by Postma, (et al. 1991) is in the lower end. This indicates that a denitrification with pyrite as electron donor is possible at EVI2. In addition, a push pull experiment conducted at EVI2, in September 2016 shows that denitrification can take place at EVI2, which may be caused by pyrite oxidation (Kofod, 2016). Similarly, Karan (et al. 2013) also expect that the presence of pyrite makes pyrite oxidation possible at the field site Hygild even though they did not test the presence of pyrite, which means that this assumption primarily is based on high sulfate concentrations.

The denitrification in EVI2 can also occur due to the present of organic material, which was not tested in this thesis and the 2D models show that the nitrate-free water that enters the field site from the northern part has a major influence at the nitrate content of the water due to dilution. However, the

fact that EVI2 is located at a sub glacial stream trench (figure 2.3), together with the chemical measurements from the summer and winter season means that the organic material with high possibility is present in the soil, which can affect the nitrate reduction and at the same time it makes sulfate reduction possible.

This means that the agricultural field at EVI2 is capable of removing nitrate, which indicates that the nitrate-polluted water with high probability does not reach the stream and groundwater naturally. However, it should be kept in mind that the drain at the agricultural field removes high amount of nitrate-polluted water from the field and leads it directly into the stream.
The influence of the drain is simulated in the 2D PHAST models B and C that show the drains removal of nitrate-polluted water, which affects the water chemistry around the drain (figure 5.55 and 5.56).

However, the same chemical processes were found by the winter and summer snap shots for controlling the water chemistry at EVI2, some differences were seen in the chemistry composition (figure 5.34).
These differences can be due to heterogeneity, a higher denitrification rate in the summer time or leaching. In order to investigate the seasonal variations it would be optimal to have measurements of the water chemistry several times a year, optimally every month and from the same positions as well as at different places at EVI2. This could optimize the data distribution in time and space. If the chemistry processes were investigated at different locations at the agricultural field and the same controlling chemistry processes were found, it could mean that the same chemistry processes are controlling the water chemistry at the entire agricultural field at EVI2. This could be used to upscale the assumptions about which chemical processes that control the water chemistry in riparian areas like EVI2. Investigation of other agricultural fields located at a former sub glacial stream trench would also be preferred to investigate in order to do this upscaling.

However, it was observed that the same chemical processes are likely to control the water chemistry in the investigated wells at the agricultural field. This may mean that it could have been enough to investigate only the TH3 well in order to explore the chemical processes controlling the water chemistry at EVI2. This well can represent the processes at the entire agricultural field. However, it can be difficult to know if one well represents the entire area without investigating other locations.

6.5 Denitrification Rates at EVI2

The rates for transformed pyrite in TH3 in 4 m.b.s due to denitrification with pyrite as electron donor was -0.076 mM/year, -0.049 mM/year and -0.089 mM/year for the 2D PHAST model A, B and C, respectively (figure 5.61).

A study in the USA of zero-order denitrification rates in shallow aquifers made by Tesoriero and Puckett, 2011, found zero-order denitrification rates from 0.015 to 0.070 mM/year for suboxic systems, which is in the same range as the simulated rates by the 2D PHAST model. However, it should be kept in mind that the simulated rates are not based on zero-order reaction.

By a comparison of the simulated rates with a push pull experiment conducted in TH3.2 in 3 m.b.s. the simulated rates are low. The push pull experiment resulted in rates of -5.5 mM/year and -10.9 mM/year, depending on which measurements the rates the calculations were based on (Kofod, 2016). The highest rate may be the most reliable because this rate was calculated based on measurements of water that had been in the aquifer for the longest period of time (Kofod, 2016).

The comparison between the simulated rates and the measured rates by the push pull experiment means that the 2D PHAST models may not be representative for simulating the pyrite oxidation rates at the agricultural field at EVI2. However, the models can be used as a framework for further investigations of the denitrification rates. This can be done by implementing the calculated rate constants from the push pull experiment in the kinetic rate expression for the pyrite rates and also the calculated pyrite content in the soil. However, the push pull experiment could optimally be repeated for a longer period than 36 hours, which was the time the injected nitrate-polluted water was in the aquifer that was used for calculating the rates (Kofod, 2016).

6.6 The origins of the nitrate-polluted water in the springs at the wetland area

It is not clear where the high nitrate concentrations measured in the springs at the wetland area at EVI2 originates from and in the following, some different possibilities will be discussed.

The 3D MODFLOW modeling shows that the high concentrations of nitrate in the springs at the wetland area are highly possible to originate from the northern part of Holtum catchment. The particle

tracking of the entering particles in the wetland area showed that the particles flow in the lowest sand layer before entering the wetland (figure 5.41). If the nitrate in the springs originated from the agricultural field at EVI2, nitrate would be likely to be found in the wells at the agricultural field and bufferzone but it is found that the nitrate is reduced at the agricultural field (section 6.3).

The age distribution analysis of the particles entering the wetland area show that the particles are mainly young, which can explain the nitrate pollution because the denitrification requires some time to reduce the nitrate as well as some electron donors as pyrite and organic material (section 3.2. Deni). Karan (et al. 2013) found that the particles in the wetland area at the study site Hygild, located in the outlet of Holtum catchment, could be divided into two zones based on CFC method. An upper zone from 3-4 m.b.s. with relatively young nitrate-polluted water with ages around 20 years and a deeper zone with older groundwater around 50 years which is free of nitrate (Karan et al., 2013). Compared to EVI2, the ages is in the same range as the 3D MODFLOW model simulates for the particles in the wetland area, but the wetland area also contains older particles aged 130 years (figure 5.44).

In addition, it is possible that the nitrate-polluted water in the springs originates from former drains or drain connections that may end in the soil, at the wetland area. If the drains are buried in the soil it will looks like a natural springs. It is especially possible that the spring with the highest nitrate concentration, which is an old drainage shaft, is connected to drains and maybe a drainage system (figure 2.3). This can allow nitrate-polluted water that originates from agricultural fields from the southern part of Holtum catchment to enter the springs even though the flow path analysis based on the modeling does not show that water flow from the southern part of the catchment towards the stream.

7. Conclusion

This thesis investigates the hydrogeology and groundwater chemistry for an agricultural riparian area, EVI2, located at a subglacial stream trench with a sandy aquifer near Holtum stream, Denmark.

The water flow in the riparian area was investigated based on hydraulic head measurement but also 3D and 2D modeling. The water in the study site EVI2 flows from the northern part of the catchment towards the stream and probably also under the stream and up in the wetland area as springs. In addition, it was found that a pre-developed 3D MODFLOW model at catchment scale could be used to investigate the flow pattern and origins of the water in the study site at local scale.

At the study area, nitrate-polluted water was found in the springs at the wetland area and in the wells at the agricultural field. The nitrate-polluted water in the springs probable flows towards the stream as surface runoff. In the wells at the agricultural field, nitrate was only found above 2.5 m.b.s., which means that it must be reduced, and the stream does not receive nitrate-polluted water that originates from the agricultural field naturally.

Investigations of the groundwater chemistry at the agricultural field at EVI2 by qualitative analysis of measured chemistry concentrations in the summer and winter season and quantitative analysis by use of 1D and 2D modeling, showed that nitrate due to fertilizer affects the water chemistry at the agricultural field. It was found that the controlling chemical processes are most likely to be denitrification with pyrite as electron donor from 2 – 3 m.b.s. denitrification with organic material as electron donor, reductive dissolution of iron oxides and sulfate reduction with organic material from 2 - 4 m.b.s. and sulfate reduction with organic material from 4 - 5 m.b.s. A pyrite content analysis at the agricultural field also showed that pyrite oxidation is possible.

This means that the nitrate at the agricultural field with high probability can be removed due to the presence of pyrite and organic material. The investigation during this thesis gives an understanding of small-scale nitrate removal processes and parameters.

8. Perspectives

Regarding the content of this thesis, the data and study area has been limited. If there was time for further studies, it could be interesting to investigate other agricultural riparian areas located at a sub glacial stream trench, in order to explore if it is the same chemical processes that controls the water chemistry and possible nitrate removal that was with high possibility found for the agricultural field at EVI2. It could be interesting to investigate if such riparian areas are able to reduce nitrate before the water enters the groundwater and stream. This could be used for optimization of a new spatially differentiated regulation of nitrate.
Furthermore the investigations of the water chemistry in the summer and winter season was only based on measurements from March, February and September. These analyses could advantageously be expanded to include more measurements, optimally from every month. Similarly, it could be interesting to investigate the pyrite content at the agricultural field in other locations and depths.

Further investigations of the denitrification rate could also be interesting. This could include optimization of the 2D PHAST models pyrite rate expressions by including the rates found by the push-pull experiment. Further analysis of the wetland could also be interesting in order to find the controlling processes for this area. This could include MEP analysis of the geology and installation of new deeper wells.

9. Reference

- Agriculture Solutions, 2016, *The why and how to testing the Electrical Conductivity of Soils*. *https://www.agriculturesolutions.com/resources/92-the-why-and-how-to-testing-the-electrical-conductivity-of-soils* downloaded 24.10.2016

- Antivakis C., 2012, *Distillations for silver sulfide,* NordCEE, Syddansk Universitet

- Appelo, C.A.J and Postma D., 2005, *Geochemistry, groundwater and pollution,* A.A. Balkema Publishers, Leiden, The Netherlands a member of Taylor & Francis Group plc. Amsterdam, 2. Ed.

- Aquaveo, 2016, *GMS Tutorials; MODFLOW – Model Calibration*, http://gmstutorials-10.1.aquaveo.com/MODFLOW-ModelCalibration.pdf , downloaded 18.10.16

- Borggaard, O. K. and Elberling B., 2013, *Pedological Biogeochemistry.* University of Copenhagen, Copenhagen, Denmark.

- Breuning-Madsen, H; Krogh L., 2005, *Jordbundsgeografi*, Institut for Geografi og Geologi, Københavns Universitet

- Clark I. and Fritz P., 1997, *Environmental Isotopes in Hydrogeology*, Lewis Publishers, CRC Press LLC.

- Cline, J. D., 1969, Spectrophotometric determination of hydrogen sulfide in natural waters. Limnol.Oceanogr, year 14, p. 454-458.

- Dahl, M., Nilsson, B., Langhoff, J.H., Refsgaard, J.C., 2007. *Review of classification systems and new multi-scale typology of groundwater–surface water interaction*. J. Hydrol. 344, 1–16.

- Enemark, T., 2015, *Modelling of interactions between groundwater and lakes Hampen and Ejstrup in Skjern River Catchment*, University of Copenhagen.

- Engesgaard, P., 2003, *Groundwater flow and solute transport*, Geological Institute, University of Copenhagen

- Ernstsen, V., 2014, *Omsætning af nitrat i undergrunden*, Geoviden Nr. 4; Nitrat. Geocenter Danmark

- Fetter, C.W., 1999, *Contaminant hydrogeology*, Prentice Hall, 2. Ed.

- Fitts, R. C., 2002, *Groundwater Science;* Academic Press, 1. Ed.

- Fitts, R. C., 2013, *Groundwater Science;* Academic Press, 2. Ed.

- Frind E.O. and Hokkanen G.E., 1987, *Simulation of the Borden Plume Using the Alternating Direction Galerkin Technique*, Water Resources Research Vol. 23, No. 5, Pages 918-930.

- GEUS, 2016, Borings databasen. Danmark og Grønlands Geologiske Undersøgelser GEUS. http://data.geus.dk/JupiterWWW/borerapport.jsp?borid=80863 downloaded 20.07.2016

- Gieskes, J. M.; Rogers, W.C., 1973, *Alkalinity determination in interstitial waters of marine sediments.* J. Sed. Petrol. V.43, P. 272-277.

- Harrison, J. A., 2016, The Nitrogen Cycle: Of Microbes and Men; *Earth Cycles*, Visionlearning.com. http://www.visionlearning.com/en/library/Earth-Science/6/The-Nitrogen-Cycle/98 Downloaded 28.8.2016

- Hendricks, Martin R., 2010, *Introduction to Physical Hydrology.* Oxford University Press

- Hill, A. R., 1996, *Nitrate removal in stream riparian zones*, J. Eviron. Qual vol. 25, July-August, 1996.

- Hunger, S.; Brenning L. G., 2007, *Greigite: a true intermediate on the polysulfide pathway to pyrite*, Geochemical Transactions, BioMed Central Ltd. 2007. https://geochemicaltransactions.springeropen.com/articles/10.1186/1467-4866-8-1

- Jessen S., Engesgaard P., Sørensen, L. T., Müller S., Leskelä J. and Postma D., 2016, *Decadal variations in groundwater quality in a sandy aquifer: a legacy from nitrate leaching and denitrification by pyrite*. *Manuscript under revision* after positive reviews at *Water Resources Research*.

- Karan, S.; Engesgaard, P.; Looms, M.C.; Laier, T.; Kazmierczak, J., 2013, *Groundwater flow and mixing in a wetland-stream system: Field study and numerical modeling;* Journal of hydrology 488 (2013) 73-83.

- Kidmose, J., Engesgaard P., Ommen D. A. O., Nilsson, B., Flindt M. R., and Andresen F. Ø., 2014, *The role of groundwater for lake-water quality and quantification of N seepage,* National Ground Water Association.

- Kofod, T., 2016, *Determining denitrification rates in riparian zones with Single-well "Push-Pull" method, Mid-Jutland in Denmark,* University of Copenhagen

- Massman, G., Tichomirowa M., Merz O., Pekdeger A., 2003, *Sulfide oxidation and sulfate reduction in a shallow groundwater system (Oderbruch Aquifer, Germany).* Journal of Hydrology, Elsevier Science.

- Müller, S., 2016, unpublished data of bulk precipitation average in Holtum catchment.

- Nichols, G., 2009, *Sedimentology and Stratigraphy.* 2nd edition, Wiley-Blackwell.

- Nørrevang, A. S. F. and van't Veen, S. G. W., 2014, *Hydrogeologiske forhold og betydningen af upwelling for nitratfjernelsen i et vådområde nær Holtum Å*, University of Copenhagen

- Parkhurst, D.L., and Appelo, C.A.J., 2013, *Description of input and examples for PHREEQC version 3—A computer program for speciation, batch-reaction, one-dimensional transport, and inverse geochemical calculations:* U.S. Geological Survey Techniques and Methods, book 6, chap. A43, 497 p., available only at http://pubs.usgs.gov/tm/06/a43.

- Parkhurst, D.L., Kipp, K.L., and Charlton, S.R., 2010, *PHAST Version 2—A program for simulating groundwater flow, solute transport, and multicomponent geochemical reactions*: U.S. Geological Survey Techniques and Methods 6–A35, 235 p.

- Pepper, I.L; Brusseau, M.L.; Gerba, C.P., 2006, *Environmental and pollution science* ; Academic Press, 2. Ed.

- Petersen, N. J., 2016, *Groundwater flow modelling and conceptualization - An investigation of the groundwater flow for an agricultural site near Holtum Stream, Denmark.* University of Copenhagen

- Postma, D.; Boesen, C.; Kristiansen, H.; Larsen, F., 1991, *Nitrate Reduction in an Unconfined Sandy Aquifer; Water Chemistry, Reduction Processes, and Geochemical Modeling*, Water Resour. 27, 2027-2045

- Postma, D.; Larsen, F.; Thai N. T.; Trang, P. T. K.; Jakobsen R.; Nhan, P. Q., Long T. V.; Viet P. H.; Murray A. S., 2012, *Groundwater arsenic concentrations in Vietnam controlled by sediment age,* NATURE GEOSCIENCE | VOL 5,

- Poulsen, J. R.; Sebok, E.; Duque, C.; Tetzlaff, D.; and Engesgaard, P. K., 2015, *Detecting groundwater discharge dynamics from point-to-catchment scale in a lowland stream: combining hydraulic and tracer methods*: Hydrology and Earth System Sciences, v. 19, no. 4, p. 1871-1886.

- Scharling M. and Kern-Hansen, C. 2002, *Klimagrid – Danmark Nedbør og fordampning 1990-2000.* Danmarks Meteorologiske Institut, TECHINICAL REPORT 02-03 *http://www.dmi.dk/fileadmin/user_upload/Rapporter/TR/2002/tr02-03.pdf* downloaded 01.08.16

- Sebok E.; Duque C.; Engesgaard P. and Boegh E., 2014, *Spatial variability in streambed hydraulic conductivity of contrasting stream morphologies: channel bend and straight channel,* Hydrol. Process. (2014), Wiley Online Library.

- Skov- og Naturstyrelsen, 1987, *Geofysik og råstofkortlægning*

- Sonnenborg, T. O. and Henriksen H. J., 2005, *Håndbog i grundvandsmodellering*, Miljøministeriet

- Steiness M., Parnanzone F. and Spitilli M., 2016, Unpublished data of discharge in the stream and springs at the wetland area at EVI2.

- Stookey, L. L., 1970, *Ferrozine - a new spectrophotometric reagent for iron.* Analytical Chemistry 42: 779-781.

- SVANA, 2016, *Vandområdeplaner*, Miljø- og Fødevareministeriet, Styrelsen for Vand- og Naturforvaltning. http://svana.dk/vand/vandomraadeplaner/vandomraadeplaner-2015-2021/vandomraadeplaner-2015-2021/ Downloaded 21.10.2016

- Tesoriero, A. J., and L. J. Puckett, 2011, *O2 reduction and denitrification rates in shallow aquifers*, Water Resour. Res., 47, W12522, doi:10.1029/2011WR010471.

- TRENDS., 2016, *Trends, a research project on Transport and Reduction of Nitrate in Danish landscapes at various Scales.* http://trends.nitrat.dk/about_us_uk/main.html Downloaded 21.10.2016

- Vidon P, G, F.; Hill A. R., 2004, *Landscape controls on the hydrology of stream riparian zones:* Journal of Hydrology, v. 292, no. 1-4, p. 2010-228

- Williamson, M.A., and Rimstidt, J.D., 1994, *The kinetics and electrochemical rate-determining step of aqueous pyrite oxidation*: Geochimica et Cosmochimica Acta, v. 58, no. 24, p. 5443–5454.

Appendix 1: Rawdata of the chemistry measurements at EVI2

Measured in November 2015, February 2016, March 2016 and September 2016

Well ID	Sampling date	Screen depth m below surf	Distance from stream (m) (Stream:	Transect	EC µS/cm	pH -	Temp. C	Alkalinity meq/L	fluoride mM	chloride mM	nitrite mM	bromide mM	nitrate mM	phosphate mM	sulfate mM	sodium mM	ammonium µm/L	potassium µm/L	calcium mM	magnesium µm/L	Fe2+ mM	H2S_mM	O2_mM
C10 S	18-02-2016	2.14	-11	2	362	5.93	5.6	0.663	0.0076	1.7640	0.0039	0.0063	0.0000	0.0000	0.2544	1.2142	0.1108	0.1130	0.4860	0.1586	0.0504	0.0004	0.0078
TH4 3mut	18-02-2016	3.9	112	3	272	6.03	5.3	2.147	0.0074	0.5013	0.0053	0.0091	0.0000	0.0000	0.0098	0.5288	0.1554	0.1370	0.7782	0.1476	0.0169	0.0014	0.0039
F4	18-02-2016	2	3	3	300	6.04	3.2	1.99	0.01	0.42	0.02	0.01	0.00	0.00	0.09	0.35	0.05	0.06	1.02	0.16	0.05	0.00	0.03
C20 D	18-02-2016	4.12	-21	2	511	5.89	7.2	0.88	0.01	2.88	0.01	0.01	0.00	0.00	0.42	2.61	0.06	0.10	0.65	0.11	0.05	0.00	0.00
TH4, 4 MU	08-03-2016	4.9	112	3	342	6.46	6.1	1.40	0.00	0.73	0.00	0.01	0.00	0.00	0.37	0.55	0.04	0.10	0.94	0.22	0.05	0.00	0.01
TH4 5 MU	08-03-2016	5.9	112	3	269	5.55	6.8	1.43	0.01	0.80	0.00	0.01	0.00	0.00	0.06	0.63	0.26	0.15	0.52	0.08	0.03	0.00	0.01
TH4 6mut	09-03-2016	6.92	112	3	232	5.76	6.4	1.28	0.01	0.67	0.00	0.01	0.00	0.00	0.08	0.54	0.22	0.09	0.54	0.18	0.02	0.01	0.01
TH3 2mut	18-02-2016	1.9	74	3	327	5.98	4.2	0.39	0.00	0.75	0.00	0.00	1.25	0.00	0.22	0.44	0.00	0.00	0.90	0.24	0.00	0.00	0.01
TH3 3mut	09-03-2016	3.2	74	3	400	5.1	5.7	0.10	0.02	0.62	0.00	0.00	0.59	0.00	1.28	0.59	0.00	0.00	1.21	0.27	0.01	0.01	0.01
TH3 4mut	09-03-2016	4.2	74	3	293	5.86	7.3	1.33	0.01	0.72	0.00	0.01	0.01	0.00	0.23	0.46	0.00	0.08	0.80	0.13	0.05	0.00	0.01
TH3 5mut	09-03-2016	5.2	74	3	288	6.05	7.9	1.91	0.01	0.75	0.00	0.01	0.01	0.00	0.03	0.50	0.00	0.06	0.80	0.17	0.05	0.01	0.01
TH2.2 2mu	09-03-2016	2.19	15	3	259	5.66	5.7	1.00	0.00	0.27	0.01	0.01	0.00	0.00	0.34	0.19	0.00	0.00	0.80	0.14	0.05	0.00	0.01
TH2.2 3mu	09-03-2016	3	15	3	306	5.48	5.9	0.67	0.01	0.40	0.00	0.00	0.00	0.00	0.81	0.35	0.00	0.00	0.97	0.14	0.05	0.00	0.00
TH1.2 2mu	09-03-2016	1.9	37	3	285	5.71	7.3	0.76	0.01	0.24	0.00	0.00	0.00	0.00	0.72	0.45	0.05	0.00	0.93	0.13	0.02	0.00	0.01
TH2.2 4mu	09-03-2016	4	15	3	320	5.57	6.3	0.67	0.01	0.41	0.00	0.00	0.00	0.00	0.86	0.38	0.00	0.00	0.97	0.16	0.05	0.00	0.01
TH6-S	09-03-2016	2	2	3	301	5.79	6.9	0.92	0.00	0.43	0.00	0.01	0.00	0.00	0.67	0.40	0.00	0.05	0.88	0.15	0.05	0.00	0.00
TH2.2 5mu	09-03-2016	5.06	15	3	333	5.53	6.5	0.44	0.01	0.44	0.00	0.00	0.00	0.00	1.03	0.37	0.00	0.00	0.97	0.15	0.05	0.00	0.01
Stream	10-03-2016	0	0	4	310	6.61	4.7	0.93	0.00	0.92	0.01	0.01	0.14	0.00	0.34	0.79	0.00	0.11	0.86	0.17	0.00	0.00	0.31
C20 S	18-02-2016	2.13	-21	2	252	5.74	5.5	0.78	0.00	0.49	0.00	0.00	0.00	0.00	0.40	0.70	0.12	0.07	0.39	0.09	0.05	0.00	0.01
TH-2.12mu	18-02-2016	11.9	15	3	326	7.48	4.6	1.81	0.01	0.61	0.01	0.01	0.00	0.00	0.24	0.52	0.00	0.00	1.14	0.17	0.03	0.00	0.01
C10 D	18-02-2016	6.16	-11	2	503	6.14	8	0.39	0.01	2.29	0.00	0.00	0.00	0.00	0.94	2.30	0.00	0.10	0.74	0.15	0.04	0.00	0.01
TH1.2 3mu	10-03-2016	2.9	37	3	357	5.96	4.5	1.03	0.01	0.51	0.00	0.01	0.00	0.00	0.98	0.38	0.00	0.05	1.11	0.22	0.02	0.00	0.01
TH1.2 4mu	10-03-2016	4.1	37	3	327	5.7	5.4	0.97	0.01	0.47	0.00	0.01	0.00	0.00	0.76	0.32	0.08	0.00	1.14	0.20	0.05	0.00	0.02
TH1.2 5mu	10-03-2016	5	37	3	281	5.7	7.7	0.63	0.01	0.38	0.00	0.00	0.00	0.00	0.75	0.36	0.12	0.05	0.86	0.15	0.05	0.00	0.01
Dræn v. at	10-03-2016	0	0.5	4	328	6.17	4.3	0.65	0.01	1.67	0.00	0.00	0.19	0.00	0.23	1.17	0.00	0.08	0.72	0.14	0.00	0.00	0.28
TH4 7mut	09-03-2016	7.9	112	3	235	6.25	7.4	1.38	0.01	0.53	0.00	0.01	0.00	0.00	0.12	0.44	0.00	0.05	0.74	0.14	0.03	0.00	0.01
overfor sø	18-02-2016	0	-97	4	556	6.49	3.8	0.48	0.00	0.64	0.01	0.00	1.19	0.00	0.25	0.53	0.00	0.32	0.75	0.26	0.00	0.00	0.30
Okker-kild	18-02-2016	0	-60	4	340	6.94	2.1	1.71	0.01	1.30	0.00	0.00	0.09	0.00	0.18	1.19	0.03	0.04	0.83	0.19	0.01	0.00	0.19
bæk ved å	18-02-2016	0	-1	4	450	7.04	4.4	0.95	0.00	1.81	0.00	0.00	0.74	0.00	0.31	1.64	0.00	0.15	0.93	0.25	0.00	0.00	0.38
TH4 8mut	09-03-2016	8.9	112	3	306	5.84	7.5	1.59	0.01	0.91	0.00	0.01	0.00	0.00	0.12	0.69	0.09	0.08	0.72	0.13	0.04	0.00	0.01
C5	18-02-2016	2.18	-7	2	320	6.02	5.2	1.02	0.01	0.90	0.00	0.00	0.00	0.00	0.27	0.79	0.09	0.09	0.60	0.15	0.09	0.00	0.01
stream	18-02-2016	0	0	4	309	6.94	4.7	1.23	0.01	0.89	0.01	0.02	0.16	0.00	0.35	0.71	0.00	0.07	0.85	0.14	0.00	0.00	0.30
C1 (nær å)	18-02-2016	2.15	-3	2	318	5.97	5.4	1.03	0.01	1.02	0.00	0.01	0.00	0.00	0.30	0.79	0.10	0.10	0.68	0.18	0.09	0.00	0.01
dræn	18-02-2016	0	10	4	330	8.3	3.8	0.62	0.01	1.65	0.01	0.01	0.21	0.00	0.23	1.15	0.00	0.00	0.69	0.12	0.00	0.00	0.32
S1	18-02-2016	2.82	0	2	344	6.66	6.7	2.33	0.00	0.42	0.01	0.01	0.00	0.00	0.28	0.33	0.00	0.00	1.22	0.13	0.05	0.00	0.02
C30	18-02-2016	3.17	-30	2	583	6.94	4.9	0.96	0.01	2.92	0.01	0.01	0.00	0.00	0.79	2.00	0.00	0.07	0.75	0.29	0.01	0.00	0.01
TH-1	18-02-2016	15.9	37	3	276	7.37	7.1	2.00	0.01	0.40	0.00	0.01	0.00	0.00	0.17	0.38	0.00	0.05	0.98	0.17	0.03	0.00	0.01
TH3 6mut	09-03-2016	6.2	74	3	345	6.22	8.4	1.78	0.01	1.01	0.01	0.02	0.00	0.00	0.16	0.59	0.00	0.09	1.07	0.16	0.05	0.00	0.01
Dræn-brøn	18-02-2016	0	-82	4	557	6.8	7.6	0.38	0.00	3.04	0.00	0.00	1.09	0.00	0.24	2.66	0.00	0.14	0.71	0.27	0.00	0.00	0.29
Jernkilde	18-02-2016	0	-56	4	458	6.44	8	0.99	0.01	1.85	0.01	0.01	0.66	0.00	0.31	1.64	0.00	0.13	0.95	0.21	0.00	0.00	0.24
TH3-D	14-09-2016	1.5	64	well	226	5.37	17	0.22	0.00	0.39	0.00	0.00	0.00	0.85	0.00	0.11	0.53	0.00	0.05	0.56	0.09	0.00	0.01
TH3-D	14-09-2016	3	64	well	281	5.48	15.4	0.13	0.01	0.43	0.00	0.01	0.51	0.00	0.63	0.59	0.00	0.03	0.69	0.17	0.00	0.00	0.00
TH3-D	14-09-2016	2	64	well	180.2	5.28	16.4	0.26	0.00	0.26	0.00	0.00	0.55	0.00	0.13	0.59	0.00	0.02	0.42	0.07	0.01	0.00	0.00
TH3-D	14-09-2016	4	64	well	274	5.63	14.4	0.55	0.01	0.63	0.00	0.01	0.04	0.00	0.71	0.47	0.01	0.07	0.71	0.14	0.04	0.00	0.00
Ditch	13-09-2016	0	-2	not well	504	6.57	15.8	0.52	0.00	2.84	0.00	0.01	0.82	0.00	0.25	2.43	0.00	0.11	0.64	0.26	0.00	0.00	0.20
TH6S	14-09-2016	2	2	well			1.53	0.00	0.58	0.00	0.01	0.00	0.56	0.63	0.01	0.06	1.07	0.16	0.04	0.00			
Spring 3. (drænbrøn	13-09-2016	0	-82	not well	489	6.57	10.7	0.35	0.00	3.38	0.00	0.01	1.32	0.00	0.31	2.37	0.00	0.13	0.64	0.26	0.00	0.00	0.26
TH3.2	12-09-216	3	74	well	365	4.86	14	0.10	0.02	0.31	0.02	0.01	0.08	0.00	1.87	0.63	0.00	0.03	1.08	0.20	0.00	0.00	0.01
TH3.2	12-09-216	2.5	74	well	221	4.9	15.8	0.18	0.00	0.20	0.00	0.01	0.00	0.00	0.84	0.46	0.00	0.03	0.57	0.10	0.04	0.00	0.01
TH3.2	12-09-216	1.5	74	well	189.7	5.5	17.5	0.31	0.00	0.35	0.01	0.01	0.84	0.00	0.22	0.58	0.00	0.02	0.47	0.09	0.01	0.00	0.00
Spring 4. (bæk ved	13-09-2016	0	-1	not well	410	6.58	14.9	1.09	0.00	1.71	0.00	0.01	0.73	0.00	0.34	1.34	0.00	0.21	0.83	0.24	0.00	0.00	0.27
TH3.2	12-09-2016	2	74	well	192.9	5.66	16.4	0.45	0.00	0.29	0.00	0.00	0.33	0.00	0.24	0.47	0.00	0.03	0.55	0.11	0.01	0.00	0.00
TH2.1	14-09-2016	12	15	well			2.12	0.00	0.46	0.00	0.01	0.00	0.00	0.00	0.18	0.48	0.00	0.04	1.04	0.13	0.02	0.00	0.00
Lake - "outlet"	13-09-2016	0	-97	not well	389	6.37	12.6	1.08	0.00	1.48	0.00	0.01	0.76	0.00	0.31	1.20	0.00	0.26	0.79	0.24	0.00	0.00	0.19
TH1.1	14-09-2016	16	37	well	299	6.52	12.5	2.01	0.00	0.43	0.00	0.01	0.00	0.00	0.22	0.42	0.00	0.04	1.04	0.15	0.03	0.00	0.00
TH2.2	14-09-2016	6	15	well				0.95	0.00	0.14	0.00	0.01	0.00	0.00	0.48	0.37	0.04	0.04	0.91	0.17	0.05	0.00	
Spring 5. (jernkilde)	13-09-2016	0	-56	not well	437	6.35	10.3	1.06	0.00	1.38	0.00	0.01	0.52	0.00	0.25	1.64	0.00	0.11	0.93	0.22	0.00	0.00	0.23
Stream	13-09-2016	0	0	not well	335	6.78	13.1	1.44	0.00	0.84	0.00	0.01	0.07	0.00	0.36	0.84	0.00	0.08	0.98	0.13	0.00	0.00	0.24
TH3-U	13-09-2016	2	84	well				1.48	0.11	0.16	0.00	0.01	0.06	0.00	0.76	0.69	0.01	0.05	1.07	0.20	0.01	0.00	

Appendix 2: The calculated EC balance for all water samples at EVI

Well ID	Sampling date	Sum kat	Sum an	EB balan	EC/100
C10 S	18-02-2016	2.77762	2.95004	-3.0103	3.62
TH4 3mu	18-02-2016	2.68766	2.68464	0.05629	2.72
F4	18-02-2016	2.87039	2.60196	4.90508	3
C20 D	18-02-2016	4.33976	4.62901	-3.22507	5.11
TH4_4 MI	08-03-2016	3.05584	2.87703	3.01392	3.42
TH4 5 MU	08-03-2016	2.26842	2.37197	-2.23145	2.69
TH4 6mu	09-03-2016	2.30374	2.11864	4.18569	2.32
TH3 2mu	18-02-2016	2.71639	2.83262	-2.09452	3.27
TH3 3mu	09-03-2016	3.5502	3.8976	-4.66438	4
TH3 4mu	09-03-2016	2.4524	2.5474	-1.90011	2.93
TH3 5mu	09-03-2016	2.53834	2.75158	-4.03109	2.88
TH2.2 2m	09-03-2016	2.12	1.95379	4.08014	2.59
TH2.2 3m	09-03-2016	2.61761	2.69612	-1.47746	3.06
TH1.2 2m	09-03-2016	2.64887	2.45341	3.83079	2.85
TH2.2 4m	09-03-2016	2.67878	2.81033	-2.39649	3.2
TH6-S	09-03-2016	2.56466	2.70334	-2.63248	3.01
TH2.2 5m	09-03-2016	2.64464	2.94739	-5.41387	3.33
Stream	10-03-2016	2.96294	2.68117	4.99227	3.1
C20 S	18-02-2016	1.89262	2.07077	-4.49487	2.52
TH-2 12m	18-02-2016	3.15663	2.92186	3.86227	3.26

Well ID	Sampling date	Sum kat	Sum an	EB balan	EC/100
C10 D	18-02-2016	4.22352	4.55876	-3.81726	5.03
TH1.2 3m	10-03-2016	3.12367	3.30946	-5.81619	3.57
TH1.2 4m	10-03-2016	3.14053	2.97952	2.63087	3.27
TH1.2 5m	10-03-2016	2.59868	2.52166	1.5041	2.81
Dræn v. a	10-03-2016	2.98195	2.9734	0.14345	3.28
TH4 7mu	09-03-2016	2.29698	2.16251	3.01541	2.35
overfor s	18-02-2016	2.87036	2.81479	0.97743	5.56
Okker-kil	18-02-2016	3.31064	3.45494	-2.13278	3.4
baek ved	18-02-2016	4.15687	4.13497	0.26408	4.5
TH4 8mu	09-03-2016	2.60768	2.76006	-2.8388	3.06
C5	18-02-2016	2.55317	2.48424	1.3683	3.2
stream	18-02-2016	2.75842	3.00864	-4.33873	3.09
C1 (nær å	18-02-2016	2.79757	2.67097	2.31497	3.18
dræn	18-02-2016	2.77442	2.95667	-3.18003	3.3
S1	18-02-2016	3.07662	3.32425	-3.86881	3.44
C30	18-02-2016	4.18153	5.46825	-13.3342	5.83
TH-1	18-02-2016	2.76513	2.75563	0.17201	2.76
TH3 6mu	09-03-2016	3.18137	3.13434	0.74473	3.45
Drænbrøn	18-02-2016	4.77755	4.98378	-2.11272	5.57
Jernkilde	18-02-2016	4.08843	4.14509	-0.68814	4.58

Well ID	Sampling date	Sum kat	Sum an	EB balan	EC/100
TH3-D	14-09-2016	1.86693	1.69243	4.90257	2.26
TH3-D	14-09-2016	4.33567	4.69244	-3.95171	5.04
TH3-D	14-09-2016	1.60136	1.33648	9.01605	1.802
TH3-D	14-09-2016	2.2796	2.657	-7.64499	2.74
Ditch	13-09-2016	4.33567	4.69244	-3.95171	5.04
TH6S	14-09-2016	3.2002	3.24267	-0.65918	0
Spring 3.	13-09-2016	4.30072	5.66559	-13.6949	4.89
TH3.2	12-09-216	3.22746	4.24122	-13.5735	3.65
TH3.2	12-09-216	1.8764	2.07706	-5.07535	2.21
TH3.2	12-09-216	1.72121	1.93722	-5.90419	1.897
Spring 4.	13-09-2016	3.69823	4.21968	-6.58577	4.1
Exp. Blan	13-09-2016	6.10754	6.48367	-2.9872	6.83
TH3.2	12-09-2016	1.8253	1.54876	8.19604	1.929
TH2.1	14-09-2016	2.86659	2.94359	-1.32518	0
Spring B	13-09-2016	3.52763	3.94987	-5.6468	3.89
TH1.1	14-09-2016	2.86766	2.89614	-0.49411	2.99
TH2.2	14-09-2016	2.65596	2.0596	12.6467	0
Spring 5.	13-09-2016	4.06158	3.46323	7.95176	4.37
Stream	13-09-2016	3.13773	3.08634	0.82564	3.35
TH3-U	13-09-2016	3.3057	1.8605	27.9749	

Appendix 3: PHEEQC 1D model for TH3

```
selected_output
-file C:\Users\Sofie\Dropbox\Holtum 2016\Data\phreeqc_model.xls
-totals O(0) S(-2) S(6) Ca Fe(2) N(5) C(-4) H(0) N(0)
-pH
-Alkalinity
-saturation_indices Calcite CO2(g) CH4(g)
-equilibrium_phases Goethite


Solution 0 #TH3 in 2 mbs.
Units mmol/l
Temp 4.2
ph 5.98
O(0) 0.0 #no oxigen present is chosen in order to make the model as simple as possible
Alkalinity 0.391
Cl 0.7546
S(6) 0.2192
Na 0.4435
K 0.000
Ca 0.8960
Mg 0.2384
Fe(2) 0.0081
N(5) 1.25

Solution 1-10 #initial values (TH3 in 2 mbs.)
Units mmol/l
Temp 4.2
ph 5.98
O(0) 0.0
Alkalinity 0.391
Cl 0.7546
S(6) 0.2192
Na 0.4435
K 0.000
Ca 0.8960
Mg 0.2384
Fe(2) 0.0081
N(5) 1.25

Equilibrium_phases 2
Goethite -0.5 #Iron present -1 means more stabil

Equilibrium_phases 3-10
pyrite 0 0 #in total precipitates only
Goethite -0.77
#siderite 0 0


reaction 2-3
pyrite
0.25 mmoles #før0.23

reaction 4-10 #kinetic is here. everything else is in equilibrium
CH2O
2 mmoles #2 is enough for sulfate to be reduced

TRANSPORT
-cells  10
-length 1 # cell length 1 m, column length 10*1 = 10 m
-dispersivity   0.1 # m
-shifts 20 # 10/20 = 2 pore volumes
-flow_direction forward
-time_step 3.15e7 # 1 meter/year
-boundary_conditions flux flux # at column ends
-diffusion_coefficient 0.3e-9 # m2/s
-punch_frequency 20 # Punching/graphing is done after each 20rd shift.


print
-reset false

end
```

Appendix 4: PHAST chemical script for Model A, B and C

SOLUTION_SPECIES # Disable NO2- and NH4+ which means that nitrate is not suddenly formed

NO3- + 2H+ + 2e- = NO2- + H2O

log_k -100 # 28.570

2NO3- + 12H+ + 10e- = N2 + 6H2O

log_k 207.080

NO3- + 10 H+ + 8 e- = NH4+ + 3 H2O

log_k -200 # 119.077

solution 1 Natural water for PHAST(bufferzonen), based on measurement for EVI2 (TH3 2 meter) without Fe2+, nitrate and with calculated oxygen.

temp 4.2

ph 5.98

Units mmol/l

O(0) 0.4

Alkalinity 0.391

Cl 0.0

S(6) 0.2192

Na 0.4435

K 0.000

Ca 0.8960

Mg 0.2384

Fe(2) 0.0

N(5) 0.0

end

solution 2 Nitrate peak agricultural area recharge for PHAST, based on TH3. Calculated oxygen and no Fe2

temp 4.2

ph 5.98

Units mmol/l

O(0) 0.4 #It is chosen that oxygen is present in the infiltration water. The oxygen concentration corresponds with equilibrium with the atmosphere

Alkalinity 0.391

Cl 0.7546

S(6) 0.2192

Na 0.4435

```
K 0.000
Ca 0.8960
Mg 0.2384
Fe(2) 0.0 #no Fe2+ because it is impossible if there is oxygen present
N(5) 1.5 #minimum 1.25.   1.3 for model A and C . 1.5 for model B
end

solution 3 Initial conditions. - Natural water just without oxygen
temp 4.2
ph 5.98
Units mmol/l
O(0) 0
Alkalinity 0.391
Cl 0.0
S(6) 0.09 #changed from 0.2192 because it is assumed that some denitrification had been going on in the measurement
from TH3 2 m.b.s.
Na 0.4435
K 0.000
Ca 0.8960
Mg 0.2384
Fe(2) 0.0
N(5) 0.0
end

equilibrium_phases 1 # 2 m.b.s. only iron oxiders
Goethite -0.35  # ironoxider that gives Fe2+ (-1 means more stable)
Siderite 0 0
end

equilibrium_phases 2 # 3-10 m.b.s. . pyrite precitates and iron oxiders is present
pyrite 0 0 #netto it only precipitates
Goethite -0.3
Siderite 0 0
end

RATES 1 #PYRITE
PR     #rate name
  -start
   1 rem            parm(1) = log10(A/V, 1/dm)      parm(2) = exp for (m/m0)
```

```
  2 rem          parm(3) = exp for NO3-                    parm(4) = exp for O2
  3 rem    parm(5) = exp for H+

  10 if (m <= 0) then goto 200
  20 if (si("Pyrite") >= 0) then goto 200
  20  rate = -10.19 + parm(1) + parm(4)*lm("O2") + parm(3)*lm("NO3-") + parm(5)*lm("H+") +
parm(2)*log10(m/m0)
  30  moles = 10^rate * time # 10^rate
  40 if (moles > m) then moles = m
  #50 if (moles >= (mol("O2")/3.5)) then moles = mol("O2")/3.5
  200 save moles
 -end

KINETICS 1 #pyrite 2-3 m.b.s.
PR      #rate name
                -formula FeS2
                -tol            1e-8  #Tolerance for integration procedure (moles)
                -m0             1 #initial moles of reactant . m0 og m  sættes begge til 1 pga forholdet indgår i rate
                -m              1          #0.00025   Current moles of reactant.
                -parms  300     1    5    .5     -0.11    #ex. From the manual: 3.0 0.67 0.5 0.5 -0.11

RATES 2
Organic_C
 -start
  10 if (m <= 0) then goto 200
  20  mO2 = mol("O2")
  30  mNO3 = tot("N(5)")
  40  mSO4 = tot("S(6)")
  50            rate = 1.57e-9*mO2/(2.94e-4 + mO2) + 1.67e-11*mNO3/(1.55e-4 + mNO3)
  60            rate = rate + 1.e-13*mSO4/(1.e-4 + mSO4)
  70  moles = rate * m * (m/m0) * time
  80 if (moles > m) then moles = m
  200 save moles
 -end

KINETICS 2  # 4-10 m.b.s. ORGANIC MATERIAL
Organic_C
-formula CH2O
-tol             1e-8                                    # m in mol/kgw
```

```
-m0                 1    #initial moles of reactant
-m                                  30    #5e-3
reaction 2 # 4-10 m.b.s. ORGANIC MATERIAL
CH2O
2 mmoles
end

selected_output
#-file              C:\Users\Sofie van't Veen\Dropbox\1. SPECIALE_Sofie\PHAST\EVI2\PHAST
MODELLER\phast_model.xls
-totals O(0) S(-2) S(6) Ca Fe(2) N(5) C(-4) H(0) N(0) Cl
-pH
-Alkalinity
-kinetic_reactants PR Organic_C
-saturation_indices Calcite CO2(g) CH4(g)
-equilibrium_phases Goethite
end
```

Appendix 5: Conductance and hydraulic conductivity in stream and drain in the PHAST models

In PHAST the conductance is used to calculate the leakage between the streambed and groundwater and to find the hydraulic conductance for the drain. The equation for the conductance is described in section 3.5.

$$Cond = \frac{K_m * A}{D}$$

Where

Cond: The conductance [m²/day]

A: The vertical flow area [m²]

Km: Hydraulic head in the closes well [m/day](TH6-S= 20 m/day)

D: Streambed thickness [m]

The stream:

*A= 2*1=2m*

D=1m

Km=20 m/day divided in 3 because of an anisotropy at 3.

$$Cond = \frac{2 * \frac{20}{3}}{1} = 13.3\ m^2$$

The drain:

Cond= 5 m²

Width=0.2m

Thickness=0.1m

$$5m^2 = \frac{(0.2*0.1)*\frac{Km}{3}}{0.1} <=> Km=25m/day$$

Appendix 6: Anisotropy and conductance sensitivity analysis

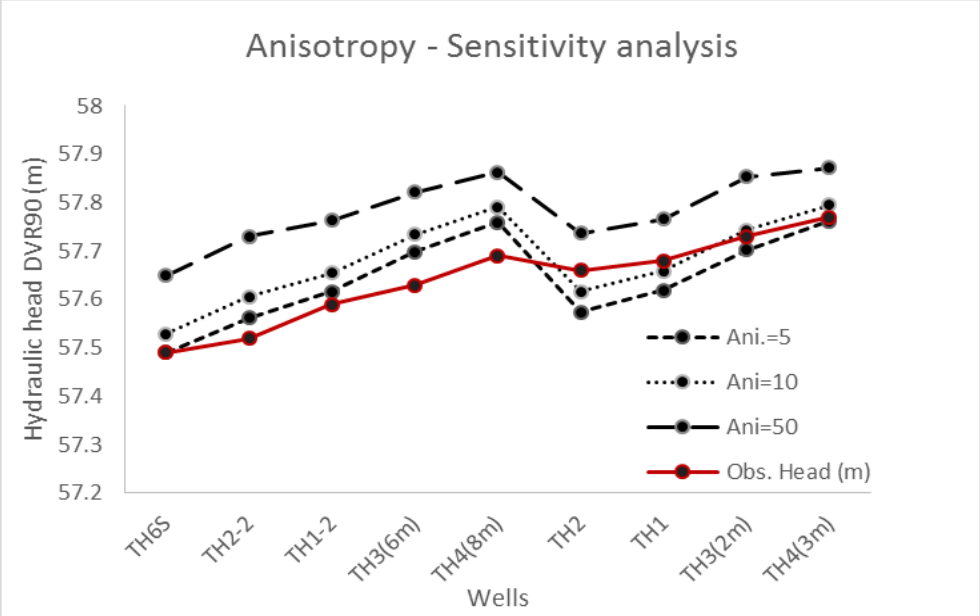

	RMSE (m)
Ani=1	**0.0814**
Ani=5	**0.0796**
Ani=10	**0.087**
Ani=50	**0.1587**

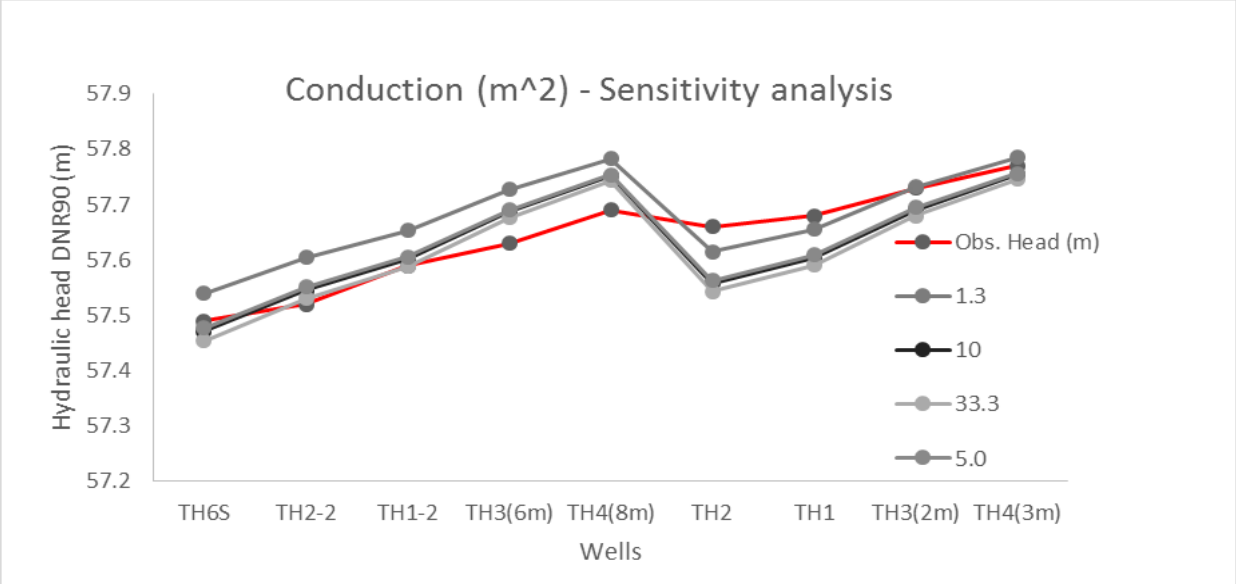

K for stream and drain(m/day)	Conductance (m2)	RMSE (m)
5	3.3	**0.0796**
7.5	5.0	**0.0809**
10	6.7	**0.0819**
15	10.0	**0.0833**
50	33.3	**0.0859**
2	1.3	**0.0845**

Appendix 7: Pyrite extraction results

Ag_2S	247.8	g/mol
S^{2-}	32.065	g/mol
Fe	55.845	g/mol
FeS_2	119.98	g/mol

By addition of 0,5 ml AgNO3: 0.00050 mol Ag

0.00025 mol S

No.	Date	Sample ID	[g] sample	[g] filter (before)	[g] filter (after)	g Ag2S	mol S	ml added 1M AgNO3	Check	% Fe_{Py}	% FeS2	Mol pyrit ideter to S i	omregne t til gram	divideret med	pyrit g/kg	Notes
1	26-09-2016	Shale 1	0.511	0.6235	0.6678	0.0443	0.000179	0.500000	ok	0.9769	2.0987	0.000358	0.0429	0.0839	83.9499	control 2% FeS2
2	26-09-2016	B1	2.0704	0	0	0.0000	0.000000	0.500000	ok	0.0000	0.0000	0.000000	0.0000	0.0000	0.0000	not crushed
3	26-09-2016	C- mix without crushing	2.1624	0.6562	0.6593	0.0031	0.000013	0.500000	ok	0.0162	0.0347	0.000025	0.0030	0.0014	1.3882	not crushed
10	26-09-2016	C mix after crushing	2.0221	0.6211	0.6231	0.0020	0.000008	0.500000	ok	0.0111	0.0239	0.000016	0.0019	0.0010	0.9578	crushed
11	26-09-2016	B5	2.0014	0.601	0.6029	0.0019	0.000008	0.500000	ok	0.0107	0.0230	0.000015	0.0018	0.0009	0.9193	crushed
12	26-09-2016	B4	2.0182	0.6368	0.6384	0.0016	0.000006	0.500000	ok	0.0089	0.0192	0.000013	0.0015	0.0008	0.7677	crushed
13	26-09-2016	B3	2.1744	0.5869	0.5891	0.0022	0.000009	0.500000	ok	0.0114	0.0245	0.000018	0.0021	0.0010	0.9798	crushed
14	26-09-2016	B2	2.1926	0.6013	0.6029	0.0016	0.000006	0.500000	ok	0.0082	0.0177	0.000013	0.0015	0.0007	0.7066	crushed

Appendix 8: Pyrite rate calculation

Based on the FeS2 concentration measured in a mixed sample from 2-3 m.b.s. and nitrate measured in TH3 in 2 m.b.s.

Vertical water flow calculation from the PHAST model A:

K = 3.33 m/d

head in 1.9 m.b.s. =57.778545 m

head in 3.2 m.b.s = 57.778061 m

L=1.3 m

Darcy q=K*dh/L=0,001 m/day

VFeS2 = V_{H2O}/R = V_{H2O}/ 1 + delta q / delta c							
delta q= difference in electron acceptor concentration							
delta c= difference in pyrite concentrationen							
					Vertical flow	0.001	m/day
	mmol/L	elektrode use			V_{H2O}	0.45	m/yr
Oxygen	0.3	4			delta c	8.7	
nitrate	1.5	5			delta q	268.2924	
FeS2	17.88616	15					
					delta q/delta c	30.8382069	
VFeS2	0.014085	0.014085	m/yr	1.408511			
The present day profile from marts has developed during the last						213.0	yr

The results from the pyrite extraction by use of silver sulfide. mMol/L is calculated by assuming a porosity at 0.3 and that the rest of the sediments are quarts with a mole weight of 2.65.

Sample ID	Meter below surface	% FeS2	Gram pyrite/kg soil	mMol/kg	mMol/L
B1	1.6	0.000	0.00	0.0	0.0
B2	1.7	0.018	0.18	1.5	9.1
B3	1.8	0.024	0.24	2.0	12.6
B4	1.9	0.019	0.19	1.6	9.9
B5	2	0.023	0.23	1.9	11.8
C before crushing	2 - 3	0.035	0.35	2.9	17.9
C after chrushing	2 - 3	0.024	0.24	1.9	12.3

Appendix 9: PHREEQC speciation based on the measurements

Speciation made in PHREEQC						
	Screen depth (m.b.s.)	si_Calcite	si_CO2(g)	pCO2	si_siderite	si_Mackinawite
TH3	1.9	-2.8	-1.7	0.0193	-2.5	-1.1
	3.2	-4.2	-1.4	0.0399	-3.6	-1.0
	4.2	-2.4	-1.0	0.0892	-1.0	0.2
	5.2	-2.0	-1.1	0.0821	-0.7	1.6
	6.2	-1.8	-1.3	0.0523	-0.5	1.2
TH4	3.9	-2.0	-1.0	0.0956	-1.1	0.5
	4.9	-1.7	-1.6	0.0231	-0.4	0.8
	5.9	-2.8	-0.7	0.1963	-1.5	0.2
	6.92	-2.7	-1.0	0.1077	-1.5	0.6
	7.9	-2.0	-1.4	0.0378	-0.7	0.6
	8.9	-2.4	-1.0	0.1118	-1.0	0.4

Appendix 10: Cations concentration measured in TH3, TH4, TH3.2 and TH3-D

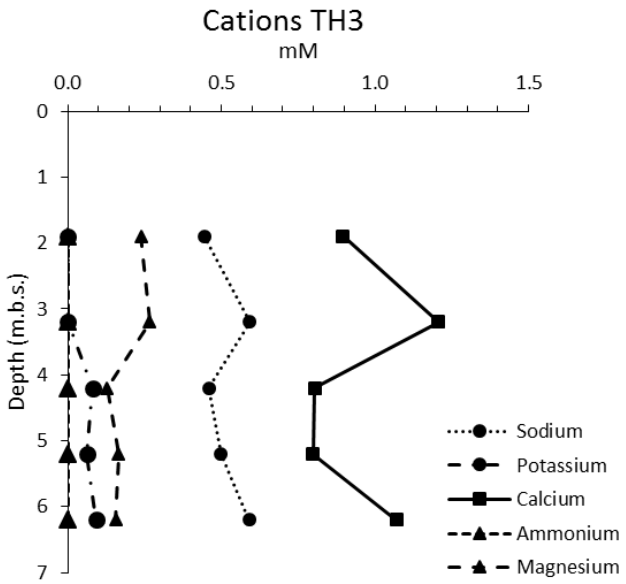

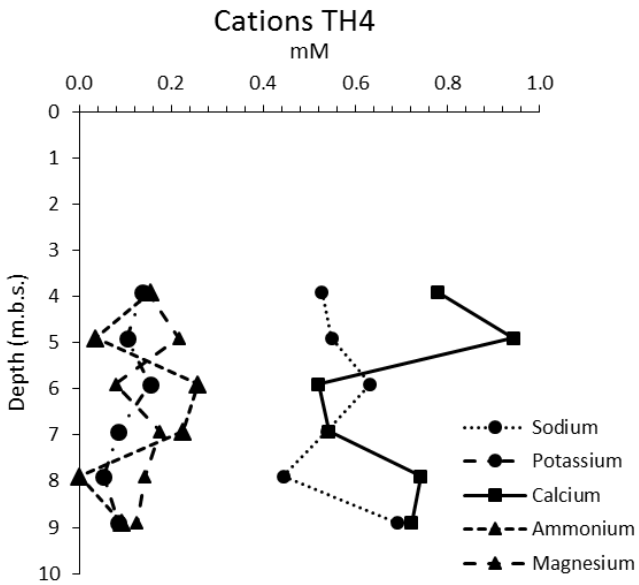

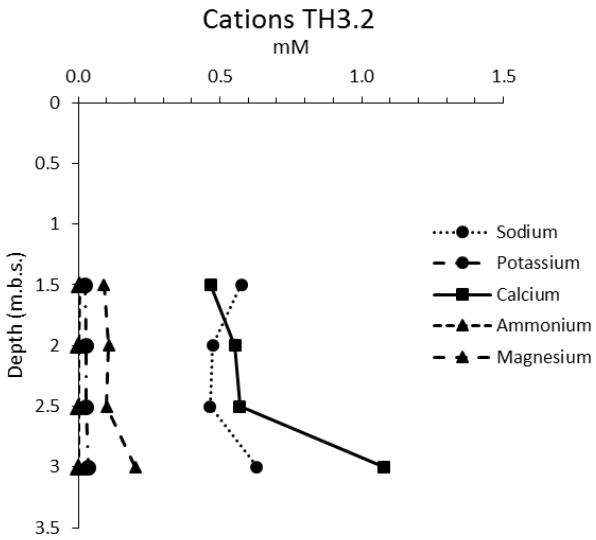

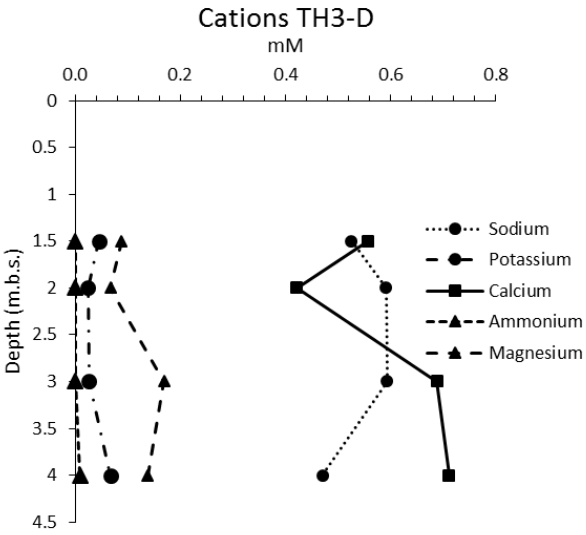

Appendix 11: 1-1 lines of observed vs. simulated heads in the 2D PHAST models

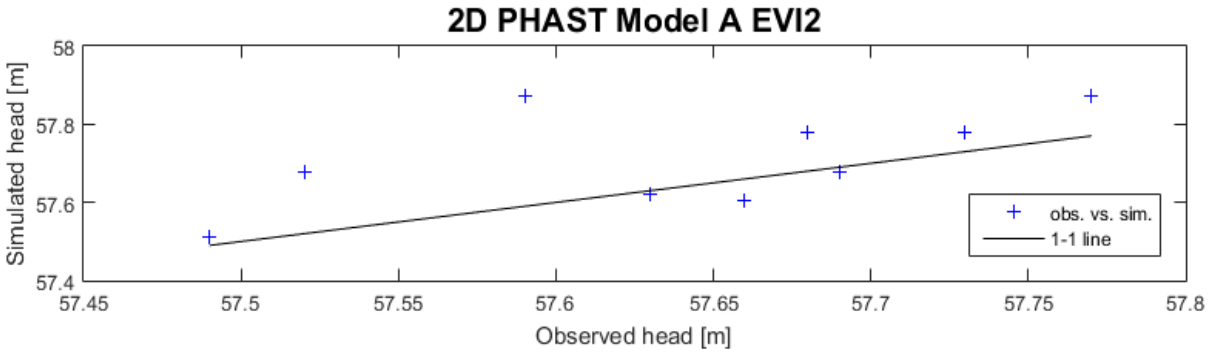

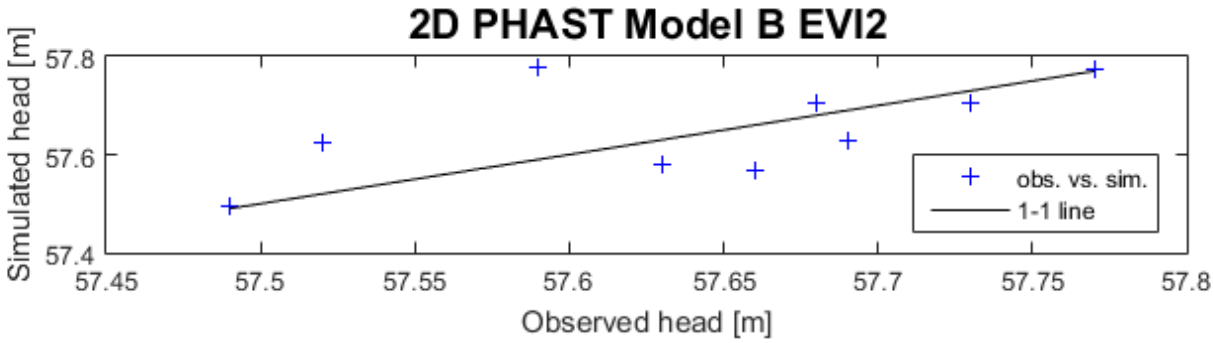

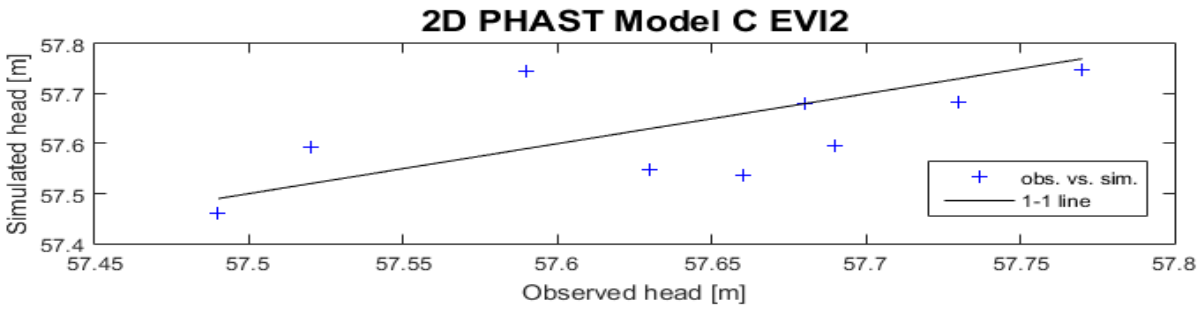

Appendix 12: MATLAB script for the water flow for the 2D PHAST models

```
clc, clear all  %Ensures that all previous provisions and characters are deleted

load velocities_ny.txt
data1=velocities_ny;
%Velocity in the cells in the model

load Evi2_modelA_ny.head.dat
data=Evi2_modelA_ny_head; %note that matlab changes file name
nx=85;
ny=2;
nz=84;

n=length(data);
j=1;
k=1;
for i=nz:-1:1
    for j=1:nx
        x(i,j)=data(k,1);
        z(i,j)=data(k,3);
        h(i,j)=data(k,4);
        vx(i,j)=data1(k,6);
        vz(i,j)=data1(k,8);
        k=k+1;
    end
    k=k+nx;
end

figure(1)
V=linspace(57.4,58,15);
[C,F]=contourf(x,z,h,V); %Please contour with fill using vector V (,V)
clabel(C,F,V) %Add labeling (,V)
colorbar % And a colorbar
colormap(jet) %color jet er farveskalaen
caxis([57.4,58]) %defines the min and max values at the colorbar
c = colorbar;  %defines a label at the colorbar
c.Label.String = 'Hydraulic head (m)'; %defines a label at the colorbar
grid off % No grid
title('2D groundwater flow - Model B','fontsize',16)
xlabel('Distance from stream (m)')
ylabel('Elevation (m)')
axis([0,170,38,60])

dx=170/nx;
dz=21/nz;


hold on
%Add velocity vectors
skip=35; %means that only every 30 flow vector are plotted
quiver(x(1:skip:end),z(1:skip:end),vx(1:skip:end),vz(1:skip:end),2,'k')
```

Appendix 13: MATLAB script for the hydraulic heads simulations in the PHAST models

```
clc, clear all  %Ensures that all previous provisions and characters are deleted

load Wells_i_phast_nyt_grid.txt
data=Wells_i_phast_nyt_grid; %note that matlab changes file name

%Data = Observed heads
depth=Wells_i_phast_nyt_grid(:,2); %depth
x=Wells_i_phast_nyt_grid(:,1); %x i meter from stream
z=Wells_i_phast_nyt_grid(:,7); %z i meter depth
y=Wells_i_phast_nyt_grid(:,6); %y i celle
h=Wells_i_phast_nyt_grid(:,3); %head measured

%data from the 2D PHAST model
load Evi2_modelA_ny.head.dat
data=Evi2_modelA_ny_head; %note that matlab changes file name

xsim=Evi2_modelA_ny_head(:,1); %x in PHAST model
ysim=Evi2_modelA_ny_head(:,2); %y in PHAST model
zsim=Evi2_modelA_ny_head(:,3); %z in PHAST model
hsim=Evi2_modelA_ny_head(:,4); %head simulated


%The simulated heads for the specific wells
con1=xsim>4&xsim<4.2&zsim>56&zsim<56.3&ysim>0&ysim<1.5
sum(con1) %gives x,y,z for TH6S
con2=xsim>14&xsim<14.2&zsim>52.1&zsim<52.2&ysim>0&ysim<1.5
sum(con2) %gives x,y,z for TH2-2
con3=xsim>36&xsim<36.5&zsim>53&zsim<53.2&ysim>0&ysim<1.5
sum(con3) %gives x,y,z for TH1-2
con4=xsim>72&xsim<72.9&zsim>52&zsim<52.2&ysim>0&ysim<1.5
sum(con4) %gives x,y,z for TH3-6m
con5=xsim>111.2&xsim<111.4&zsim>50&zsim<50.2&ysim>0&ysim<1.5
sum(con5) %gives x,y,z for TH4-8m
con6=xsim>14&xsim<14.2&zsim>46&zsim<46.2&ysim>0&ysim<1.5
sum(con6) %gives x,y,z for TH2
con7=xsim>36&xsim<36.5&zsim>42.7&zsim<42.9&ysim>0&ysim<1.5
sum(con7) %gives x,y,z for TH1
con8=xsim>72&xsim<72.9&zsim>56.1&zsim<56.3&ysim>0&ysim<1.5
sum(con8) %gives x,y,z for TH3-2m
con9=xsim>111.2&xsim<111.4&zsim>55.2&zsim<55.3&ysim>0&ysim<1.5
sum(con9) %gives x,y,z for TH4-3m

datasim=cat(1,hsim(con1),hsim(con2),hsim(con3),hsim(con4),hsim(con5),hsim(con6),hsim(con7),hsim(con8),hsim(con9))
%head for every well. 1 is the dimension


figure (2)
plot(h,datasim,'b+') %obs. head vs. sim. head in a scatter plot. (1-1 line)
title('2D PHAST Model A EVI2','fontsize',16)
xlabel('Observed head [m]')
ylabel('Simulated head [m]')
hold on
plot(h,h,'k-') %1-1 line
legend('obs. vs. sim.','1-1 line',2)
%grid


figure (3)
plot(x,h,'b+') %obs. head vs. distance to stream in a scatter plot
title('Observed heads and simulated heads','fontsize',16)
hold on
plot(x,datasim,'r+') %simulated head vs. distance to stream in a scatter plot.
xlabel('Distance to stream [m]')
ylabel('Heads [m]')


%RMSE is calculated for the PHAST model
rmse(h,datasim)
```

Appendix 14: MATLAB script for TH3 and TH4 in the 2D PHAST models

```
clc, clear all %Ensures that all previous provisions and characters are deleted

load TH3_obs_values.txt
data0=TH3_obs_values; %note that matlab changes file name

%TH3- Observed data
x=TH3_obs_values(:,3); %x in meter from stream
z=TH3_obs_values(:,2); %z in meter depth
y=TH3_obs_values(:,4); %y in cells
Alk=TH3_obs_values(:,11); %alkalinity
pH=TH3_obs_values(:,6); %pH
Fe2=TH3_obs_values(:,24); %Fe2
nitrat=TH3_obs_values(:,16); %nitrate
sulfate=TH3_obs_values(:,18); %sulfate

load TH4_obs_values.txt
data2=TH4_obs_values; %note that matlab changes file name

%TH4- Observed data
TH4x=TH4_obs_values(:,3); %x in meter from stream
TH4z=TH4_obs_values(:,2); %z in meter depth
TH4y=TH4_obs_values(:,4); %y in cell
TH4Alk=TH4_obs_values(:,11); %alkalinity
TH4pH=TH4_obs_values(:,6); %pH
TH4Fe2=TH4_obs_values(:,24); %Fe2
TH4nitrat=TH4_obs_values(:,16); %nitrate
TH4sulfate=TH4_obs_values(:,18); %sulfate


%-----------------------------------------------------------------
%data from the 2D PHAST model

load EVI2_modelA_ny_123_ikkdrain.txt
data=EVI2_modelA_ny_123_ikkdrain; %note that matlab changes file name

xsim=data(:,1); %x in PHAST model
ysim=data(:,2); %y in PHAST model
zsim=data(:,3); %z in PHAST model
n5sim=data(:,20); %nitrate simulated
s6sim=data(:,17); %sulfate simulated
phsim=data(:,12); %ph simulated
alksim=data(:,14); %alk simulated
fe2sim=data(:,19); %fe2 simulated
time=data(:,4); %time for print
ilt=data(:,15); %oxygen
rate=data(:,31); %rate

%-----------------------------------------------------------------
%TH3 - data for the specific time step
con1=time>9.5&time<11&xsim>72&xsim<72.9
sum(con1) %All columns for time step 10 for TH3

Tid_n5sim=cat(1,n5sim(con1)) %Nitrat
Tid_s6sim=cat(1,s6sim(con1)) %Sulfate
phsim1=cat(1,phsim(con1)) %pH
Tid_alksim=cat(1,alksim(con1)) %alk
Tid_fe2sim=cat(1,fe2sim(con1)) %Fe2
zsim_ny=cat(1,zsim(con1)) %z(because z in obs. is in the wrong order)
Tid_ilt=cat(1,ilt(con1)) %oxygen for step 10
Tid_rate=cat(1,rate(con1)) %rate pyrit


%Simulated data is multiplied with 1000 for the units to be in mmol.
n5sim1=Tid_n5sim*1000;
s6sim1=Tid_s6sim*1000;
alksim1=Tid_alksim*1000;
fe2sim1=Tid_fe2sim*1000;
iltsim1=Tid_ilt*1000;
ratesim1=Tid_rate*1000;


% %TH4 - Data for the specific time step 10 years
con2=time>9.5&time<11&xsim>110&xsim<112
sum(con2) %gives all columns for time step 10 for TH4

TH4Tid_n5sim=cat(1,n5sim(con2)) %nitrate
TH4Tid_s6sim=cat(1,s6sim(con2)) %sulfate
TH4phsim1=cat(1,phsim(con2)) %pH
TH4Tid_alksim=cat(1,alksim(con2)) %alk
TH4Tid_fe2sim=cat(1,fe2sim(con2)) %Fe2
TH4zsim_ny=cat(1,zsim(con2)) %z(because z in obs. is in the wrong order)
```

```
%Simulerede data multiplied with 1000 for mmol.
TH4n5sim1=TH4Tid_n5sim*1000;
TH4s6sim1=TH4Tid_s6sim*1000;
TH4alksim1=TH4Tid_alksim*1000;
TH4fe2sim1=TH4Tid_fe2sim*1000;


%-----------------------------------------------------------------------
%The figures. data vs depth
%TH3
figure (1) %Alk and pH, and Fe
%Alk and pH
subplot (2,1,1)
plot(Alk,z,'k-','linewidth',1.5) %obs. alk vs depth
title('Alkalinity and pH - TH3 Model A','fontsize',16)
xlabel('[meq/L and pH]')
ylabel('Depth DVR90[m]')
hold on
plot(pH,z,'k-','linewidth',1.5) %obs. pH vs depth
hold on
plot(alksim1,zsim_ny,'k--','linewidth',1.5) %sim. alk vs depth
hold on
plot(phsim1,zsim_ny,'k:','linewidth',1.5) %sim. pH vs depth
legend('Alk measured','pH measured','Alk simulated','pH simulated',2)
axis([0,7,47,58])
%grid

% Fe2
subplot (2,1,2)
plot(Fe2,z,'k-','linewidth',1.5) %obs. head plottes vs. distance to stream in a scatter plot.
title('Fe2 - TH3 Model A','fontsize',16)
hold on
plot(fe2sim1,zsim_ny,'k--','linewidth',1.5) %simulated head plottes vs. distance to stream in a scatter plot.
xlabel('[mM]')
ylabel('Depth DVR90[m]')
legend('Fe2 measured','Fe2 simulated',2)
axis([0,0.13,47,58])

figure (2)%Nitrat og sulfat
%Nitrate
subplot (2,1,1)
plot(nitrat,z,'k-','linewidth',1.5) %obs. head plottes vs. sim. head in a scatter plot. (1-1 linjen)
title('Nitrate - TH3 Model A','fontsize',16)
xlabel('[mM]')
ylabel('Depth DVR90[m]')
hold on
plot(n5sim1,zsim_ny,'k--','linewidth',1.5) %nitrat simulated
legend('Nitrate measured','Nitrate simulated',2)
axis([0,1.5,47,58])

%Sulfate
subplot (2,1,2)
plot(sulfate,z,'k-','linewidth',1.5) %obs. head plottes vs. distance to stream in a scatter plot.
title('Sulfate - TH3 Model A','fontsize',16)
hold on
plot(s6sim1,zsim_ny,'k--','linewidth',1.5) %simulated head plottes vs. distance to stream in a scatter plot.
xlabel('[mM]')
ylabel('Depth DVR90[m]')
legend('Sulfate measured','Sulfate simulated',2)
axis([0,1.5,47,58])

figure (5)%simuleret ilt og  rate
plot(iltsim1,zsim_ny,'k-','linewidth',1.5) %plottes vs. distance to stream in a scatter plot.
title('TH3 Model A','fontsize',16)
hold on
plot(ratesim1,zsim_ny,'k--','linewidth',1.5) % plottes vs. distance to stream in a scatter plot.
xlabel('[mM] and [mM/year]')
ylabel('Depth DVR90[m]')
legend('Oxygen','Transferred pyrite',2)
axis([-0.1,0.4,47,58])

%-----------------------------------------------------------------------
%TH4

figure (3) %Alk and pH, and Fe TH4
%Alk and pH
subplot (2,1,1)
plot(TH4Alk,TH4z,'k-','linewidth',1.5) %obs. alk vs depth
title('Alkalinity and pH - TH4 Model A','fontsize',16)
xlabel('[meq/L]')
ylabel('Depth DVR90[m]')
hold on
plot(TH4pH,TH4z,'k-','linewidth',1.5) %obs. pH vs depth
hold on
```

```
plot(TH4alksim1,TH4zsim_ny,'k--','linewidth',1.5) %sim. alk vs depth
hold on
plot(TH4phsim1,TH4zsim_ny,'k:','linewidth',1.5) %sim. pH vs depth
legend('Alk measured','pH measured','Alk simulated','pH simulated',2)
axis([0,7,47,58])

% Fe2
subplot (2,1,2)
plot(TH4Fe2,TH4z,'k-','linewidth',1.5) %obs. head plottes vs. distance to stream in a scatter plot.
title('Fe2 - TH4 Model A','fontsize',16)
hold on
plot(TH4fe2sim1,TH4zsim_ny,'k--','linewidth',1.5) %simulated head plottes vs. distance to stream in a scatter
plot.
xlabel('[mM]')
ylabel('Depth DVR90[m]')
legend('Fe2 measured','Fe2 simulated',2)
axis([0,0.13,47,58])

figure (4)%Nitrat og sulfat TH4
%Nitrate
subplot (2,1,1)
plot(TH4nitrat,TH4z,'k-','linewidth',1.5) %obs. head plottes vs. sim. head in a scatter plot. (1-1 linjen)
title('Nitrate - TH4 Model A','fontsize',16)
xlabel('[mM]')
ylabel('Depth DVR90[m]')
hold on
plot(TH4n5sim1,TH4zsim_ny,'k--','linewidth',1.5) %nitrat simulated
legend('Nitrate measured','Nitrate simulated',2)
axis([0,1.5,47,58])

%Sulfate
subplot (2,1,2)
plot(TH4sulfate,TH4z,'k-','linewidth',1.5) %obs. head plottes vs. distance to stream in a scatter plot.
title('Sulfate - TH4 Model A','fontsize',16)
hold on
plot(TH4s6sim1,TH4zsim_ny,'k--','linewidth',1.5) %simulated head plottes vs. distance to stream in a scatter plot.
xlabel('[mM]')
ylabel('Depth DVR90[m]')
legend('Sulfate measured','Sulfate simulated',2)
axis([0,1.5,47,58])
```

Appendix 15: MATLAB script for TH1 and TH2 in the 2D PHAST models

The plotting of the figure are not showed for this script because it is the same script as for TH3 and TH4 (appendix 14)

```
load TH1_obs_values.txt
data0=TH1_obs_values; %note that matlab changes file name

%TH1- Observed data
x=TH1_obs_values(:,3); %x in meter from stream
z=TH1_obs_values(:,2); %z in meter depth
y=TH1_obs_values(:,4); %y in cell
nitrat=TH1_obs_values(:,5); %nitrate
sulfate=TH1_obs_values(:,6); %sulfate

%TH2
load TH2_obs_values.txt
data2=TH2_obs_values; %note that matlab changes file name

%TH2- Observed data
TH2x=TH2_obs_values(:,3); %x in meter from stream
TH2z=TH2_obs_values(:,2); %z in meter depth
TH2y=TH2_obs_values(:,4); %y in cell
TH2nitrat=TH2_obs_values(:,5); %nitrate
TH2sulfate=TH2_obs_values(:,6); %sulfate

%-----------------------------------------------------------------
%simulated data from the 2D PHAST model

load EVI2_modelA_ny_123.txt
data=EVI2_modelA_ny_123; %note that matlab changes file name

xsim=data(:,1); %x in the PHAST model
ysim=data(:,2); %y in the PHAST model
zsim=data(:,3); %z in the PHAST model
n5sim=data(:,20); %nitrate simulated
s6sim=data(:,17); %sulfate simulated
time=data(:,4); %time for print

%-----------------------------------------------------------------
%TH1 - The data for the specific time step and well
con1=time>9.5&time<11&xsim>36&xsim<36.5
sum(con1) %giver alle kolonner for timestep 10 for TH1

Tid_n5sim=cat(1,n5sim(con1)) %nitrat for step 10
Tid_s6sim=cat(1,s6sim(con1)) %sulfate for step 10
zsim_ny=cat(1,zsim(con1)) %z for step 10 (because z in obs. is in the wrong order)

%Simulerede data is multiplied with 1000 to get the unit in mmoles
n5sim1=Tid_n5sim*1000;
s6sim1=Tid_s6sim*1000;

% %TH2 - Data fot the specific time step
con2=time>9.5&time<11&xsim>14&xsim<15
sum(con2) %gives all columns for time step 10 for TH2

TH2Tid_n5sim=cat(1,n5sim(con2)) %nitrat for step 10. 1 is the dimension
TH2Tid_s6sim=cat(1,s6sim(con2)) %sulfate for step 10
TH2zsim_ny=cat(1,zsim(con2)) %z for step 10 (because z in obs. is in the wrong order)

% Simulerede data is multiplied with 1000 to get the unit in mmoles
TH2n5sim1=TH2Tid_n5sim*1000;
TH2s6sim1=TH2Tid_s6sim*1000;
```

Appendix 16: Flow budget from the 3D GMS model

The 3D model without drain

Sources	m3/day	percentag	**Sinks**	m3/day	percentag
Lakes	1.95	0.001	Wells boundary	43268.4	25.8
Recharge	167884.6	99.998	Lakes	957.22	0.6
Stream	0.96	0.001	Stream	123500.4	73.6
Total	167887.5		Total	167726	

The 3D model with drain

Sources	m3/day	percentag	**Sinks**	m3/day	percentag
Lakes	5.06	0.003	Wells boundary	43268.4	25.4
Recharge	167884.6	99.288	Lakes	715.9	0.4
Stream	1198.74	0.709	Drain	21427.45	12.6
			Stream	104806.1	61.6
Total	169088.4		Total	170217.9	

Flow budget for A: The cells at the wetland area at EVI2 and B: for the agricultural field at EVI2

A

	Flow In	Flow Out
Sources/Sinks		
CONSTANT HEAD	0.0	0.0
WELLS	0.0	0.0
DRAINS	0.0	-1709.780670166
HEAD DEP BOUNDS	0.0	0.0
RECHARGE	57.913076877594	0.0
STREAM LEAKAGE	72.718788146973	-3.711812496185
Total Source/Sink	**130.63186502457**	**-1713.492482662**
Zone Flow		
FLOW RIGHT FACE	17.476151823997	-22.17388910055
FLOW FRONT FACE	78.680668592453	0.0
FLOW LOWER FACE	1624.5500490367	-112.6128002405
FLOW LEFT FACE	16.46329498291	0.0
FLOW UPPER FACE	0.0	0.0
FLOW BACK FACE	4.2602316141129	-23.57502958179
Total Zone Flow	**1741.4303960502**	**-158.3617189229**
TOTAL FLOW	**1872.0622610748**	**-1871.854201585**
Summary	**In - Out**	**% difference**
Sources/Sinks	**-1582.860617638**	**-171.6652805569**
Cell To Cell	**1583.0686771274**	**166.65704259435**
Total	**0.208059489727**	**0.0111145369723**

B

Zone 55 Use all ti

Budget Term	Flow (m^3/d)
Flow Budget for Zone 55	
IN:	
CONSTANT HEAD	0.0
WELLS	0.0
DRAINS	0.0
HEAD DEP BOUNDS	0.0
RECHARGE	13.948999166489
STREAM LEAKAGE	60.87296295166
Zone 11 to zone 55	0.0
Zone 100 to zone 55	5.5184046924114
Zone 200 to zone 55	23.114715576172
Total IN	103.45508238673
OUT:	
CONSTANT HEAD	0.0
WELLS	0.0
DRAINS	85.780143737793
HEAD DEP BOUNDS	0.0
RECHARGE	0.0
STREAM LEAKAGE	0.0
Zone 55 to zone 11	0.0
Zone 55 to zone 100	8.3356248736382
Zone 55 to zone 200	9.4798812270164
Total OUT	103.59564983845

Appendix 17: 1-1 lines for the 3D MODFLOW model with and without drain

RMSE(head) with drain: 3.84 m

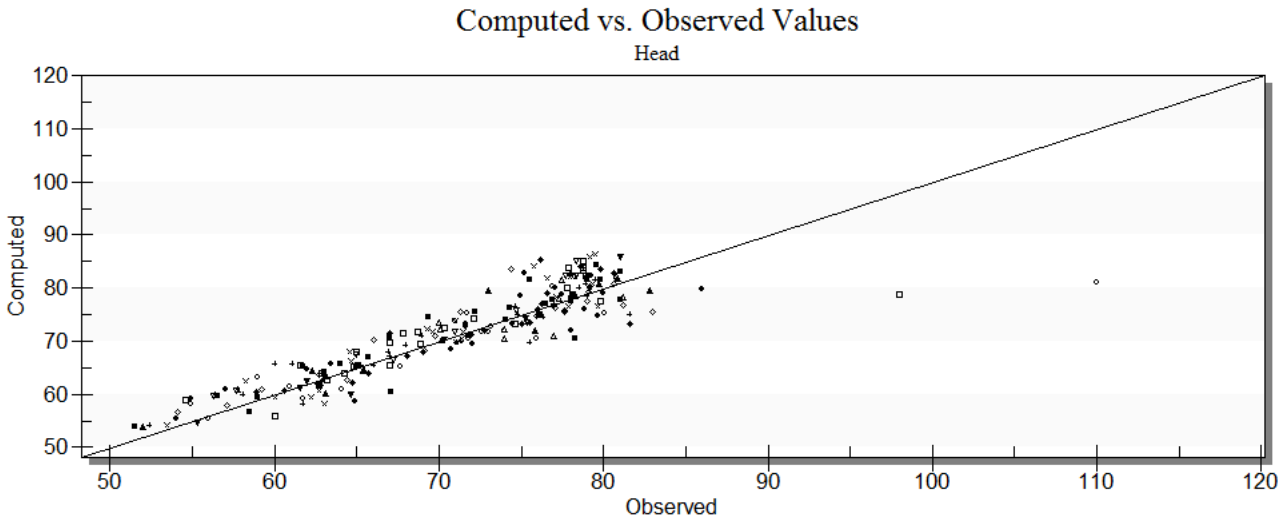

RMSE(head) without drain 4.13m

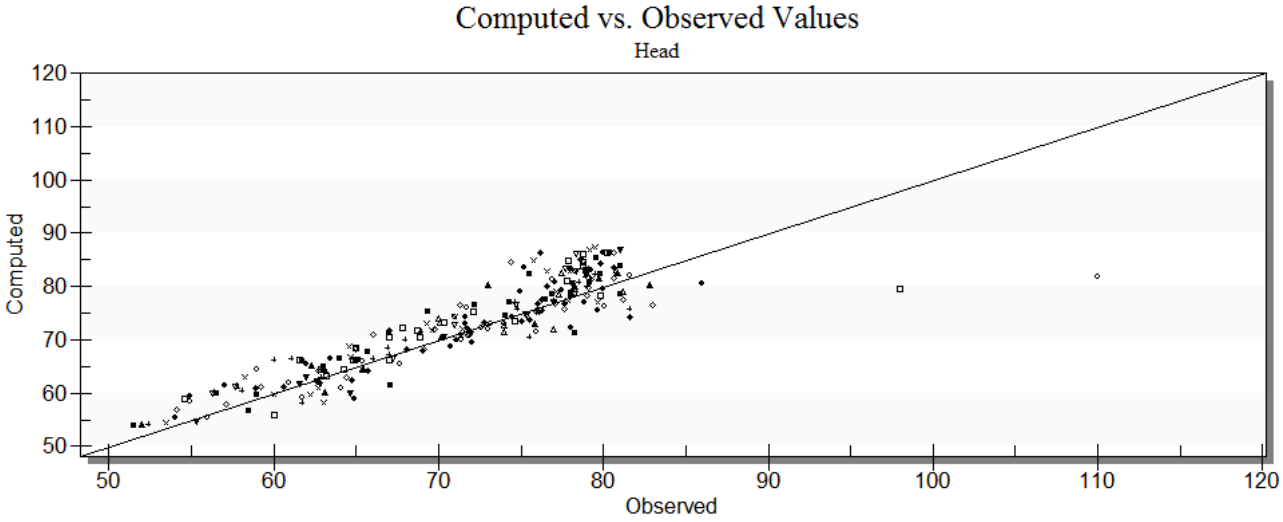

Appendix 18: Push pull experiment

The puch-pull experiment was conducted in TH3.2 in 3 m.b.s. in order to investigate the rate of denitrification.

The figure is created by Jessen S. 2016 and show three synthetically constructed graphs of the consumption of 1 mM NO3- over time (days) with three different k values/hour: -0.0025 in red, -0.01 in green and -0.025 in blue (Kofod, 2016).

One can argue that the highest rate is the one you can trust the most because the concentrations of nitrate that has been used to find this rate has been in the aquifer the longest time (36 hour) and by that the denitrification can have taken place without the influence of oxygen (Kofoed, 2016).

By differentiate the rate k by assuming a 1. order reaction (Appelo and Postma, 2005) of the denitrification with nitrate as electron donor the following denitrification rate is found:

-0.025 /hour * 0.05 mM = 0.00125 mM/hour = -0.03 mM/day = -10.9 mM/year

-0.0025/hour *0.25mM= 0.00063 mM/hour = -0.015 mM/day = -5.5 mM/year